AD NUMBER
AD324548
CLASSIFICATION CHANGES
TO: unclassified
FROM: confidential
LIMITATION CHANGES
TO: Approved for public release, distribution unlimited
FROM: Distribution authorized to U.S. Gov't. agencies and their contractors; Administrative/Operational Use; MAY 1961. Other requests shall be referred to Office of Naval Research, 800 North Quincy Street, Arlington, VA 22217-5660.
AUTHORITY
31 May 1973, DoDD 5200.10; ONR ltr, 28 Jul 1977

NOX

MASSACHUSETTS INSTITUTE OF TECHNOLOGY
NAVAL SUPERSONIC LABORATORY

Technical Report 448

(UNCLASSIFIED TITLE)
FINAL REPORT ON A STUDY OF
ROCKET THRUST CONTROL BY
GAS INJECTION

by

Fred L. Gunter
and
Fred E. Fahrenholz

May 1961

Massachusetts Institute of Technology
Naval Supersonic Laboratory
Cambridge, Massachusetts

Technical Report 448

(UNCLASSIFIED TITLE)
FINAL REPORT ON A STUDY OF ROCKET THRUST CONTROL BY GAS INJECTION*

by

Fred L. Gunter
and
Fred E. Fahrenholz

May 1961

AL Log No. 3945
Copy 20 of 100 copies.
xii and 110 pages

*This report is based in part on a thesis by Fred L. Gunter entitled "Thrust Vector Control by Secondary Gas Injection" and submitted in partial fulfillment of the requirements for the degrees of Bachelor of Science and Master of Science at the Massachusetts Institute of Technology, January 1961

FOREWORD

The research described in this report was sponsored in whole or in part by the Office of Naval Research under Contract Nonr 1841 (61) which has been monitored by Lt. Comdr. F. T. Hemmler, Lt. Cmdr. W. L. Miller and Mr. J. R. Patton, Jr.

ABSTRACT

A theoretical and experimental investigation of thrust control by secondary gas injection has been completed. Thrust control is treated from the two aspects of thrust modulation and vector control with the emphasis being on the former.

The thrust modulation study is concerned with the use of injection as a means of throttling the main nozzle flow. Since experimental data shows that thrust is proportional to total nozzle flow, the thrust is thus also proportional to flow throttling or injection rate. The performance (flow throttling and thrust) of a variety of secondary injection configurations was measured with a low pressure-ratio, axially symmetric nozzle as well as a high pressure-ratio, two-dimensional nozzle. Cold air (530°R) was the working fluid in the primary and secondary flows. The flow throttling results agree with an analysis based on three flow models and the schlieren photographs (from the two-dimensional tests) show that all three types of flow occur. The effects of the important variables are determined analytically and/or experimentally.

The vector control study concerns asymmetric secondary gas injection as a means of controlling the direction of the thrust vector. Some experimental data was obtained from the two-dimensional nozzle tests. This data is compared to data from other sources and an explanation is given for the process which governs the generation of side force.

TABLE OF CONTENTS

TABLE OF CONTENTS (Concluded)

LIST OF ILLUSTRATIONS

LIST OF ILLUSTRATIONS (Continued)

LIST OF ILLUSTRATIONS (Concluded)

LIST OF SYMBOLS

A_e	Nozzle exit area
A_{inj}	Nozzle area at injection station
A_{2_s}	Secondary flow area at station 2 (see sketches on pages 9 and 11)
A_{*_s}	Secondary injection orifice area (local Mach number of unity)
b	Injection throat height (0.08", see Fig. 11)
C	Orifice coefficient (see page 13)
d	Throat height (1.5", see Fig. 9)
F	Thrust
F_s	Side force
F_0	Thrust with unrestricted primary flow ($w_s = 0$)
M	Mach number
p	Pressure
p_0	Primary stagnation pressure
p_{0_s}	Secondary stagnation pressure
R	Gas constant
R	Radius of primary flow (see sketches on pages 5, 9, and 11)
T	Temperature
T_0	Primary stagnation temperature
T_{0_s}	Secondary stagnation temperature
w_p	Primary flow
w_{p_0}	Unrestricted primary flow ($w_s = 0$)
w_s	Secondary flow
x	Axial distance

LIST OF SYMBOLS (Concluded)

β	Circumferential angle over which injection takes place
γ	Ratio of specific heats $\frac{C_p}{C_v}$
ρ	Density
ρ_0	Primary stagnation density
ρ_{0_s}	Secondary stagnation density
ϕ	Injection angle (see sketch on page 5)

Subscripts

$()_1$	Flow stations in primary flow, see sketches on pages 5, 9, and 11.
$()_2$	
$()_{2s}$	Flow station in secondary flow, see sketches on pages 9 and 11
$()_{*s}$	Value at sonic speed (M = 1) in secondary flow
$()_s$	Secondary flow
$()_s$	Asymmetric injection configuration
$()_*$	Value at sonic speed (M = 1) in primary flow

SECTION I

INTRODUCTION

The wide variety of missions presently associated with vehicles using large rocket engines has made apparent the need for versatility in engine performance. Of particular importance in this respect is the capability of rocket thrust control. Although much work has been done on this subject, the state of the art certainly does not preclude the possibility of further improvements. The conventional gimbal system, especially in the largest engines, is enormously complicated and not the ultimate in efficiency. In the case of solid propellant engines, the problem of thrust control is particularly critical in view of the inherently "uncontrollable" nature of the burning process. Liquid propellant devices, however, are not as rigidly fixed in their basic mode of operation and thus may be better suited to modifications designed to incorporate thrust control capability. In either case, the need for more efficient systems is great.

The Naval Supersonic Laboratory (NSL) has conducted an investigation of a promising method of thrust control. The method is one in which a secondary flow is injected into a main nozzle to change the magnitude and/or direction of the nozzle flow. Since nozzle thrust is directly proportional to the product of mass flow and velocity, any change in these quantities implies a change in thrust. The present study deals with symmetric injection for flow throttling (thrust modulation) and asymmetric injection for flow direction control (vector control). Most of the work, however, concerns symmetric injection configurations.

A variety of parameters have been investigated in the two phases of research which constitute the overall program. The Phase I portion centered around three-dimensional air flow tests and included analytical studies. This work is reported in detail in Ref. 1 and summarized briefly herein. Two-dimensional air flow tests formed the basis of the Phase II effort which is described in detail in this report.

SECTION II

THRUST MODULATION

Analytical and experimental studies have been carried out which investigated symmetric secondary injection as a means of thrust modulation. The first portion of this section briefly summarizes the most important features of the work accomplished in the Phase I program. The Phase I program included both analytical and experimental studies. The second portion of this section presents further analytical work. This involves an analogy between the secondary injection and blunt body problems as well as extensions of the Phase I analytical developments. A presentation of the details of the Phase II two-dimensional air flow tests constitutes the third part of this section while the fourth and final one is a correlation and comparison of NSL and other data.

A. PHASE I - THEORY

The first thorough attempt to find an analytical solution to the flow throttling problem was made by A. I. Martin in Ref. 2. Martin regarded secondary injection as a possible method of obtaining a variable-throat nozzle for use in controlling the performance of a jet engine at different operating conditions. Two theoretical models were developed although this procedure was adopted merely as a simplification necessary to generate an amenable analytical problem. Martin expected that the real case would be a combination of the features of both models.

The problem solutions obtained by Martin came from appropriate application of simplified forms of the equations of fluid motion. He compared numerical results to some test data and the agreement between theory and experiment was not very good. In addition, appropriate use of Martin's solutions gave results which, like his own data, disagreed with NSL experimental data (reported in Section B).

Further study of the Martin analyses led to the development of

several NSL analytical models. There are three NSL flow models of which two are modifications of the Martin ones. These are the "secondary mixing" (modified "mixing process") model and the "sheet flow" (modified "vortex sheet") model. An entirely new one has also been developed called the "secondary expansion" model. The most important features of the NSL analyses are described below while a detailed treatment may be found in Ref. 1.

Although the theoretical flow configurations are treated separately below, some simplifying assumptions are common to all of them. The most basic one is that the flow is one-dimensional. In addition, the primary and secondary fluids are assumed to be perfect gases whose flow is isentropic. These assumptions may not be satisfied but their use leads to an approximately correct choice of dependence of problem variables.

The assumption of one-dimensional, perfect gas flow immediately relates certain problem variables. The equation of state for a perfect gas,

$$p = \rho R T \tag{1}$$

relates the pressure, density, and temperature at any point in the flow. As shown in Ref. 3, the energy equation may be written in the following appropriate form:

$$\frac{T}{T_0} = \left[1 + \frac{\gamma - 1}{2} M^2 \right]^{-1} \tag{2}$$

The energy equation is also useful in obtaining the following one-dimensional isentropic flow relations:

$$\frac{p}{p_0} = \left[1 + \frac{\gamma - 1}{2} M^2 \right]^{-\frac{\gamma}{\gamma - 1}} \tag{3}$$

$$\frac{\rho}{\rho_0} = \left[1 + \frac{\gamma - 1}{2} M^2 \right]^{-\frac{1}{\gamma - 1}} \tag{4}$$

All of the above equations apply throughout the flow in all of the theoretical models.

1. Secondary Mixing Model

In the secondary mixing case the secondary flow mixes with the primary stream to produce a combined stream. The important features of the flow configuration are shown in the sketch below.

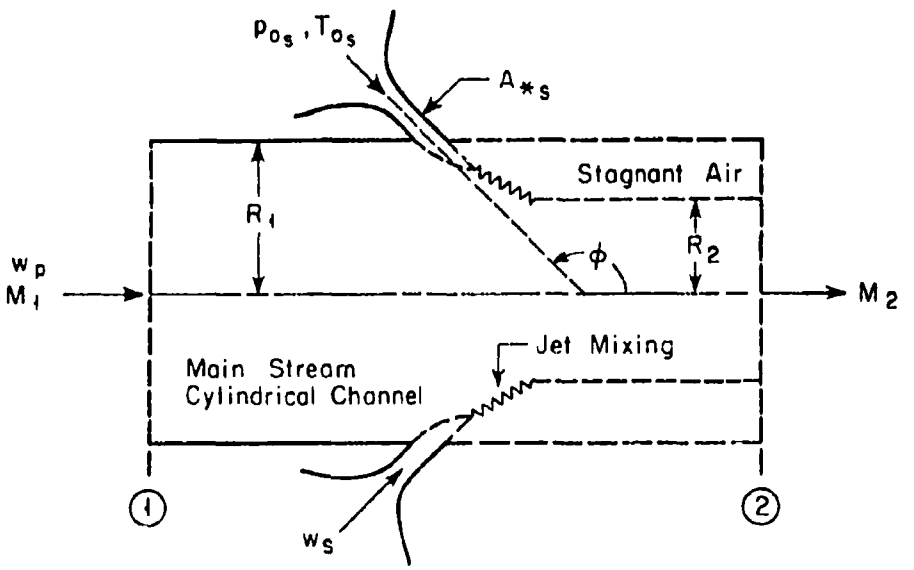

The secondary flow (rate w_s) enters the nozzle (radius R_1) through a sonic orifice (area A_{*s}) and is directed at an angle ϕ with respect to the nozzle axis. The primary and secondary streams mix to form a final stream tube of radius R_2. The primary stream (rate w_p) flows uniformly at Mach number M_1 at station 1 while at station 2 a uniform combined stream flows at Mach number M_2.

The equations of continuity and momentum are applied to the flow and, in particular, are evaluated at stations 1 and 2. The continuity

equation may be written as

$$\left[\frac{\rho_2}{\rho_0}\right]\left[\frac{R_2}{R_1}\right]^2 M_2 \left[\frac{T_2}{T_0}\right]^{\frac{1}{2}} = \left[\frac{\rho_1}{\rho_0}\right] M_1 \left[\frac{T_1}{T_0}\right]^{\frac{1}{2}}$$

$$+ \frac{A_{*s}}{\pi R_1^2}\left[\frac{\rho_{*s}}{\rho_{0s}}\right]\left[\frac{\rho_{0s}}{\rho_0}\right]\left[\frac{T_{*s}}{T_{0s}}\right]^{\frac{1}{2}}\left[\frac{T_{0s}}{T_0}\right]^{\frac{1}{2}} \qquad (5)$$

where the primary and secondary fluids are the same gas.

The momentum equation is given by

$$\frac{p_1}{p_0}\left[1 + \gamma M_1^2\right] - \gamma\left[\frac{A_{*s}}{\pi R_1^2}\right]\left[\frac{p_{*s}}{p_{0s}}\right]\left[\frac{p_{0s}}{p_0}\right]\cos\phi$$

$$= \frac{p_2}{p_0}\left(\frac{R_2}{R_1}\right)^2\left[1 + \gamma M_2^2\right] \qquad (6)$$

in which the primary and secondary gases are again the same. This equation has the additional assumption that the stagnation conditions of the combined stream are equal to those of the primary stream. Equation (6) also has an assumption which concerns the "stagnant air" zone shown in the sketch on page 5. It was felt that this separated flow zone might exist at some very low pressure. That is, the centrifugal force on the secondary flow as it changes direction by $(\pi - \phi)$* might leave little flow near the wall just downstream of the injection point. Therefore, for the purposes of analysis, it was assumed that the pressure in this zone is negligible (mathematically, zero) compared to that in the primary and secondary streams.

*All of the work in this report concerns configurations where $\phi \leq 90°$.

It should be pointed out that Eqs. (5) and (6) are not in a form which corresponds to the general representation of the problem. This is due to the assumption that the primary and secondary flows are the same gas. The case of different gases, however, does not permit the use of the simplified equations shown above. The values of the gas constant R and the ratio of specific heats γ must be determined for the combined stream from trial values of the primary flow associated with a given secondary flow. This iterative procedure is thus superimposed on the remainder of the method of solution. Apart from this matter, the method of solution is complicated above and beyond that of the "same gas" case due to another factor. This factor is that the mixing of gases implies an increase in entropy (which also means a loss in efficiency). Thus Eqs. (3) and (4) (and thus (5) and (6)) would be replaced by the more complicated relationships appropriate to the situation. However, here again the procedure is an iterative one since the entropy increase is a function of the amount of each gas or, in effect, the primary flow associated with a given secondary flow. It is fairly obvious at this point that the "different gas" case thus becomes indeed complicated. In fact, its complexity is out of proportion to that of the other models as well as its usefulness as an approximate analysis. Furthermore, by way of experience with data, it is difficult to justify in view of the fact that the "same gas" case is the poorest (compared to data) of the theoretical models. Therefore, the remainder of this discussion concerns the "same gas" case and all references to the secondary mixing model pertain to this case only.

The flow configuration sketch on page 5 shows that the secondary flow is injected through a sonic orifice of area A_{*_s} from stagnation pressure and temperature p_{0_s} and T_{0_s}, respectively. In the form of a non-dimensional ratio which compares it to the original ($w_s = 0$) primary flow, the secondary flow rate is

$$\frac{w_s}{w_{p_0}} = \frac{\dfrac{A_{*_s}}{\pi R_1^2}\left[\dfrac{\rho_{*_s}}{\rho_{0_s}}\right]\left[\dfrac{\rho_{0_s}}{\rho_0}\right]\left[\dfrac{T_{*_s}}{T_{0_s}}\right]^{\frac{1}{2}}\left[\dfrac{T_{0_s}}{T_0}\right]^{\frac{1}{2}}}{\left[\dfrac{\rho_2}{\rho_0}\right] M_2 \left[\dfrac{T_2}{T_0}\right]^{\frac{1}{2}}} \qquad (7)$$

where the two flows are the same gas. Equation (7) is the special case (primary gas = secondary gas) of the general form given in the next section (A2). The choice of this parameter (w_s/w_{p_0}) as an index of the secondary flow rate is somewhat arbitrary although its usefulness is made apparent by the discussion in the next paragraph.

When certain final assumptions are made the continuity and momentum equations ((5) and (6)) yield a solution to the problem. The geometry is specified by the assumption of values for the parameters $A_{*_s}/\pi R_1^2$ and ϕ while the particular gas employed designates γ. The final assumption necessary is an overall pressure ratio (p_2/p_0) which implies the value of the Mach number* M_2. Since the pressure, density, and temperature ratios are functions of Mach number (according to Eqs. (2), (3), and (4)), Eqs (5) and (6) thus become a pair of simultaneous equations with unknowns $[R_2/R_1]^2$ and M_1. The particular procedure used in solving the equations is described in Appendix A. As shown in this appendix, flow throttling results are conveniently handled in terms of non-dimensional ratios. Thus, the results for a typical case are shown in Fig. 1, taken from Ref. 1, where primary flow ratio is plotted against secondary flow ratio. For purposes of comparison, also shown is the Martin mixing process result.

It should be noted that in Fig. 1 as well as subsequent figures the flow throttling curves do not begin at $w_s/w_{p_0} = 0$. This results from the assumption of sonic injection of secondary flow. The lower limit of w_s/w_{p_0} is thus determined according to the assumption that the sonic secondary pressure is approximately the same as the sonic primary pressure. In equation form,

$$\frac{\frac{p_{0_s}}{p_{*_s}}}{\frac{p_0}{p_2}} \approx \frac{p_{0_s}}{p_0} \quad \text{if } p_{*_s} \approx p_2$$

* Results show that maximum flow throttling occurs when $M_2 = 1\ (p_2/p_0 = 0.5283)$. This is understandable since the primary stream occupies a minimum of area at sonic conditions. In all of the theoretical calculations, therefore, M_2 is unity.

which determines the minimum p_{0_s}/p_0. Since p_2/p_0 is the sonic ($M_2 = 1$) pressure ratio for air, if the secondary gas is also air, then the minimum p_{0_s}/p_0 is unity.

2. Sheet Flow Model

The basic assumption in the sheet flow model is that the primary and secondary flows do not mix. The flow configuration is sketched below.

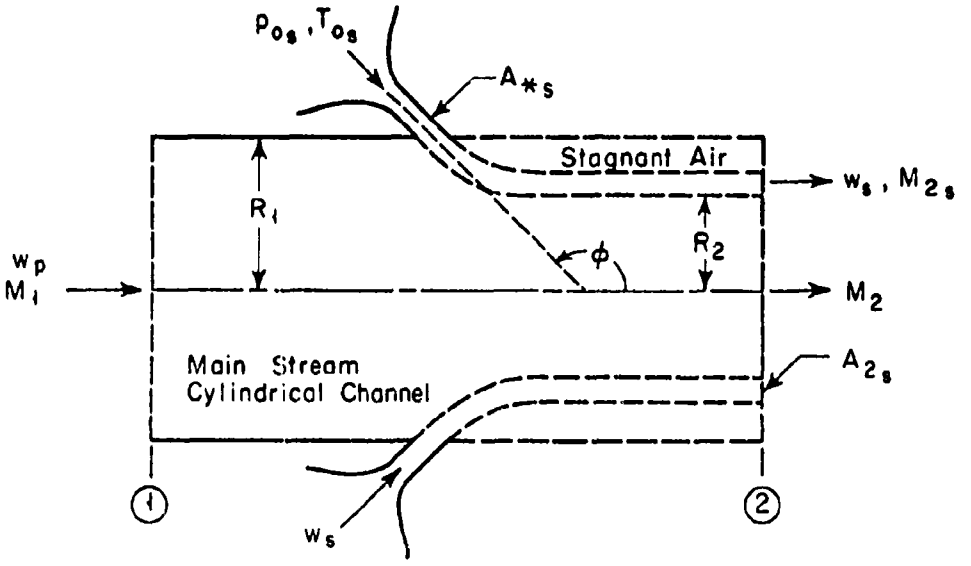

The secondary flow enters the nozzle in the same manner as that in the secondary mixing model. In the present model, however, the secondary stream flows in a sheet circumjacent to the primary one and there are two distinct streams at station 2. At this station, the secondary stream occupies an area A_{2_s} while it flows at Mach number M_{2_s}. The pressure in the stagnant air zone is again assumed to be negligible (mathematically, zero) compared to that in the primary and secondary streams.

The equations of continuity and momentum are applied to the flow as in the secondary mixing model. Now there are two continuity equations written as

$$\frac{\rho_2}{\rho_0}\left[\frac{R_2}{R_1}\right]^2 M_2 \left[\frac{T_2}{T_0}\right]^{\frac{1}{2}} = \frac{\rho_1}{\rho_0} M_1 \left[\frac{T_1}{T_0}\right]^{\frac{1}{2}} \tag{8}$$

for the primary flow, and

$$\frac{\rho_{2_s}}{\rho_0}\left[\frac{A_{2_s}}{A_{*s}}\right] M_{2_s} \left[\frac{T_{2_s}}{T_{0_s}}\right]^{\frac{1}{2}} = \left[\frac{T_{1_s}}{T_{0_s}}\right]^{\frac{1}{2}} \tag{9}$$

for the secondary flow.

The momentum equation, after substitution of Eq. (9), is

$$\frac{p_1}{p_0}\left[1 + \gamma M_1^2\right] - \left[\frac{A_{*s}}{\pi R_1^2}\right]\left[\frac{p_{*s}}{p_{0_s}}\right]\left[\frac{p_{0_s}}{p_0}\right]\gamma_s \cos\phi$$

$$= \frac{p_2}{p_0}\left(\frac{R_2}{R_1}\right)^2\left[1 + \gamma M_2^2\right] + \frac{p_2}{p_0}\left[\frac{A_{2_s}}{A_{*s}}\right]\left[\frac{A_{*s}}{\pi R_1^2}\right]$$

$$+ \left[\frac{A_{2_s}}{A_{*s}}\right]\left[\frac{A_{*s}}{\pi R_1^2}\right]\left[\frac{p_{2_s}}{p_{0_s}}\right]\left[\frac{p_{0_s}}{p_0}\right]\gamma_s M_{2_s}^2 \tag{10}$$

where the primary and secondary streams may be different gases. The area ratio A_{2_s}/A_{*s} is the isentropic area ratio which corresponds to M_{2_s} where M_{2_s} is implied by the assumption that the static pressures in both streams are one and the same ($p_{2_s} = p_2$). This is explained in Appendix B.

The general form of Eq. (7) for the secondary flow ratio is

$$\frac{w_s}{w_{p_0}} = \frac{\frac{A_{*s}}{\pi R_1^2}\left[\frac{\rho_{*s}}{\rho_{0_s}}\right]\left[\frac{\rho_{0_s}}{\rho_0}\right]\left[\frac{T_{*s}}{T_{0_s}}\right]^{\frac{1}{2}}\left[\frac{T_{0_s}}{T_0}\right]^{\frac{1}{2}}\left[\frac{\gamma_s R_s}{\gamma R}\right]^{\frac{1}{2}}}{\left[\frac{\rho_2}{\rho_0}\right] M_2 \left[\frac{T_2}{T_0}\right]^{\frac{1}{2}}} \tag{11}$$

where the primary and secondary gases may be different.

The final assumption of values for $A_{*_s}/\pi R_1^2$ and ϕ as well as the gases involved leads, as in the secondary mixing model, to a final set of simultaneous equations in the unknowns $[R_2/R_1]^2$ and M_1. Appendix A describes the graphical technique used to solve these equations. Typical results are shown in Fig. 1 (taken from Ref. 1) where the comparable Martin vortex sheet model has been added.

3. Secondary Expansion Model

In the secondary expansion model the flow behavior is somewhat different from either of the preceding cases. The secondary flow enters the nozzle in the same way and, as in the sheet flow model, does not mix with the primary stream. However, in the present model the secondary stream expands as it flows downstream, as shown in the sketch below, filling the region between the wall and the primary stream.

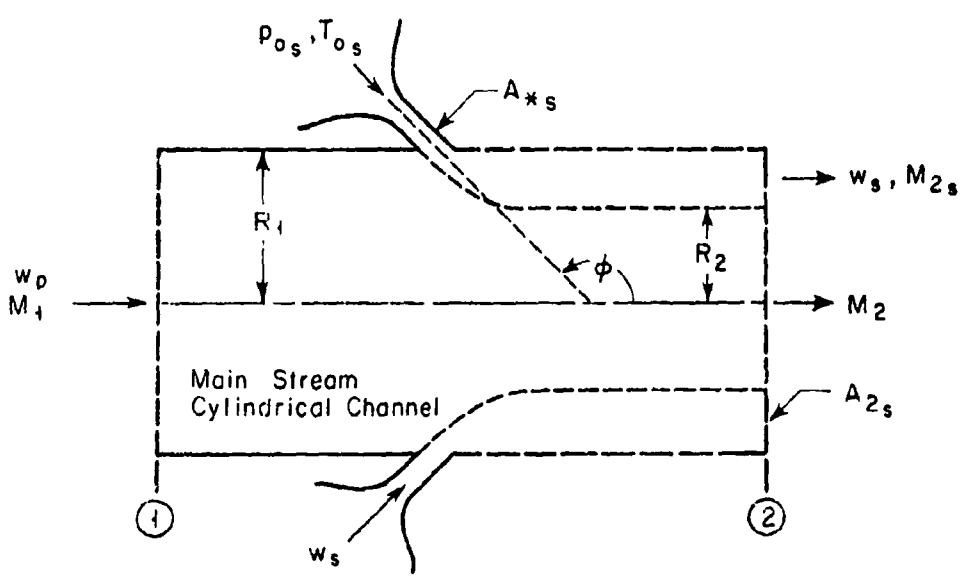

This secondary expansion is isentropic and the Mach number M_{2_s} is given by the area ratio* A_{2_s}/A_{*_s} rather than being implied by the assumption that $p_2 = p_{2_s}$. Thus the secondary expansion model assumes

* See the first part of Appendix B.

that the flow does not separate from the wall.

The continuity equations for the present model are Eqs. (8) and (9) while the momentum equation is

$$\frac{p_1}{p_0}\left[1+\gamma M_1^2\right]-\left[\frac{A_{*_s}}{\pi R_1^2}\right]\left[\frac{p_{*_s}}{p_{0_s}}\right]\left[\frac{p_{0_s}}{p_0}\right]\gamma_s\cos\phi$$

$$=\frac{p_2}{p_0}\left(\frac{R_2}{R_1}\right)^2\left[1+\gamma M_2^2\right]+\left[\frac{p_{2_s}}{p_{0_s}}\right]\left[\frac{p_{0_s}}{p_0}\right]\left[1+\gamma_s M_{2_s}^2\right]\left[1-\left(\frac{R_2}{R_1}\right)^2\right] \tag{12}$$

where trial values of A_{2_s}/A_{*_s} (which determines M_{2_s}) are used according to the iterative procedure explained in Appendix C. Equation (12) takes account of the fact that the primary and secondary gases may not be the same as does Eq. (11) which is the secondary flow ratio appropriate to the present model.

The final specification of problem geometry and primary and secondary gases again yields the simultaneous equations (in unknowns $[R_2/R_1]^2$ and M_1) which were solved by the graphical technique in Appendix A. The results for a typical case are again shown in Fig. 1 (taken from Ref. 1).

B. PHASE I--EXPERIMENT

A series of experiments were performed as part of the Phase I program in which secondary injection was used in an axially symmetric nozzle. A variety of injection configurations were tested with air as the working fluid in both the primary and secondary streams. The objective of these tests was to determine some of the flow throttling and attendant thrust control characteristics peculiar to the injection method. A detailed treatment of this work is reported in Ref. 1 while

a brief summary is presented in this section.

Air for the primary and secondary flows was obtained from auxiliary wind tunnel equipment at the NSL. Flow rate, stagnation pressure, and stagnation temperature were measured in both flows. The primary stagnation pressure was 100 psia in nearly all of the tests and held constant regardless of the amount of primary flow throttling. Model forces were measured directly by means of strain gage balance systems.

The axially symmetric nozzle used in these tests was conical having a subsonic cone semi-vertex angle of 30° and a supersonic cone semi-vertexangle of 15°. The design flow rate was one pound per second with a stagnation pressure of 100 psia and stagnation temperature of 530°R. The exit Mach number of the nozzle, according to the exit-to-throat area ratio, was 2.1. Secondary flow rates varied up to about 0.15 pounds per second corresponding to a secondary stagnation pressure of about 300 psia.

Secondary flow was injected from various orifice configurations. These were usually holes equally spaced around the circumference of the nozzle throat. In one case a slot replaced the holes. Injection angles (ϕ) of 60° and 90° were tested. The circumferential injection angle β was also varied.

Some typical flow throttling data, taken from Ref. 1, is presented in Fig. 2 where it is compared to the results for the sheet flow and secondary expansion models. Configuration F has 32 holes 0.032 inches in diameter while configuration J has a slot 0.020 inches in width. The analytical calculations are based on the assumption that the flow throttling takes place at or near the nozzle throat. Thus the throat area ($0.430\,in^2$) is assumed to be πR_1^2. In addition, since the analytical methods do not contain an orifice coefficient* (C) in the secondary mass flow equation, the area ratio $A_{*_s}/\pi R_1^2$ was replaced, in the analytical calculations, by $CA_{*_s}/\pi R_1^2$. This procedure was adopted, somewhat arbitrarily, so that the theoretical and experimental stagnation pressure ratios (p_{0_s}/p_0) would be about the same for a given w_s/w_{p_0}.

* An approximation to the average value of C was used for each configuration.

The agreement between theory and experiment shown in Fig. 2 is typical of all of the Phase I data*. These models encompassed almost all of the data and this pattern seems reasonable since, in a sense, they are "extremes" of a type of flow behavior. In the sheet flow model the secondary pressure (at station 2 in the analysis) is determined by the primary stream and, since the change in flow direction (120°) is large, the secondary stream is separated from the nozzle wall. In the secondary expansion model, however, the secondary stream expands to fill the area between the primary stream and the wall. In this case the secondary pressure is independent of the adjacent primary value and there is no separated flow region. Some crude Phase I water table observations indicated that both flow configurations exist and, as the air data seems to prove, this may actually be the case.

Thrust control is directly proportional to total nozzle flow with symmetric or asymmetric injection. In over 97 percent of the test runs the nozzle thrust ratio (F/F_0) divided by the total flow ratio $[(w_p + w_s)/w_{p_0}]$ varies between 0.96 and 1.04. This indicates that the exhaust velocity does not change appreciably with injection rate and the flow may behave as though the throttling had been accomplished by an "effective geometric throat".

C. FURTHER ANALYTICAL STUDY--FLOW FIELD ANALOGY

The NSL theoretical models (sheet flow and secondary expansion) seem to correlate the data fairly well. However, due to the extrinsic nature of such analyses (consideration of the flow through a control volume) only a vague picture is acquired of the actual flow field. A next step would seem to be the development of an analysis which gives a clear understanding of the detailed nature of the flow process. An effort has been made to formulate such an analysis of the flow field induced by secondary injection into a supersonic stream.

The water table flow observations, mentioned in connection with the theoretical models, showed that the main nozzle flow with injection

* The experimental uncertainties (for all of the Phase I data) in the flow measurements are ±0.01 in w_p/w_{p_0} and ±0.003 in w_s/w_{p_0}.

resembled the flow past a blunt body. This suggested that if the primary stream does not mix greatly with the secondary stream perhaps the primary flow is analogous to a blunt body flow.

The "flow field analogy" analysis is formulated in two main parts. First, the primary flow field is treated in accordance with the approximate method of Li and Geiger (Ref. 4) for finding the flow field in the stagnation region of a blunt body. Second, the flow field of the secondary stream is formulated in accordance with similar considerations. The two flow fields are then combined according to certain conditions which must hold at the boundary which separates the streams. Since the combined-flow problem is non-linear, a solution must be obtained by approximate numerical methods. Although a solution was not obtained the work accomplished is nevertheless felt to be worthy of mention.

1. Li and Gieger Blunt Body Analysis

Since the analysis of the primary flow field is based on a direct analogy to this method, a review is necessary of the work done by Li and Geiger in Ref. 4. This method, as opposed to other more exact methods, lends itself to simple calculation.

The basic equations of inviscid fluid motion are the starting point of the analysis. Certain assumptions are then made which allow their simplification to a degree where a closed form solution is possible. The solution permits the specification of the flow parameters throughout the stagnation region.

The momentun equations, written in terms of orthogonal curvilinear coordinates, for inviscid flow are

$$u \frac{\partial u}{\partial x} + (1 + Ky) v \frac{\partial u}{\partial y} + Kuv + \frac{1}{\rho} \frac{\partial p}{\partial x} = 0 \qquad (13)$$

$$u \frac{\partial v}{\partial x} + (1 + Ky) v \frac{\partial v}{\partial y} - Ku^2 + \frac{1}{\rho} \frac{\partial p}{\partial y} = 0 \qquad (14)$$

The continuity equation, reduced to two dimensional flow, is

$$\frac{\partial}{\partial x} (\rho u) + \frac{\partial}{\partial y} [(1 + Ky) \rho v] = 0 \qquad (15)$$

The curvilinear coordinate system is shown below where the origin is taken at the stagnation point with y measured normal to the body and x along the body. The parameter K which may be a function of x, is the local curvature

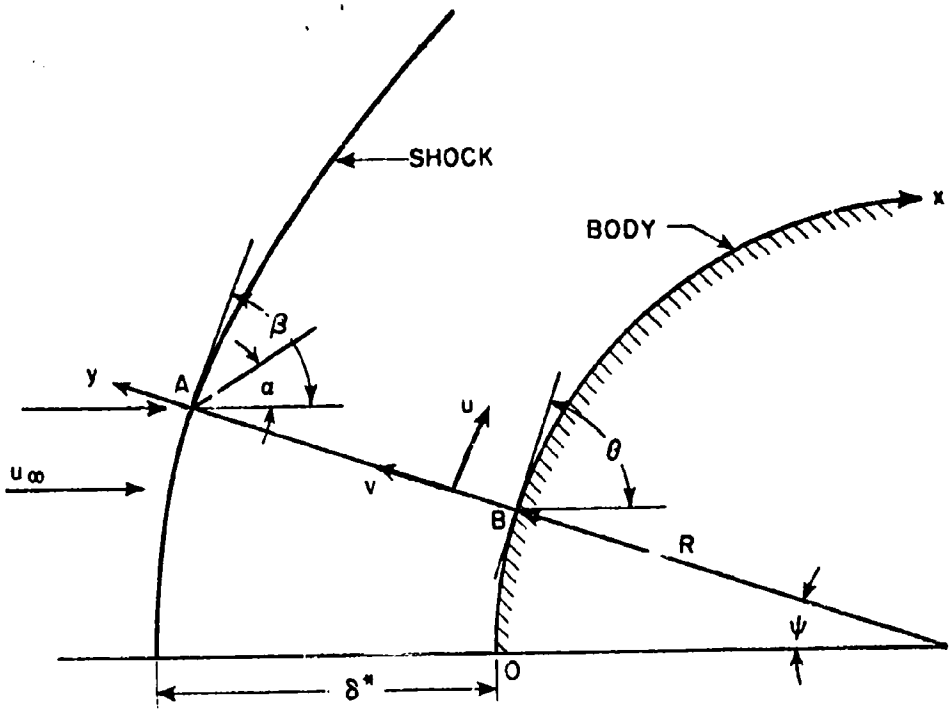

of the body ($K = -d\theta/dx = -1/R_B$).

In the stagnation region of the body Eqs. (13), (14) and (15) may be simplified by use of the following conditions:

1. In the stagnation region u/u_∞, $v/u_\infty = 0(k)$ where k (density ratio across shock) is very small. Thus higher order terms Kuv, Ku^2, etc., can be neglected.
2. Between the shock and body $Ky = 0[\delta/R_B]$ and can be neglected for $\delta/R_B \ll 1$.
3. For $M_\infty > 3$ the Mach number immediately behind the shock rapidly approaches $\sqrt{(\gamma - 1)/2\gamma}$. Thus, the flow field in the

stagnation region may be assumed incompressible $\rho \simeq \rho_2 = \rho_\infty / k$. These simplifications reduce the basic equations, Eqs. (13), (14) and (15) to

$$u\,(\partial u/\partial x) + v\,(\partial u/\partial y) = (-k/\rho_\infty)\,(\partial p/\partial x) \tag{16}$$

$$u\,(\partial v/\partial x) + v\,(\partial v/\partial y) = (-k/\rho_\infty)\,(\partial p/\partial y) \tag{17}$$

$$(\partial u/\partial x) + (\partial v/\partial y) = 0 \tag{18}$$

A solution of these differential equations must be found subject to the following boundary conditions:
at the body $y = 0$, $v = 0$, and at a point A just behind the shock wave

$$y = 5 \qquad u_A = q_A \cos(\theta - \alpha)$$

$$v_A = -q_A \sin(\theta - \alpha) \tag{19}$$

$$q_A = \sqrt{(k u_\infty \sin\beta)^2 + (u_\infty \cos\beta)^2}$$

$$p_A = p_\infty + \rho_\infty u_\infty^2\,(1 - k)\sin^2\beta$$

Also, at the stagnation point ($x = 0$, $y = 0$), $u = v = 0$.

Near the stagnation point it is assumed that

$$u = x f'(y) = x\,(df/dy) \tag{20}$$

It is seen that Eq.(18) is satisfied if

$$v = -f(y) \tag{21}$$

Elimination of the pressure from Eqs. (16) and (17) results in the equation

$$u\,(\partial\omega/\partial x) + v\,(\partial\omega/\partial y) = 0 \tag{22}$$

where the vorticity, ω, is written

$$\omega = (\partial v/\partial x) - (\partial u/\partial y)$$

Equations (20), (21) and (22) yield a total differential equation for f(y) which is

$$f' f'' - f f''' = 0 \tag{23}$$

This is an ordinary third order differential equation which has the general solution

$$f(y) = A_0 \exp(A_2 y) + A_1 \exp(-A_2 y)$$

where the constants of integration A_0, A_1 and A_2 are determined by the boundary conditions. An evaluation of the constants in the region near the stagnation point (i.e., $x_A \to 0$ and A → C on sketch) allows limiting values of the angles to be taken and $\delta \to \delta^*$.

Substitution of the constants into Eqs. (20), (21) and (22) yields the following results:

$$u/u_\infty = (-x/R_s)\sqrt{k(2-k)}\cosh\left\{(y/\delta^*)\sinh^{-1}\left[(1-k)/\sqrt{k(2-k)}\right]\right\} \tag{24}$$

$$v/u_\infty = -k\left[\sqrt{k(2-k)}/(1-k)\right]\sinh\left\{(y/\delta^*)\sinh^{-1}\left[(1-k)/\sqrt{k(2-k)}\right]\right\} \tag{25}$$

$$\omega = (x/\delta^*)(u_\infty/R_s)\sqrt{k(2-k)}\sinh^{-1}\left[(1-k)/\sqrt{k(2-k)}\right]\sinh\left\{(y/\delta^*)\sinh^{-1}\left[(1-k)/\sqrt{k(2-k)}\right]\right\}$$

It is also found as part of the solution that

$$\delta^* = \left[(-kR_s)/(1-k)\right]\sinh^{-1}\left[(1-k)/\sqrt{k(2-k)}\right] \tag{26}$$

and

$$C_p = (2-k)\left[1-(x/R_s)^2\right] \tag{27}$$

Equations (24), (25), (26) and (27) yield simple determination of any of the flow variables in the stagnation region of a blunt body in hypersonic flow.

Although the assumptions made hold only near the stagnation point in hypersonic flow (i.e., $K \ll 1$), the theory gives a good

approximation to pressure and velocity data for stream Mach numbers as low as 2.0. Also, the approximate theoretical limit of the theory is at an angular position $\psi = 6°$; however, good results are obtained for values of ψ up to about 30°.

2. Primary Flow Field

The flow field of the primary stream may be considered directly analogous to the blunt body problem for injection normal to a supersonic stream. This analogy is based on the assumption that no mixing occurs between the primary and secondary streams. In this case there is some boundary separating the streams. Restricting the problem to two dimensions, the boundary may be considered analogous to the wall of a cylinder. The primary flow field is then analogous to the flow past a cylinder. A comparison of the sketches below makes the analogy clear.

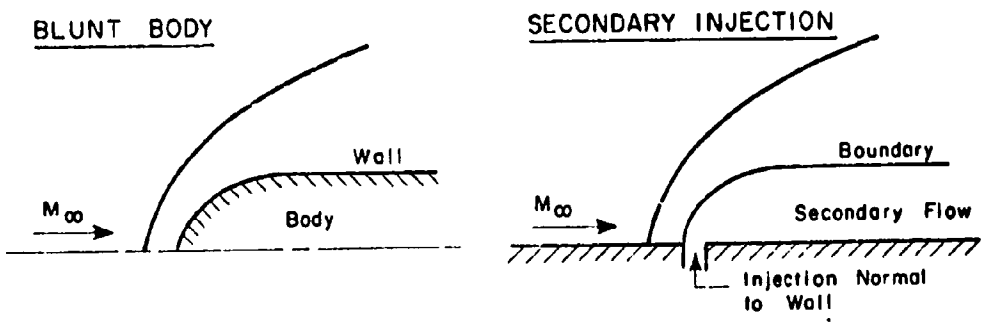

Figure 3 is a schlieren photograph of injection into the supersonic portion of a nozzle at an angle 60° upstream of the normal to the wall. Although the photograph does not seem to substantiate the sketch shown above, an explanation is apparent. The analogy assumes inviscid flow whereas in reality the viscous fluid boundary layer permits disturbances to be transmitted upstream along the wall. The disturbances separate the boundary layer from the surface causing an oblique shock to emanate from the point where separation occurs.

Closer examination of the photograph, however, reveals a curved shock formation (arrow in Fig. 3) which would be present for a blunt body in low Mach number supersonic flow. Therefore, Fig. 3 may be regarded as lending some support to the blunt body analogy.

Equations (24), (25), (26) and (27) of the previous section yield values for all the primary flow variables in the region corresponding to the stagnation region of the blunt body once the free stream Mach number and shape of the secondary flow region are specified. The criteria for this specification are discussed below under the heading of Combined Flow Field.

3. Secondary Flow Field

The secondary flow field is contained within the region occupied by the body in the blunt body problem and is, in fact, the blunt body of the analogy. Thus the problem consists of trying to find a flow field to occupy the region marked secondary flow in the sketch on page 19. Only one possible flow field will be discussed here.

Consider the following sketch of a secondary flow.

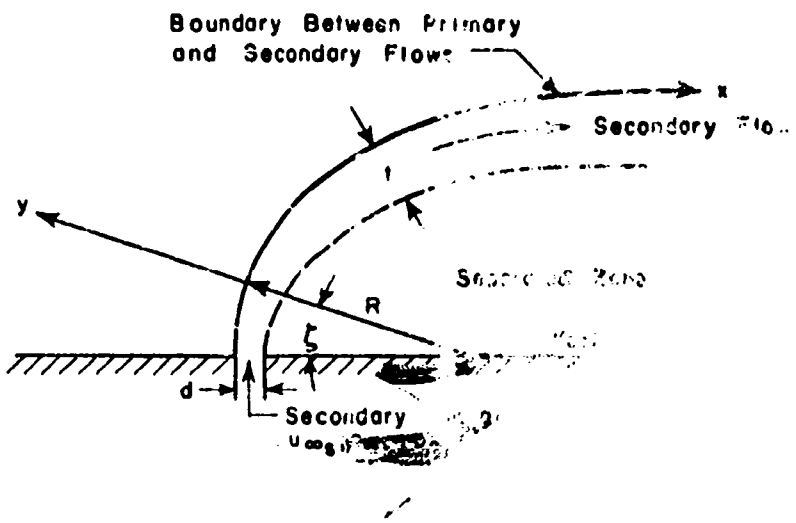

The secondary flow is injected through a slot of width d with velocity u_{∞_s}, pressure p_{∞_s}, and density ρ_{∞_s}. It is assumed that the secondary flow

A further assumption is now made that the secondary stream is a perfect gas in isentropic flow. This permits the use of the pressure-density relation

$$p = \text{const}\ \rho^{\gamma} \tag{36}$$

With this assumption the pressure and density may be eliminated from Eqs. (28) and (29) by cross differentiation to yield:

$$\left(\frac{\partial u}{\partial y}\right)\left(\frac{\partial u}{\partial x}\right) + u\,\frac{\partial^2 u}{\partial x \partial y} + \left(\frac{\partial v}{\partial y}\right)\left(\frac{\partial u}{\partial y}\right) + v\,\frac{\partial^2 u}{\partial y^2} + Ku\,\frac{\partial v}{\partial y} + kv\,\frac{\partial u}{\partial y}$$

$$-\left(\frac{\partial u}{\partial x}\right)\left(\frac{\partial v}{\partial x}\right) - u\,\frac{\partial^2 v}{\partial x^2} - \left(\frac{\partial v}{\partial x}\right)\left(\frac{\partial v}{\partial y}\right) - v\,\frac{\partial^2 v}{\partial x \partial y} + u^2\,\frac{\partial K}{\partial x} + 2Ku\,\frac{\partial u}{\partial x} = 0 \tag{37}$$

where K is considered to be a function of x. Combining Eqs. (33), (34) and (37) yields a total differential equation for K and f(x) which is

$$y(ff''' - f'f'') + K'f^2 + Kff' = 0 \tag{38}$$

where the primes denote differentiation with respect to x. It should be noted that Eq. (38) is similar to Eq. (23) obtained by Li and Gieger except for the terms containing K and its derivative. These terms arise from the fact that v/u_{∞_s} and u/u_{∞_s} are not necessarily small compared to unity. In order to solve Eq. (38) various K functions have to be assumed and the corresponding f functions determined numerically.

4. Combined Flow Field

The remaining boundary conditions on the secondary flow field are imposed when the flows are combined. Since the steady state problem must be in equilibrium, it is necessary that the static pressures of the primary and secondary streams match across the boundary. For any particular K(x) the pressure on the boundary exerted by the primary flow is specified when the values of p_∞, ρ_∞, and u_∞ are known in the primary flow. For the particular K(x) chosen the function f(x) is determined and therefore the pressure of the secondary flow on the boundary.

fills only a portion of the region between the wall and the boundary separating the primary and secondary flows. The remainder of the region is a separate zone. It is also assumed $t/R_B \ll 1$ so that $ky = 0(t/R_B)$ may be neglected. However, u/u_∞ and v/v_∞ may not be neglected in the secondary flow as they were in the primary flow.

Equations (13) (14) and (15) are simplified by the assumptions made above and may be written as follows:

$$\rho u(\partial u/\partial x) + \rho v(\partial u/\partial y) + Kuv = -\frac{1}{\rho}\frac{\partial p}{\partial x} \tag{28}$$

$$\rho u(\partial v/\partial x) + \rho v(\partial v/\partial y) - Ku^2 = -\frac{1}{\rho}\frac{\partial p}{\partial y} \tag{29}$$

$$\partial(\rho u)/\partial x + \partial(\rho v)/\partial y = 0 \tag{30}$$

These differential equations must be solved to yield solutions subject to certain boundary conditions. Two of the required boundary conditions arise from the geometry of the sketch and are as follows.

The tangency condition at the boundary between the primary and secondary streams

$$y = 0, \quad v = 0 \tag{31}$$

and the conditions at the injection port

$$x = 0, \quad u = u_\infty \qquad d < y < 0 \tag{32}$$

The remaining boundary conditions are discussed when the flow fields are combined in the next section.

In the thin region of secondary flow, it may be assumed that

$$u = f(x) \tag{33}$$

$$v = -yf'(x) = -y(df/dx) \tag{34}$$

The continuity equation, Eq. (30) is satisfied if

$$\rho = \rho_\infty + yf \tag{35}$$

The choice of the particular form of v satisfies Eq. (31).

A further assumption is now made that the secondary stream is a perfect gas in isentropic flow. This permits the use of the pressure-density relation

$$p = \text{const}\ \rho^{\gamma} \tag{36}$$

With this assumption the pressure and density may be eliminated from Eqs. (28) and (29) by cross differentiation to yield:

$$\left(\frac{\partial u}{\partial y}\right)\left(\frac{\partial u}{\partial x}\right) + u\,\frac{\partial^2 u}{\partial x \partial y} + \left(\frac{\partial v}{\partial y}\right)\left(\frac{\partial u}{\partial y}\right) + v\,\frac{\partial^2 u}{\partial y^2} + K u\,\frac{\partial v}{\partial y} + k v\,\frac{\partial u}{\partial y}$$

$$- \left(\frac{\partial u}{\partial x}\right)\left(\frac{\partial v}{\partial x}\right) - u\,\frac{\partial^2 v}{\partial x^2} - \left(\frac{\partial v}{\partial x}\right)\left(\frac{\partial v}{\partial y}\right) - v\,\frac{\partial^2 v}{\partial x \partial y} + u^2\,\frac{\partial K}{\partial x} + 2Ku\,\frac{\partial u}{\partial x} = 0 \tag{37}$$

where K is considered to be a function of x. Combining Eqs. (33), (34) and (37) yields a total differential equation for K and f(x) which is

$$y(ff''' - f' f'') + K' f^2 + Kff' = 0 \tag{38}$$

where the primes denote differentiation with respect to x. It should be noted that Eq. (38) is similar to Eq. (23) obtained by Li and Gieger except for the terms containing K and its derivative. These terms arise from the fact that v/u_{∞_s} and u/u_{∞_s} are not necessarily small compared to unity. In order to solve Eq. (38) various K functions have to be assumed and the corresponding f functions determined numerically.

4. Combined Flow Field

The remaining boundary conditions on the secondary flow field are imposed when the flows are combined. Since the steady state problem must be in equilibrium, it is necessary that the static pressures of the primary and secondary streams match across the boundary. For any particular K(x) the pressure on the boundary exerted by the primary flow is specified when the values of p_∞, ρ_∞, and u_∞ are known in the primary flow. For the particular K(x) chosen the function f(x) is determined and therefore the pressure of the secondary flow on the boundary.

Since a numerical solution was not obtained, it is not known whether an exact pressure match across the boundary is possible by varying K(x). At best it would seem that an approximate pressure match over some portion of the boundary would have to be met by this approach.

The secondary stream pressure on the boundary as a function of x is determined by the relation

$$p_s = p_{\infty s} + \int_y^{\cdot 0} \frac{\rho_s u^2}{r} \tag{39}$$

where

$$r = y - R = y + \frac{1}{K} = \frac{Ky + 1}{K}$$

thus

$$p_s = p_{\infty s} + \int_y^{\cdot 0} \frac{\rho_s (Ky + 1)}{K} u^2 \, dy \tag{40}$$

The lower limit of the integral in Eq. (40) is the value of y on the interface between the secondary flow and the separated region for a particular value of x. The interface is the path followed by a particle being injected from the edge of the slot y = - d.

The analogy is limited to small values of the angle ψ due to the fact that the analysis of Li and Geiger is valid only near the stagnation point of a blunt body. However, the analogy might be useful as a means of examining a portion of the flow field generated by secondary injection normal to a supersonic stream.

D. FURTHER ANALYTICAL RESULTS-NSL FLOW MODELS

The Phase I data corroborated the sheet flow and secondary expansion models to an encouraging extent. However, all of the data corresponds to the case of secondary air injection into a primary stream which is also air. In addition, the ratio of primary to secondary stagnation temperature was approximately unity. The range of the experimental data obviously does not provide exhaustive coverage of the variables but it should also be noted that this was not the intention of the investigation. Nevertheless, in spite of a lack of data, some attention was given to the effects of differences in gas and temperature

between the primary and secondary streams. This work is based on calculations in which temperature and gas effects were studied to determine their effect on flow throttling.

1. Temperature Effect

The effect of temperature has been studied through the use of the ratio of secondary-to-primary stagnation temperatures. It has been found that this temperature ratio plays an important part in the effectiveness of secondary injection as a means of flow control. The following discussion concerns the stagnation temperature ratio effect on flow throttling performance as predicted by the sheet flow and secondary expansion models. It should be noted that no change has been made in the analyses to account for heat transfer between the primary and secondary streams. In view of the nature of the flow models, in which the two streams flow without mixing, this seems a satisfactory approach for a first approximation.

The continuity and momentum equations for the sheet flow and secondary expansion models are given by Eqs. (8), (9), (10) and (12). The stagnation temperature ratio does not appear in any of these equations. Thus, flow throttling performance is specified for a given secondary-to-primary stagnation pressure ratio. This means that the temperature ratio effect is felt only through the expression for the secondary flow ratio. In particular, examination of the secondary flow ratio (Eq. (11)) shows that it varies inversely with the square root of the secondary-to-primary stagnation temperature ratio. This variation is illustrated by the results shown in Fig. 4 where flow throttling performance is given for a typical configuration. Although this is the somewhat ideal case of air injection into an air stream, the trend is nevertheless clear regarding the decreasing effectiveness of injection as the stagnation temperature ratio decreases. Furthermore, at a temperature ratio of 0.2 the level of constant total flow is being approached wherein the thrust remains approximately constant. Morover, this flow throttling behavior is discouraging in view of the fact that in a real application a practical value of the temperature ratio would probably

be less than unity.

At present there is no flow throttling data available for the case of injection at the throat in which the stagnation temperature ratio differs significantly from unity. Rocketdyne reported in Ref. 5 that secondary injection just upstream of the throat at a stagnation temperature ratio of 0.25 did not throttle the primary flow. This seems to disagree somewhat (although not greatly) with the trend predicted by the NSL flow models. However, the low secondary flow rates (w_s/w_{p_0} up to a maximum of 0.04) and subsonic injection associated with the Rocketdyne tests are of sufficient importance to account for the discrepancy.

It should be mentioned that UAC (Ref. 6) found the effectiveness of vector control by injection to vary with the square root of the secondary-to-primary stagnation temperature ratio. Furthermore, the form of this dependence is the same as that of the NSL flow models. That is, performance (some measure of side force) as a function of secondary flow varies in the same manner as flow throttling. Thus, there is some support (admittedly meager) for the effect of temperature given by the NSL models. However, until conclusive flow throttling data is available the predictions of the effect of temperature must be regarded as unsubstantiated.

2. Injection Gas Effect

The generalized form of the continuity, momentum, and secondary flow equations for the sheet flow and secondary expansion models permits the variation of the gases in the primary and secondary streams. Examination of these equations reveals that a low ratio of specific heats and low molecular weight are desirable properties for the secondary gas. That this is indeed the case is shown by the flow throttling results in Fig. 5. Helium injection into air is shown for a typical configuration*. Several stagnation temperature ratios are considered and the results for air injection are shown for comparison. Helium injection** obviously makes

*The curves shown for helium, like those for air, start at the point where secondary injection becomes sonic, as explained in the last paragraph on page 8.

**Although helium has a high γ, its low molecular weight makes it a good injectant since the effect of molecular weight is stronger than that of γ.

n difference in flow throttling performance being a good deal better than air injection. In spite of such encouraging results, there is, once again, no data to support or deny these predictions.

3. Combustion Effect

The effect of combustion has been very crudely estimated for the sheet flow and secondary expansion models. This was done by substituting real engine values of the specific heat ratio and molecular weight (gas constant) for the primary stream in the appropriate equations. The results are shown in Fig. 6 where flow throttling is given for several cases*. Helium injection into hydrogen peroxide and hydrazine or liquid oxygen and gasoline is not as good as helium injection into air. A stagnation temperature ratio of 0.2 was chosen since this corresponds to a case where helium at 1200°R might be injected into a 6000°R chamber. In spite of the decrease in effectiveness due to the combustion gas parameters (and low injection temperature), helium injection still shows some potential for flow throttling. A mentioned before, no data is available for comparison.

E. PHASE II -- TWO-DIMENSIONAL NOZZLE TESTS

The Phase II portion of the NSL program was a study of secondary injection into two-dimensional nozzles. One objective of the tests involved was to determine the effect on flow throttling of various parameters whose importance had not been thoroughly established by the Phase I experiments. These parameters were injection angle, nozzle throat region pressure gradient, and nozzle pressure ratio. The other objective was to gain some understanding of the basic nature of the flow throttling process through schlieren photography. Schlieren flow observations were made through glass windows which formed the major portion of the nozzle sidewalls.

---

*See first footnote on page 25.

The first part of this section describes the model and test conditions. The remainder is a presentation and discussion of the data. The vector control aspect of the Phase II study is presented in a subsequent section.

1. Model Details and Test Conditions

a. Air Supply System

The schematic diagram of Fig. 7 shows the supply system for both the primary and secondary air. Chicago Pneumatic Compressors pumped the imary air through a drier into three storage tanks denoted in the diagram as receivers. A main control valve throttled the air as it entered a surge tank before passing to the primary flowmeters. The flowmeters were used to measure the primary mass flow of air through the model. From the flowmeters the air flowed to a settling chamber at the model. Auxiliary vacuum pumps exhausted the nozzle flow after it passed through a diffuser. A thermocouple and pressure gage located in the settling chamber were used to measure the primary stream stagnation conditions. The main control valve was operated so as to maintain a constant stagnation pressure irrespective of the amount of primary flow throttling. Stagnation pressures of 40, 50, 60 and 70 psia were used during these tests.

Secondary air for these experiments was obtained from an Ingersoll-Rand compressor which pumped air into 3000psia storage tanks. This system supplies air at a working pressure of 600 psia. The mass flow rate of secondary air was measured by an orifice plate in combination with pressure measurements upstream and downstream of the orifice. A manually operated control valve was used to regulate the secondary air flow to obtain a desired stagnation pressure. A 3000 psia Heise pressure gage was used to measure the secondary stagnation pressure in the model settling chambers. The secondary stagnation temperature was obtained by thermocouple as in the primary flow.

b. Model Arrangement

The model was arranged approximately as it is shown in the schematic diagram of Fig. 7. Since no forces were being measured directly, the model was mounted rigidly in place.

c. Nozzle Design

Three nozzles were tested in the Phase II experiments. The first one tested was conical, as shown in Fig. 8, and it was found that a shock pattern originated from overexpansion at the throat. Since this shock pattern interferred with flow observations, the remaining two nozzles were designed for essentially shock-free flow. These nozzles were designed mainly to have widely different throat-region pressure gradients. The "high" and "low" throat-region pressure gradient nozzle contours are shown in Figs. 9 and 10, respectively. The high pressure gradient is four times greater than the low one and, incidentally, the pressure gradient of the nozzle in Fig. 8 is 5.5 times that of Fig. 10 (low one). The nozzle in Fig. 10 is a portion of the contour of the Mach number 3.5 main NSL wind tunnel nozzle blocks (Ref. 7) whereas the nozzle of Fig. 9 was designed according to the method of Ref. 8. Aside from the throat-region pressure gradient, the only difference in nozzles is the exit-to-throat area ratio (which determines the exit Mach number). The exit-to-throat area ratios (and exit Mach numbers) for the nozzles in Figs. 8, 9, and 10 are 5.38 (M = 3.25), 4.34 (M = 3.02), and 2.89 (M = 2.60), respectively. All three nozzles were designed for a mass flow of 2 pounds per second at a stagnation pressure of 70 psia and a stagnation temperature of 530°R.

The contoured nozzles were designed to accommodate interchangeable injection-section inserts at the throat and in the supersonic portion of the nozzle in Fig. 10. Injection angle was varied through the use of different sets of inserts all of the important features of which are shown by the one in Fig. 11.

Each nozzle was instrumented with a number of static pressure taps along the middle of the nozzle surface. The pressure tap locations are shown approximately by the ticks on the nozzle contours in Figs. 8, 9, and 10. Other pressure taps were used to measure the stagnation pressure upstream and diffuser pressure downstream of the nozzle.

The windows, which were an integral part of the nozzle sidewalls, were 1.25 inches thick with optically flat ground surfaces. The window diameter of 8 inches (see Figs. 8, 9, and 10) permitted flow observation through most of the nozzle.

d. Injection Configurations

The nozzle and injection configurations tested are listed in the table below. In all cases the nozzle throat was 1.5" in height by 0.8" in width. The injection slot extended the width of the nozzle and was 0.08" in the nozzle-axis direction measured normal to the injection slot axis (see Fig. 11).

Configuration*	Nozzle	ϕ(deg)	p_0 (psia)
N	45° convergent 25° divergent	60	40, 50, 60, 70
P	10° convergent 25° divergent	60	70
Q	high pressure gradient contoured	60	40, 50, 60, 70
R	same as Q	30	40, 50, 60, 70
S	low pressure gradient contoured	60	50, 70
T	same as S	45	50, 70
U	same as S	30	50, 70
V	same as S	75	50, 60
	Injection at the inflection point in the divergent portion of the nozzle.		
W	same as S	45	40, 50, 60
	Injection at the inflection point in the divergent portion of the nozzle.		

* Unless otherwise specified all injection locations are at the nozzle throat. The injection angle is the angle included between the primary nozzle axis and the axis of injection. The configurations listed are all two dimensional.

Asymmetric injection data was obtained for each of the configurations listed by simply cutting off the air supply to one of the injection slots. The subscript s is used to denote an asymmetric configuration (for example V_s).

2. Influence of Test Parameters

The primary objective of the two-dimensional tests was, as mentioned before, to determine the effects of certain parameters on flow throttling performance. These parameters were injection angle, throat-region pressure gradient, and injection station and their influence on flow throttling is discussed in this section.

Although the Phase I test results showed that nozzle pressure ratio was not an important parameter, a check on this was made in the Phase II tests. As shown in the configuration list of the previous section, several primary stagnation pressure levels were tested for most models. The data shown in Figs. 12, 13 and 14 is typical of all of the data as regards the effect of primary stagnation pressure.* The flow throttling results for configurations Q, R, and S are plotted in the form of primary and secondary flow ratios normalized by the appropriate value of unrestricted primary flow. It is evident from the data in Figs. 12 and 13 that there is no effect of primary stagnation pressure on the flow throttling of configurations Q and R. There is a slight effect observable in Fig. 14 where the data of configuration S indicates that flow throttling is increased by a decrease in p_0 from 70 to 50 psia. The effect is small, however, and agrees with the trend reported in Ref. 9 which is discussed further in Ref. 1. It is sufficient to state here that the primary stagnation pressure does not affect flow throttling if the overall nozzle pressure-ratio and/or the throat-region pressure gradient are sufficiently large.

a. Injection Angle

The effect of injection angle (ϕ) on flow throttling was measured with the high and low pressure gradient nozzles. The flow throttling data for corresponding configurations is typified by that shown in Figs. 15 and 16. The data in these figures corresponds to injection at the nozzle throat. Flow throttling increases with decreasing injection angle and is evidently independent of nozzle throat-region pressure

*The experimental uncertainties in the flow measurements of the Phase II tests are ±0.01 in w_p/w_{p_0} and ±0.005 in w_s/w_{p_0}.

gradient. In addition, the data in Fig. 16 indicates that the increase in throttling becomes smaller as injection angle decreases. Both of these trends substantiate qualitatively the analytical results. In the analytical models decreasing injection angle means that the axial component of injection momentum is increasing as indicated by the cos ϕ in Eqs. 6, 10 and 12. Increases in this injection stream momentum decrease the primary flow ratio (increase flow throttling). Furthermore, since this momentum varies as cos ϕ flow throttling increases should become smaller as ϕ becomes smaller. Quantitative support of the theoretical ϕ effect is not possible in view of the uncertainty in the data; however, it is believed that the data does indicate a physically correct analytical representation.

Injection into a nozzle at a station where the flow is supersonic will obviously not throttle the flow until the secondary flow is large. This is so not only because the primary stream has more momentum at a supersonic station but also because the secondary stream expands downstream more rapidly due to the increasing area in that direction. The data shown in Fig. 17 for supersonic station injection into the low pressure gradient nozzle shows the large secondary flow required for choking. It is perhaps obvious that this data also points out that flow throttling should be controlled at the nozzle throat. Also apparent in Fig. 17 is the fact that injection angle partially determines the secondary flow rate for choking. Finally, once the nozzle is choked primary flow throttling varies with secondary flow as though injection were at the throat (which, in effect, it is).

b. Pressure Gradient

Nozzle throat-region pressure gradient was investigated as a factor which might partially determine the secondary flow necessary to separate the primary flow and achieve a given amount of throttling. Typical pressure distributions for the high and low pressure gradient nozzles are shown in Figs. 18 and 19. As mentioned before, the throat-region pressure gradients are in the ratio of about 4 to 1. The pressure distributions which correspond to flow with secondary injection are discussed in connection with flow observations in a later section.

The effect of pressure gradient on flow throttling is illustrated in Figs. 20 and 21 for the injection angles of 30° and 60°. The effect is apparently small and independent of injection angle. A decrease in throat-region pressure gradient produces an increase in flow throttling and this change in throttling is very slightly attenuated by increasing stagnation pressure (p_0).

The small increase in flow throttling which results from a reduction in pressure gradient may be explained by the fact that the primary stream is actually not sensitive to nozzle contour once there is a large secondary flow. That is, large secondary flow generates an effective throat which throttles the primary flow and changes its path considerably. Since the secondary flow thus provides an effective or "fluid" nozzle, the primary flow does not feel the wall directly. Therefore, the "pressure gradient" influence is actually a geometry one in which the effective ("fluid") nozzle is partially determined by the physical nozzle throat.

c. Injection Station

The influence of injection station was mentioned in part above but will be reviewed here for clarity and completeness. The data in Fig. 17 shows that primary flow throttling does not take place until the nozzle is choked by secondary injection. This indicates further that the nozzle throat is the station at which throttling should be most efficient (require the least secondary flow). The data also indicates that throttling is the same function of secondary flow once the nozzle is choked. This again indicates injection should be at the throat since that avoids the need for the additional secondary flow required for choking.

d. Thrust Control

In a conventional nozzle the thrust is directly proportional to the product of mass flow and exit velocity. The thrust of a nozzle being throttled by secondary injection has similarly been found to be proportional to the total (secondary plus primary) flow (Refs. 1 and 9). The Phase II test data also agrees with this result as described on the following page.

The value of a thrust parameter, defined in Ref. 1 as

$$\frac{\frac{F}{F_0}}{\frac{w_p + w_s}{w_{p_0}}}$$

was calculated for a large sample of the Phase II tests. The thrusts F and F_0 correspond to the flow rates w_p+w_s and w_{p_0}, respectively, and were calculated from pressure integrations together with estimates of axial-component jet reaction forces (of the secondary flow). All of the thrust parameter values fell between 0.98 and 1.07 and the sampling included asymmetric as well as symmetric injection. This range agrees closely with the corresponding one for the Phase I tests (Ref. 1) in which the values fell between 0.96 and 1.04.

The variation of the thrust ratio* (F/F_0) and total flow ratio ($w_p+ w_s/w_{p_0}$) are shown as a function of secondary flow in Figs. 22 and 23. The data in Fig. 22 shows that results are independent of stagnation pressure (p_0), an observation common to all configurations. Also evident is the fact that thrust is related to total nozzle flow by a constant. This is not so, however, for the configurations of Fig. 23 where the proportionality varies with secondary flow. These results are typical of the other low pressure gradient nozzle and side injection configurations whereas those of Fig. 22 are typical of the high pressure gradient nozzle configurations. It is apparent in Fig. 23 that the total flow decreases faster than the thrust as secondary flow increases, a result which is opposite to the trend observed in the Phase I tests (Ref. 1). There are two obvious possible factors involved in this discrepancy. First, the Phase I tests concerned an axially symmetric nozzle while the present nozzles are two-dimensional. Second, the proportionality (between thrust and total flow) varies with secondary flow only in configurations where the nozzle does not expand to a high exit-to-throat area ratio except for two-dimensional side injection. Thus, nozzle geometry and

*The experimental uncertainty in F/F_0 is ± 0.015

expansion ratio are possibly of some importance*. It is believed that nozzle geometry is the key factor, at least qualitatively, but the quantitative nature of the data makes it inconclusive.

3. Flow Observations

One of the main purposes of using two-dimensional nozzles in the Phase II tests was to permit the use of schlieren photography. It was felt that extensive flow observations would reveal the nature of the throttling process. Although the analytical model assumptions were formulated primarily on the basis of intuition, Phase I data indicated that the assumptions were sound. The schlieren photographs discussed in this section further afford visual substantiation to the throttling analysis.

The flow patterns associated with various rates of secondary injection are shown in Fig. 24. This series of photographs concerns the high pressure gradient nozzle (configuration Q). The wide disturbance at the throat in Fig. 24a is due to the injection slot while the narrow one just upstream emanates from the insert joint (see Fig. 9). The weak shock wave downstream of the throat is caused by some slight overexpansion in the throat region. In Fig. 24b the overexpansion must have increased with injection since the resultant shock wave is stronger. The secondary flow evidently diffuses without separation since the overexpansion shock proceeds to the nozzle wall. The density gradient in the secondary injection vicinity is so strong that flow details are obscured. In Fig. 24c, however, new flow features become apparent with a higher secondary flow rate. The primary flow moves at low velocity upstream of injection as indicated by the faint circular waves which propagate from the injection slots. A thick boundary layer is apparent just downstream of injection and the overexpansion shock waves have increased in intensity. Figs. 24d and 24e make the subsonic region waves more evident and show even stronger overexpansion shock waves. More important, however, these photographs show clearly the features of a flow which is a combination of mixing, sheet flow, and secondary expan-

*It should be noted that in all cases injection effects extend only a short distance downstream of the injection station as shown in Figs. 18 and 19. Thrust variation with injection in the supersonic portion of the nozzle is thus tied strongly to geometry and expansion ratio.

sion. The flow configuration appears to be arranged as shown in the sketch below.

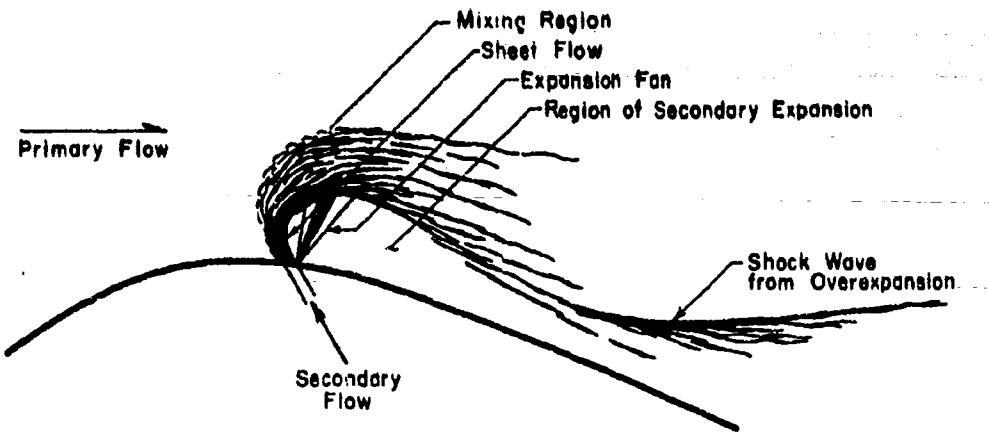

All of these details are quite apparent in Figs. 24d and 24e and the flow configuration as a whole substantiates the basic nature of the throttling analysis.

The schlieren photograph in Fig. 25 shows a typical flow field produced by injection at the throat in the low pressure gradient nozzle. The higher pressures of this flow can be seen to change the angles of the overexpansion shock wave compared to those in Fig. 24d. Higher pressure is also responsible for the fact that the expansion fan does not extend very far downstream. It is quite evident, however, that the flow pattern is basically the same as that in Fig. 24 and the configuration sketched above.

The series of schlieren photographs shown in Fig. 26 correspond to injection into the supersonic portion of the low pressure gradient nozzle. Flow separation upstream of the injection station is quite apparent along with the shear layer which bounds the separated region. After the p_{0_s}/p_e ratio exceeds unity the flow just downstream of the injection station becomes sonic. Finally, secondary flow chokes the nozzle and

moves the effective throat to the injection location where the flow is being throttled. This final flow pattern (Fig. 26e) is easily recognized as the same as that in Figs. 24e and 25.

Typical pressure distributions along the nozzle contour are shown in Figs. 18 and 19 for the high and low pressure gradient nozzles with secondary injection. These pressure distributions may be compared to the schlieren photographs in Figs. 24d and 25. This comparison shows agreement in revealing the essentially stagnant region upstream of injection and low pressure expansion just downstream. Furthermore, it is evident that downstream of the overexpansion shock wave the pressure distribution is not very different from that in the nozzle without injection.

It should be noted that an important assumption in the theoretical models is borne out by the schlieren photographs of Figs. 24, 25, and 26. This assumption is that the flow throttling process occurs in a short axial distance and thus may be treated as taking place in a constant area duct. The flow observations as well as the pressure distributions in Figs. 18 and 19 make it apparent that this is approximately the case.

In summary, it may be said that the flow observations substantiate the analytical models in that all three (mixing, sheet flow, expansion) types of flow are present. It is not possible to obtain a quantitative measure of the extent of each from the schlierens but relative density gradients* indicate that, qualitatively speaking, the sheet flow is the dominant type. This seems to agree with the general trend of the throttling data.

F. CORRELATION OF NSL EXPERIMENTAL RESULTS

In this section the Phase II data is compared to the results given by the analytical flow models. This correlation is discussed further in light of the Phase II flow observations.

---

*It can be seen, for example, that in Figs. 24d and 24e that the sheet flow portion is black, rather than one black and one white on both the upper and lower injection flows in the schlieren. This only occurs when the density gradient is so strong that light deflection becomes excessive (white areas become black).

Some Phase I results are compared to those of Plase II and both are compared to available data from other sources.

1. Phase II Data Compared to Analytical Results

The flow throttling of Phase II configurations N, Q, R, S, and U was calculated for the secondary mixing, sheet flow, and secondary expansion theoretical models. In the calculations, as explained on page 13, the ratio of injection throat area to nozzle throat area* is multiplied by an orifice coefficient C so that the theoretical and experimental stagnation pressure ratios (p_{0_s}/p_0) are approximately the same. The experimental data and analytical results are shown in Figs. 27 through 31. It is evident that the data falls primarily between the sheet flow and secondary mixing curves. It was noted in the preceding section, however, that all three types of flow are present according to schlieren observations. Nevertheless, an explanation cannot be given for how the flows are quantitatively proportioned to yield the experimental throttling results. It is very probable that the proportions are somewhat different for two- and three-dimensional flows. This is so because, in contrast to the two-dimensional data, the three-dimensional results fall between the theoretical curves for the sheet flow and secondary expansion models. The situation is further complicated by the fact that the flow type proportions may change with injection rate. In any event, it may be said that a qualitative grasp is within reach with the analytical models giving reasonably good correlation.

2. Comparison of Phase I and Phase II Data

All of the Phase I and Phase II flow throttling data for an injection angle of 60° has been represented by "average" curves in Fig. 32. The averaging process consisted of fairing a curve by eye on a plot which displayed all of the data. It is evident from the curves that three-dimensional throttling is consistently more effective than that in the two-dimensional case. However, the discrepancy diminishes with increasing injection rate beyond a secondary flow ratio of 0.06. In

*In the Phase II two-dimensional case, this ratio is 2b/d where b is the slot height (0.08", see Fig. 11) and d is the nozzle throat height (1.5").

spite of the apparent difference, the general character of flow throttling is the same in two- and three-dimensional flow.

The obvious factor which may at least partially explain the difference in flow throttling behavior is the basic difference between two- and three-dimensional flow. That is, the injection arrangement in the three-dimensional case may yield a better distribution of secondary flow in which losses are smaller. Thus, the secondary flow may be more efficiently utilized for absorbing primary stream momentum and throttling the primary flow.

Another factor which may contribute to the difference was mentioned before and is the proportion of secondary mixing, sheet flow, and secondary expansion. It seems reasonable that different proportions might be associated with two- and three-dimensional flows.

A small part of the difference in flow throttling might be due to the effect of injection-to-nozzle throat area ratio (A_{*_s}/A_{*}). In the two-dimensional case this ratio was about twice that in the three-dimensional one. The results in Ref. 9 showed that flow throttling tends to be more effective at lower injection-to-nozzle throat area ratio. However, this effect is not pronounced at high overall nozzle pressure ratios and in the present instance could be only a minor part of the difference between two- and three-dimensional throttling.

3. Comparison of NSL and Other Data

Comparative flow throttling data obtained by Rocketdyne (Ref. 5) and the NASA (Ref. 10) are shown with some NSL Phase I data in Fig. 33. The injection angle of 90° is common to all three configurations although the Rocketdyne data corresponds to asymmetrical injection. The Rocketdyne data would have shown very slightly more effective flow throttling had injection been symmetrical. In view of experimental uncertainties it is evident that the agreement between the various data is good. All of the configurations in question are three-dimensional.

SECTION III

THRUST VECTOR CONTROL

The majority of studies of secondary injection have been concerned with the use of this method as a means of obtaining thrust vector control. In the Phase I work done by the NSL, asymmetric throat injection was investigated to determine vector control characteristics. It was found that the side force (component of the thrust vector normal to the nozzle axis) generated was about the same as the jet reaction force*. In the Phase II experiments the side force produced by asymmetric injection at the throat was small (a fraction of the secondary jet reaction force) and opposite in direction to the secondary jet reaction force. These Phase I and Phase II results (comparable to those of Rocketdyne, Ref. 5) offer experimental proof of the fact that asymmetric injection for vector control should not be at the nozzle throat. This may be explained qualitatively by the following considerations. Side force will be maximized by the production of a very asymmetrical wall pressure distribution with the high pressure side being on the injection side (so that pressure force adds to jet reaction force). Much data has shown that the injection effects do not extend far downstream so that essentially all of the asymmetry in pressure distributions must necessarily be restricted to the subsonic nozzle walls. However, the asymmetry of pressure distribution is precluded to a large extent by the fact that the flow field is subsonic. It is apparent by this reasoning that injection at a supersonic station (with little or no throttling) will make the pressure distribution asymmetrical only in the supersonic portion of the nozzle. The degree of asymmetry will depend on nozzle geometry, injection rate, and Mach number at the injection station. Injection station Mach number largely determines the position (if it exists) at which the injection-induced shock wave reaches the opposite nozzle wall. Maximum side force obviously depends on the

*The side force, as mentioned in Ref. 1, was measured with much uncertainty so that only a qualitative indication was obtained.

shape of this asymmetrical pressure distribution and how it is related to the nozzle shape (or to be more precise, the nozzle area distribution).

Asymmetric injection at a supersonic nozzle station was also investigated in the Phase II tests and significant values of side force were measured. These results are discussed in the following section while a correlation with other data is presented in the final section.

A. NSL SIDE FORCE DATA

The measurements of side force presented here correspond to injection at the inflection point of the low pressure gradient nozzle. Side force, normalized by the thrust for zero injection, is plotted in Fig. 34 as a function of secondary flow ratio. The nozzle area ratio (A_{inj}/A_*) at the injection station is 1.85 which corresponds to a local Mach number of 2.1 according to one-dimensional flow equations. The side force ratio* is a linear function of secondary flow rate at low flow rates. However, it then levels off and decreases toward zero as secondary flow is increased. This behavior is due to the impingement of the injection-induced shock wave on the wall opposite injection. The change in flow with injection angle is seen to be significant since more side force is generated at the lower injection angle configuration in spite of a smaller jet reaction force. The jet reaction forces shown are only the components in the side force direction (normal to the nozzle axis). The values of side force ratio at the high secondary flow rates are of little significance since shock "interference" on the wall opposite injection has nullified the effectiveness of the configuration. Injection at even higher flow rates will not improve matters since the induced shock wave will become more normal (with nozzle choking possible, eventually) and an essentially symmetrical pressure distribution which produces little side force will be maintained.

A series of schlieren photographs of asymmetric injection flow patterns is shown in Fig. 35. The flow configuration near the wall with injection is generally similar to that in the case of symmetric injection (Fig. 26). The process whereby side force is reduced with increasing secondary flow is quite apparent in Fig. 35. The injection-induced shock

*The uncertainty in F_s/F_0 is ±0.005.

wave impinges on the wall opposite the injection side of the nozzle. The higher pressure generated opposes the high pressure on the injection side and a force is produced in opposition to the side force. As secondary flow is increased this effect attenuates the side force further as the injection-induced shock moves farther upstream. Losses in side force are also due to the decrease in pressure downstream of the injection station at large secondary flow rates.

An amplification factor defined (in Ref. 5) as the side force ratio (F_s/F_0) divided by the secondary flow ratio (w_s/w_{p_0}) was calculated for the asymmetric injection configurations. A typical plot of this amplification factor as a function of secondary flow is shown in Fig. 36. This factor is a maximum at low injection rates but falls off rapidly with increasing injection eventually approaching some equilibrium value relatively near zero. It is also a weak function of injection angle with performance being slightly improved with decreasing injection angle. The variation of the amplification factor is obviously a function of nozzle shape, exit-to-throat area ratio, and injection station. Best performance will be with a configuration where the fall-off of K is slow and takes place at a high injection rate.

Fig. 37 shows axial thrust, normalized by the thrust without secondary injection, plotted against secondary flow ratio. The thrust increases in direct proportion to secondary flow because a portion of the momentum of the secondary flow is in the axial direction. That is, the ratio of secondary stagnation pressure to nozzle exit pressure determines the ultimate velocity and some of the corresponding change in momentum appears as pressure on the nozzle wall and thus axial thrust. A portion of this momentum is negative thrust due to the direction of the injection slot. The increase in thrust, as shown in Fig. 37, is an increasing function of injection angle as would be expected.

B. CORRELATION OF NSL AND OTHER DATA

The side force measurements discussed in the preceding section are shown in Figs. 38 and 39 along with comparable data from other investigations. The data corresponds to references as follows:

UAC (Ref. 6), NOTS (Ref. 11), Rocketdyne (Ref. 5), and NASA (Ref. 12). The nozzle exit-to-throat area ratios (A_e/A_*), injection angles (ϕ), and injection stations (A_{inj}/A_*) are seen to vary over a wide range so that a high degree of quantitative correlation cannot be expected. The qualitative agreement, however, is good for several reasons. The NSL and NOTS data agree at low secondary flow rates and examination shows that they are closest in A_e/A_*, ϕ, and A_{inj}/A_*. No comparison is possible at higher injection rates because of the lack of NOTS data. This is also partially true for the Rocketdyne and NASA measurements. However, the Rocketdyne and NASA data does not show the loss in effectiveness that is apparent in the NSL data. Nevertheless, the Rocketdyne data at least shows a small decrease in slope with increasing secondary flow. It is believed that in the Rocketdyne and NASA cases (and in the NOTS one also) serious pressure forces have not begun to develop due to injection-induced shock impingement on the wall opposite injection. This is probably due to the use of bell-shaped rather than conical (or slowly diverging) nozzles which tend to be short and thus less vulnerable to shock capture by the opposite wall.

In the UAC experiments, however, the data is obviously similar in showing the onset of side force nullification. Schlieren photographs are also shown (Ref. 6) from these tests which indicate the actual location of the shock impingement. In spite of the large A_e/A_*, shock impingement took place because the nozzle was long owing to a conical shape and 15° semi-vertex angle. The smaller slopes (at low secondary flow rates) of the UAC curves are probably due to a less effective injection angle (less in terms of induced flow configuration only, since the side force component of jet reaction force is the same for UAC and NSL cases because sin 75° = sin 105°) and the difference between two- (NSL) and three-dimensional (UAC) flow.

A graphical method for assessing the relative merits of vector control schemes has been reported in Ref. 13. This method compares the side force ratio (F_s/F_0) to a specific impulse decrement parameter ($\Delta I/I$) as shown in Fig. 40. On the assumption that the injectant is equivalent to the main (primary) flow, the loss in specific impulse is

$$\frac{\Delta I}{I} = \frac{\dfrac{w_s}{w_{p_0}}}{1 + \dfrac{w_s}{w_{p_0}}} - \frac{F_s}{F_0} \sin \psi$$

where the increment in thrust due to injection is of the order of $F_s \sin \psi$ and ψ is the nozzle wall angle* (at injection station) relative to the axis. Since Ref. 13 shows that range losses are directly proportional to loss in specific impulse, the most desirable means of control is one with a maximum slope which extends to a large ordinate. The shapes and locations of the curves in Fig. 40 are about the same (relative to one another) as in Fig. 38 and 39. The Hausmann data from UAC is viewed with caution as the shroud involved may have been asymmetrical which could markedly influence the data (more favorable side force with more nozzle area on the high pressure, injection side). It should be noted that although the hot firing data shows poor performance it corresponds to a very high A_{inj}/A_{*}. The performance of the configurations in Fig. 40 should be regarded merely as a range of possibilities. That is, they should be viewed as establishing the characteristics of the method and the influence of the important variables. The maximum potential of the injection method should be evaluated on the basis of performance of an optimization study design. Furthermore, in the final analysis all schemes (injection and otherwise) must also be judged in view of their relative weight penalties and control complexity.

*It is believed that tan ψ should be used rather than sin ψ when F_s is measured in the direction normal to the axis. Ref. 13 quotes the sin ψ as shown above but for the range of ψ of interest here the difference between sin ψ and tan ψ is not important.

SECTION IV

CONCLUSIONS

A study of rocket thrust control by gas injection* has been completed. The conclusive results of this investigation form the basis of the remarks below. Tha material in this section breaks down, as it did in the investigation itself, into two parts: thrust modulation and vector control.

Thrust Modulation

The following items characterize the method of gas injection as a means of thrust modulation.

1. Thrust varies directly with total nozzle flow. In many cases the proportionality is the same as that in the nozzle with no injection. In some two-dimensional cases the proportionality factor increases slowly with injection rate while certain three-dimensional ones show a similar decrease. These changes from the zero injection proportionality approach (linearly) values somewhat under 10 percent at an injection rate of $w_s/w_{p_0} \cong 0.3$. The proportionality is further a function (weak) of only nozzle geometry with sensitivity being atteunated by increasing expansion ratio.

2. An analysis of flow throttling** was devised based on three flow models. Schlieren photographs verify the fact that all three types of flow occur. The secondary mixing and sheet flow models correlate the two-dimensional flow throttling data while the sheet flow and secondary expansion models correlate the three-dimensional flow throttling data. The reduction in primary flow in the three-dimensional case is about $2\frac{1}{2}$ times the injected secondary flow while in the two-dimensional case the reduction is somewhat less. The constant-area duct assumption in the analysis was verified by schlieren photographs and pressure distribution data which showed that the throttling process takes place

*Unless otherwise specified, injection is at the nozzle throat.

**Flow throttling means reduction in primary flow.

in a short axial distance. In addition, experimental data supports the analysis indication that flow throttling is maximized by injection at the throat. Since thrust varies with total nozzle flow, a knowledge of the flow throttling implies a knowledge of the thrust.

3. Flow throttling is insensitive to orifice geometry. That is, a given secondary injection orifice area may be distributed as a slot or holes of various sizes and flow throttling is unchanged. It is believed that shaped injection ports (supersonic nozzles) will not significantly improve flow throttling; the injection stagnation pressures required for filling an injection port nozzle of large Mach number ($M > 2$) fast become too high to be practical.

4. Primary nozzle geometry has a small effect on flow throttling which is attenuated by increasing overall nozzle pressure ratio. Flow throttling is increased (at a given w_s/w_{p_0}) as the pressure gradient (implies throat shape) is decreased. The nozzle shapes (i.e., bell-shaped) presently in use have a high $\partial p/\partial x$ in the throat region and thus are unfavorable in this respect without modification (which would be major and perhaps not worth the small gain).

5. Primary pressure ratio does not affect flow throttling at pressure ratios greater than about 3. This means that for probably all rocket engines (exit Mach numbers greater than about 1.5) primary pressure ratio is unimportant as regards gas injection flow throttling.

6. Flow throttling varies with injection angle (ϕ) primarily due to the axial momentum contribution of the injected gas. The flow throttling analysis (with which experimental data seems to agree, at least qualitatively) indicates that at a given w_s/w_{p_0} the primary flow is further (beyond that for $\phi = 90°$) reduced by an amount directly proportional to the product of the secondary flow and the cosine of ϕ.

7. The circumferential angle (β) over which injection takes place does not affect flow throttling for configurations which are symmetrical about a plane through the nozzle axis.

8. The flow throttling analysis indicates that performance is improved by using an injectant which possesses a low specific heat ratio (γ) and a low molecular weight.

The increase in performance comes from the increase in the axial momentum component (which opposes primary stream momentum) of the injected gas. In the same manner, flow throttling is increased by increasing the stagnation temperature of the secondary gas.

9. All of the theoretical and experimental study is based on the maintenance of a constant primary stagnation pressure regardless of the amount of flow throttling. This implies that primary supply throttling takes place upstream of the nozzle stagnation chamber as it indeed did in the experiments. However, such a capability in the rocket engine is hard to imagine in a solid propellant one and not presently attainable in liquid propellant ones. The turbopump compressors in liquid propellant engines pump at a constant flow rate to a constant total head with performance being variable only over a small range. Therefore, the use of gas injection as a means of flow throttling is in reality contingent upon a flow throttling capability upstream of the combustion chamber which can maintain a constant chamber pressure.

Vector Control

The following items characterize the method of gas injection as a means of vector control.

1. The asymmetric injection position for maximum side force is in the supersonic portion of the nozzle. Asymmetric injection at the throat is inefficient since the injection-induced asymmetry in pressure distribution is not effective in the subsonic region and falls off rapidly with distance in the supersonic region so that the area affected is small (near the throat). As injection station is moved toward the throat from the exit, side force increases until enough of the injection-induced shock is "captured" by the opposite wall to produce a significant counter-force which opposes the side force. The optimum position will thus be somewhere between these extremes and a strong function of nozzle geometry. The short, bell-shaped nozzles in use in present rocket engines might be favorable since shock "capture" may be attenuated.

2. Side force varies in direct proportion to secondary flow rate before the onset of serious shock capture (up to w_s/w_{p_0} of about 0.06 in configurations tested to date).

3. The ratio of side force ratio (F_s/F_0) to secondary flow ratio (w_s/w_{p_0}) is a maximum at low injection rates and numerically about 2.

4. Side force varies with injection angle (ϕ) through the injection-induced pressure distribution and the reaction force component (which part varies as sin ϕ) normal to the nozzle axis. Since the induced pressure distribution becomes more favorable with decreasing ϕ but the reaction component falls off as sin ϕ the optimum injection angle will be less than 90°.

5. Injection ports shaped for supersonic flow increase the effectiveness of a configuration in producing side force.

6. It is believed that distribution of injection area over a circumferential angle (β) will net only very small gains, if any.

7. The optimum gas injection configuration as regards ϕ, β, and injection station will depend on the particular geometry of a nozzle. It is believed that increasing injected gas momentum, by the use of a high temperature gas with a low γ and low molecular weight, will increase the resultant side force (at a given w_s/w_{p_0}).

REFERENCES

1. Blaszak, John J. and Fahrenholz, Fred E. Rocket Thrust Control by Gas Injection, Massachusetts Institute of Technology, Naval Supersonic Laboratory, Technical Report 430, November 1960 CONFIDENTIAL.

2. Martin, A.I. "The Aerodynamic Variable Nozzle", Journal of the Aeronautical Sciences, Vol. 24, No. 5, p. 357, May 1957.

3. Equations, Tables, and Charts for Compressible Flow, by the Ames Research Staff, NACA TR 1135, 1953.

4. Li, Ting-Yi and Geiger, Richard E. "Stagnation Point of a Blunt Body in Hypersonic Flow", Journal of the Aeronautical Sciences, Vol. 24, No. 1, p. 25, January 1957.

5. Rocketdyne Engineering F-1 Thrust Vector Control Study, Rocketdyne Report R-1717, October 28, 1959 CONFIDENTIAL.

6. Lingen, A. Jet-Induced Thrust-Vector Control Applied to Nozzles Having Large Expansion Ratios, Research Report No. R-0937-33, United Aircraft Corporation, March 1, 1957.

7. Baron, Judson R., Analytic Design of a Family of Supersonic Nozzles by the Friedrichs Method, Massachusetts Institute of Technology, Naval Supersonic Laboratory, Wind Tunnel Report 66, WADC Technical Report 54-279, June 1954.

8. Beckwith, Ivan E. and Moore, John A. An Accurate and Rapid Method for the Design of Supersonic Nozzles, NACA TN 3322, February 1955.

9. McArdle, Jack G. Internal Characteristics and Performance of an Aerodynamically Controlled, Variable Discharge Convergent Nozzle, NACA TN 4312, July 1958.

10. McAulay, John E. Cold-Air Investigation of Three Variable-Throat-Area Covergent-Divergent Nozzles, NASA TM X-42, September 1959, CONFIDENTIAL.

11 McCullough Jr., Foy Thrust Vector Control by Secondary Injection, Inside Distribution Publication 765, U.S. Naval Ordnance Test Station. September 14, 1959 CONFIDENTIAL.

REFERENCES (Concluded)

12. McAulay, John E. and Pauli, Albert J. A Cold-Flow Investigation of Jet-Induced Thrust-Vector Control, NASA TM X-416, December 1960, CONFIDENTIAL.

13. McVey, F. D. and Lawson, W. A., A Survey of Thrust Deflection Methods, (Part I), Cleveland Pneumatic Industries, Systems Engineering Division, Technical Report 6602-5a, July 1960, CONFIDENTIAL.

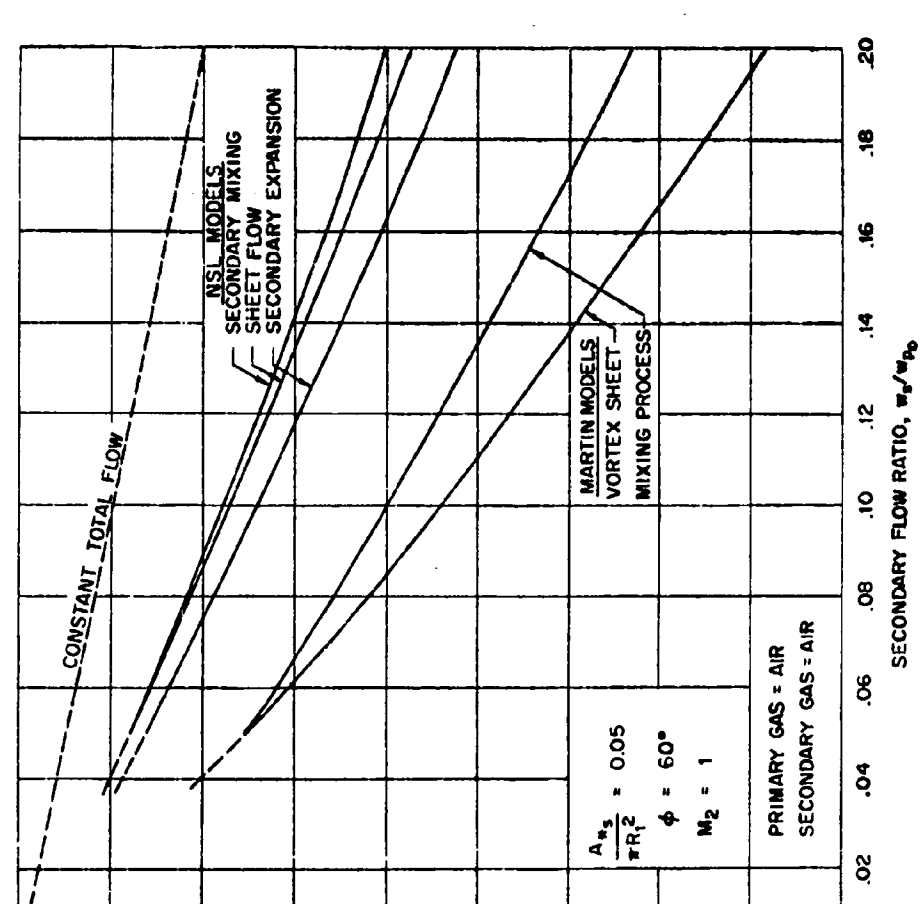

Figure 1. Flow throttling results for the NSL and Modified Martin models

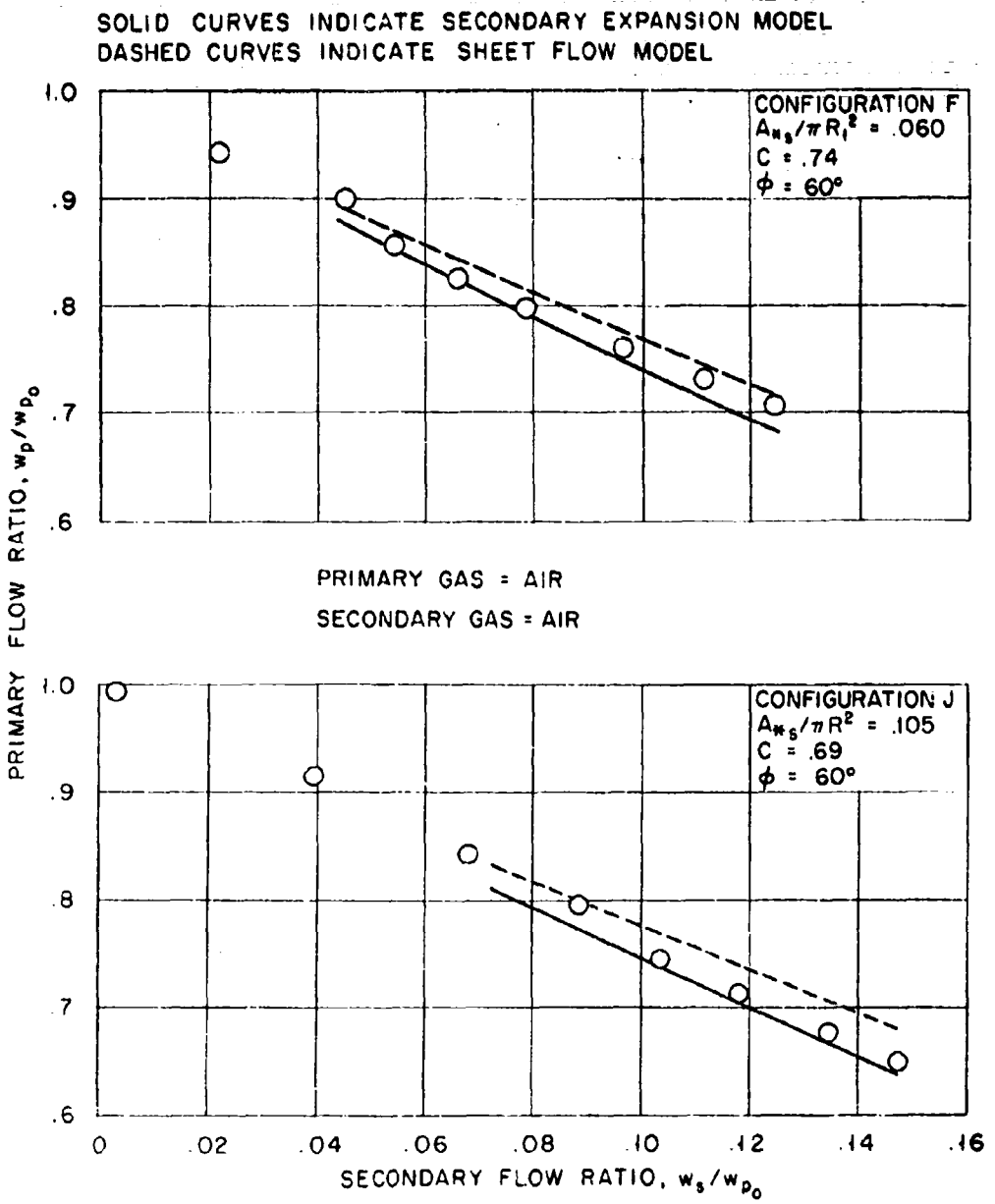

Figure 2. Typical Phase I flow throttling data

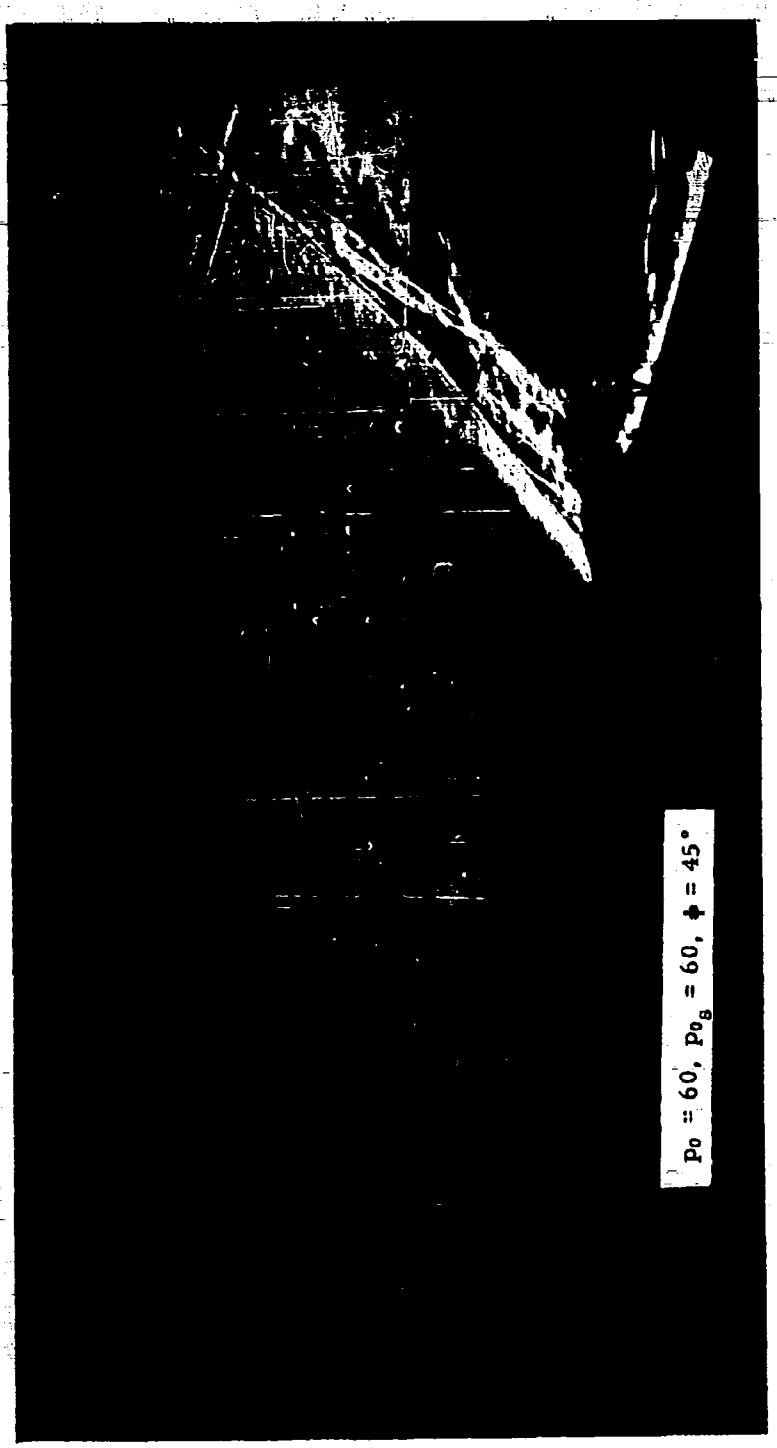

Figure 3. Schlieren photograph of injection into a supersonic stream.

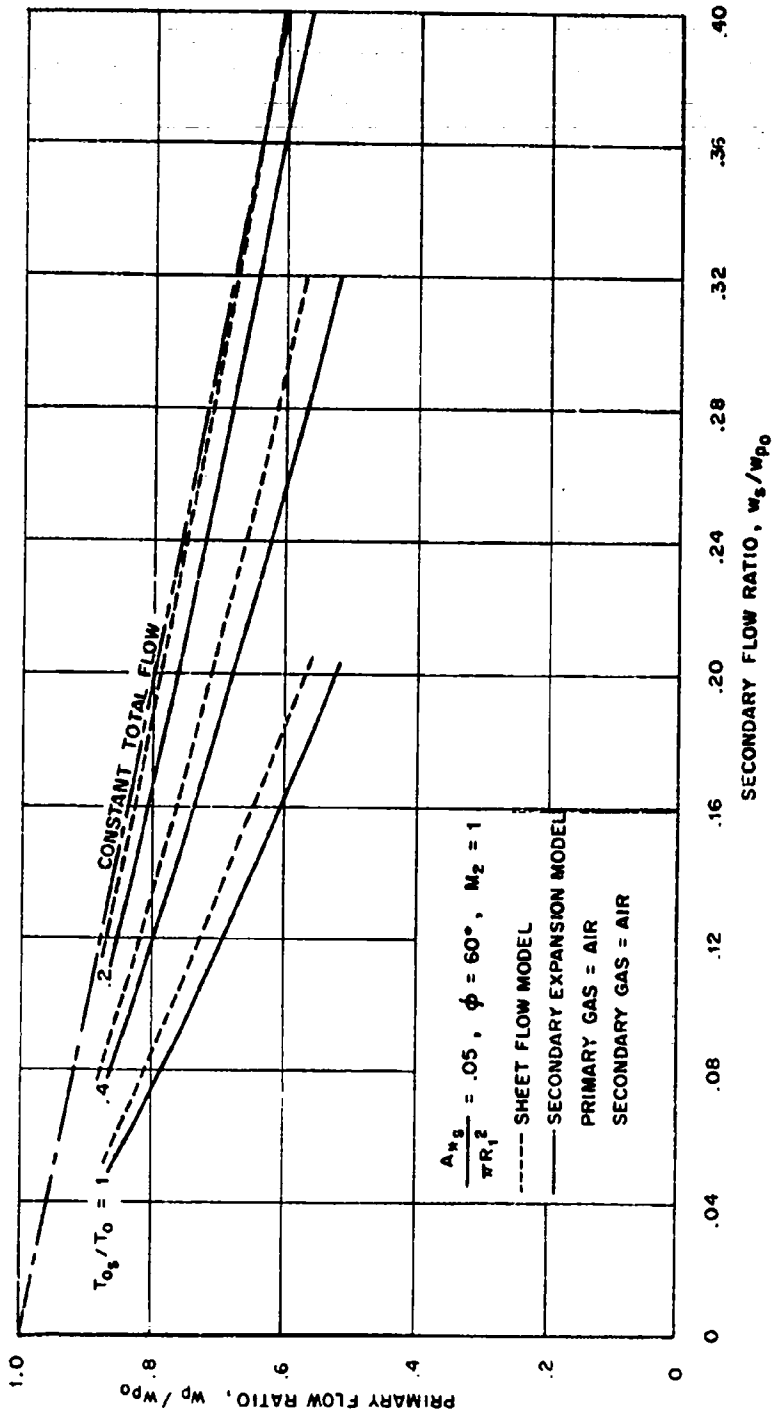

Figure 4. Effect of temperature on theoretical flow throttling

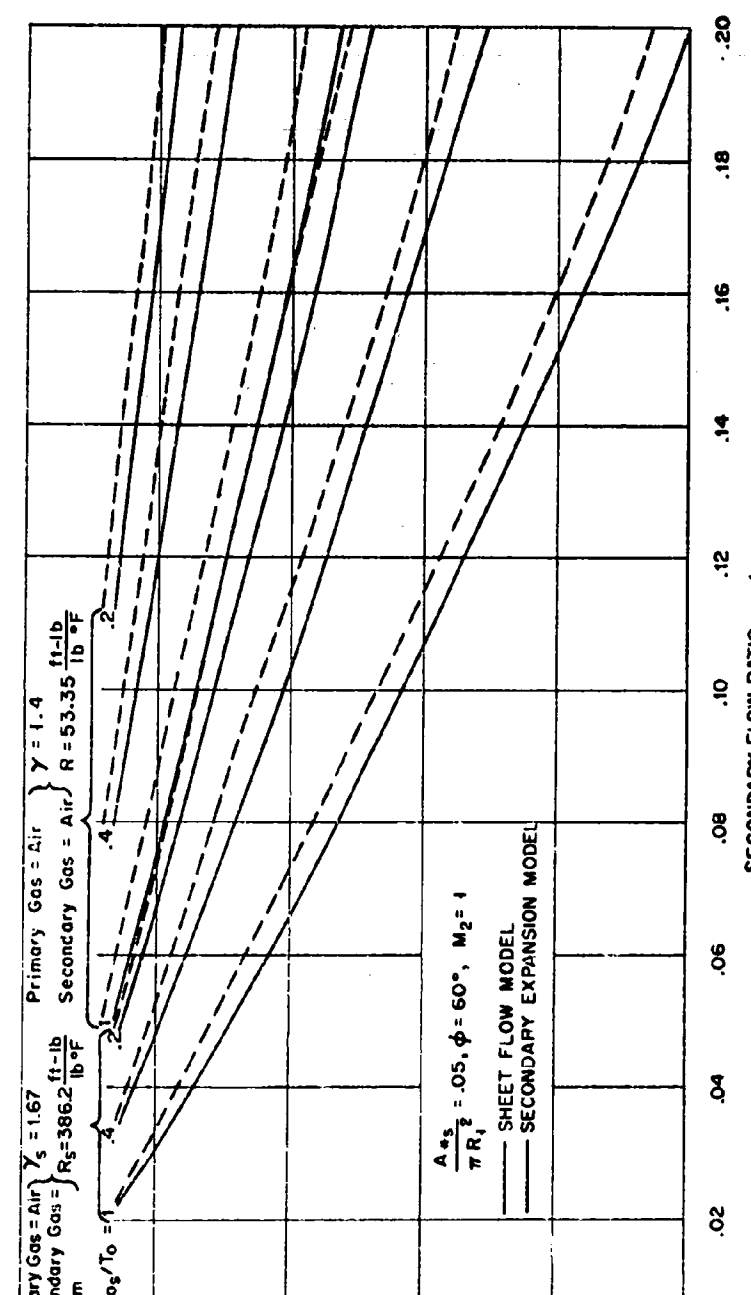

Figure 5. Effect of injection gas on theoretical flow throttling

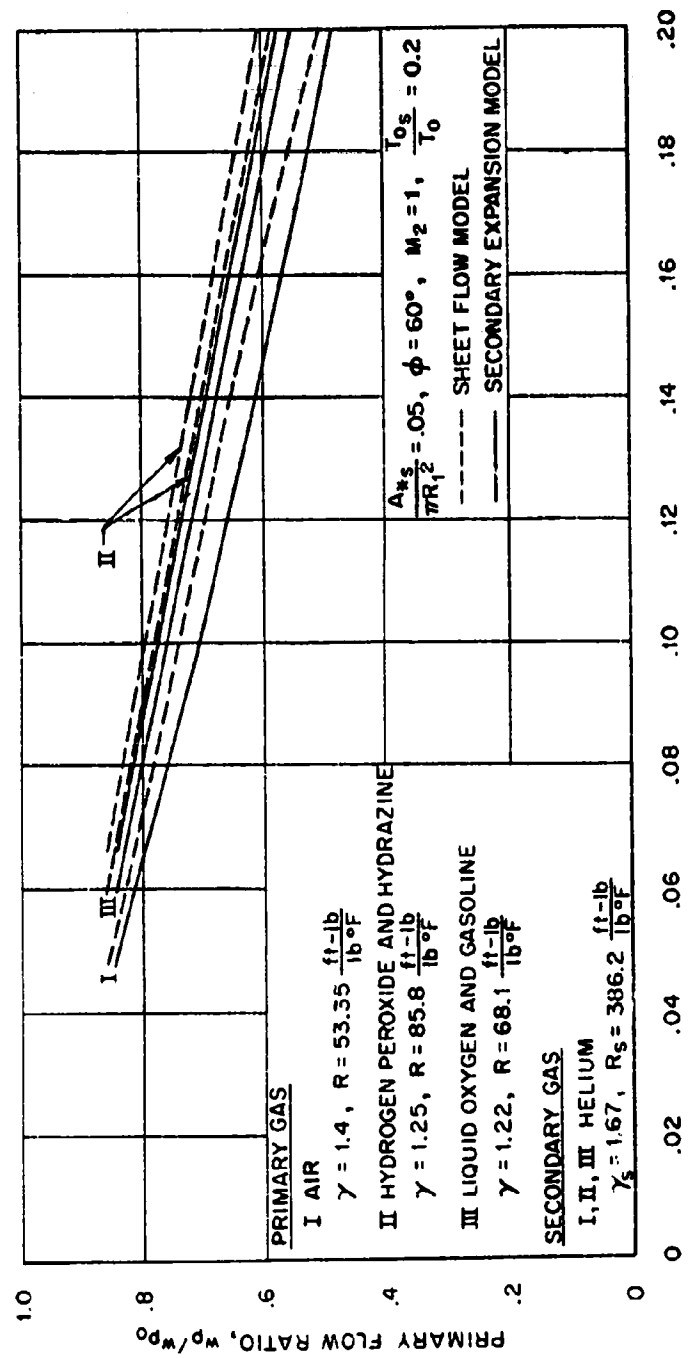

Figure 6. Effect of combustion gas on theoretical flow throttling

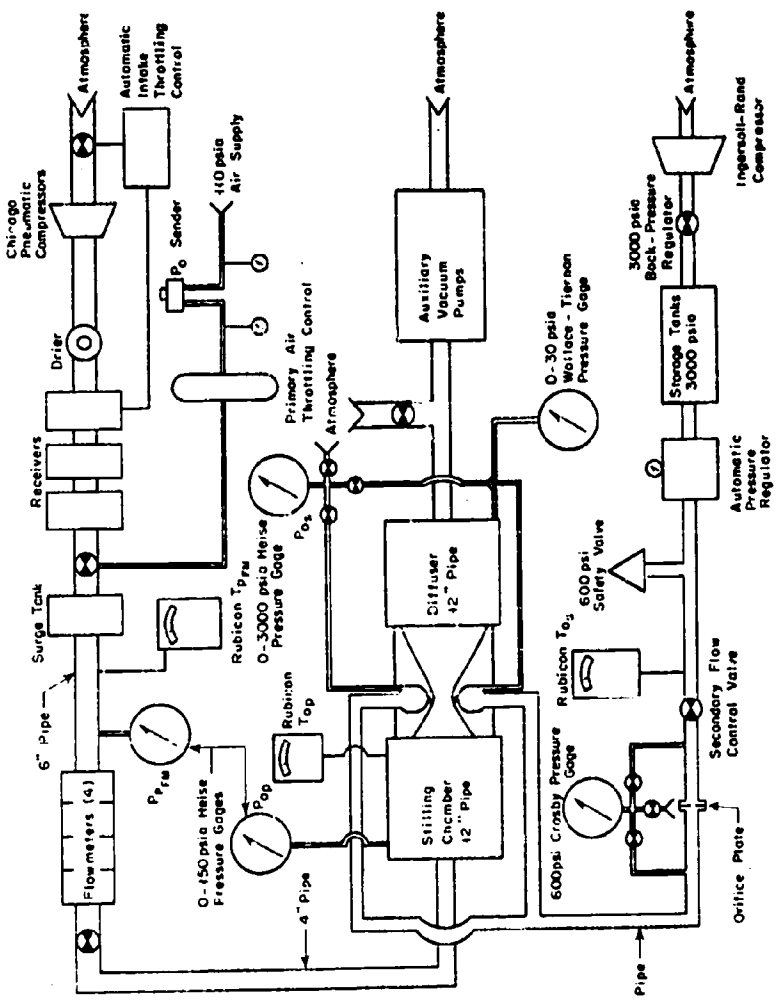

Figure 7. Schematic diagram of Phase II model arrangement

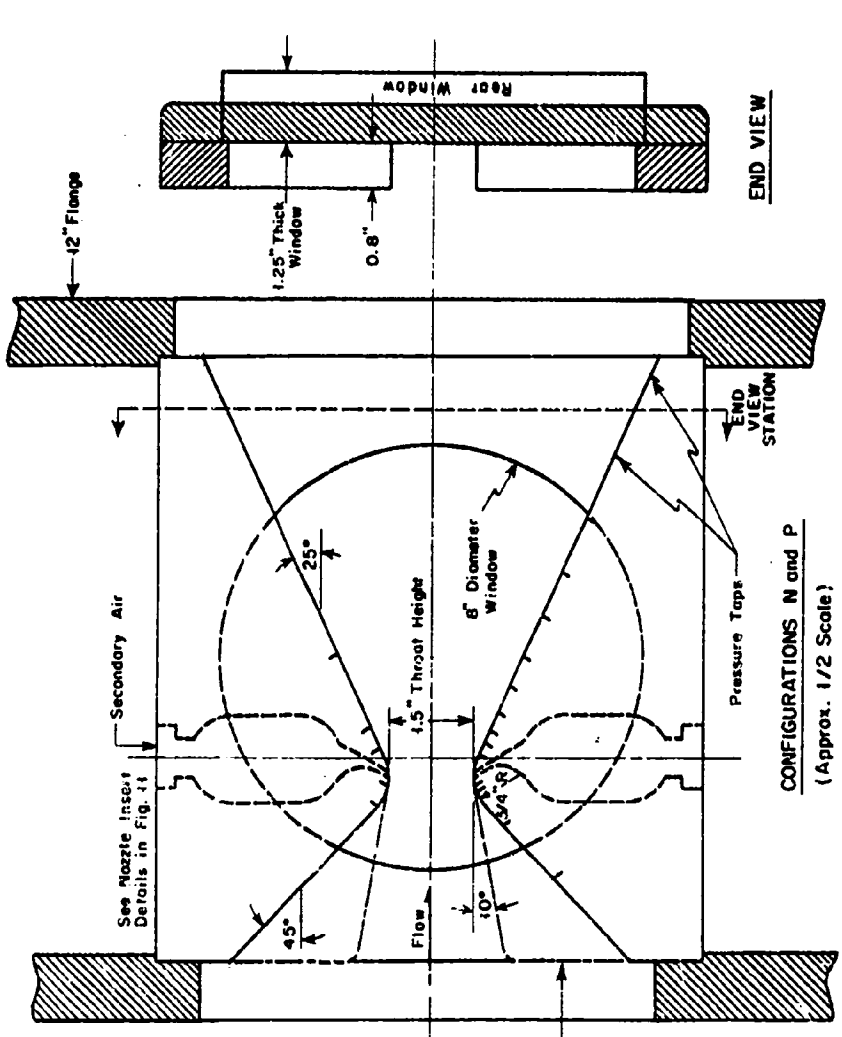

Figure 6. Model detail showing conical nozzle

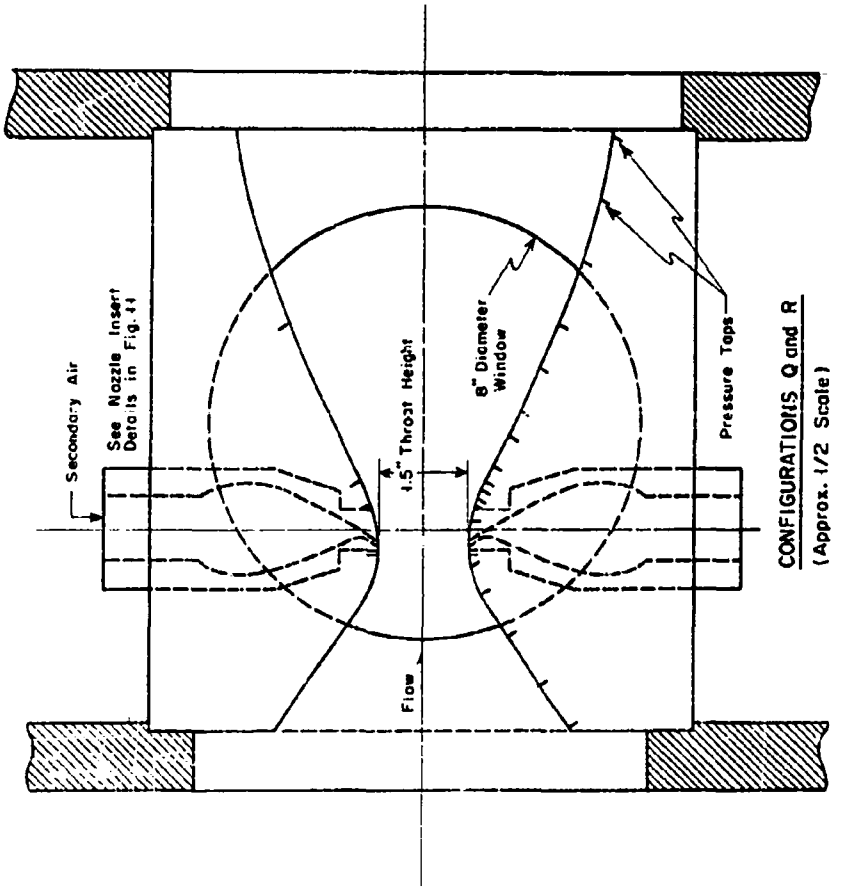

Figure 9. High pressure gradient nozzle

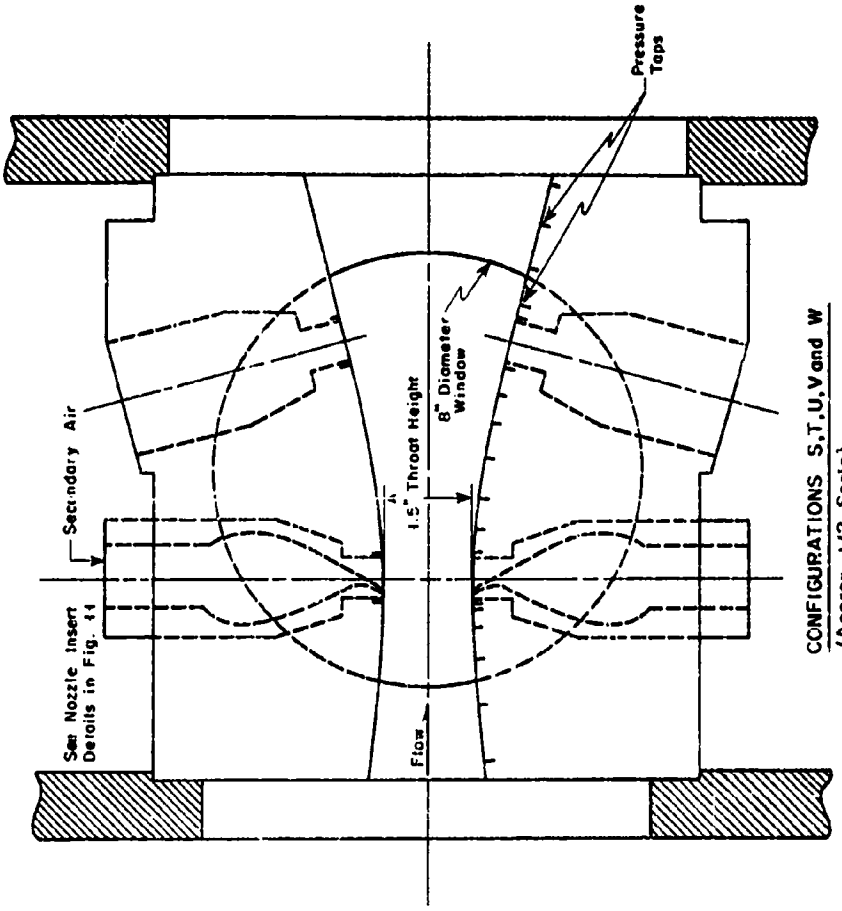

Figure 10. Low pressure gradient nozzle

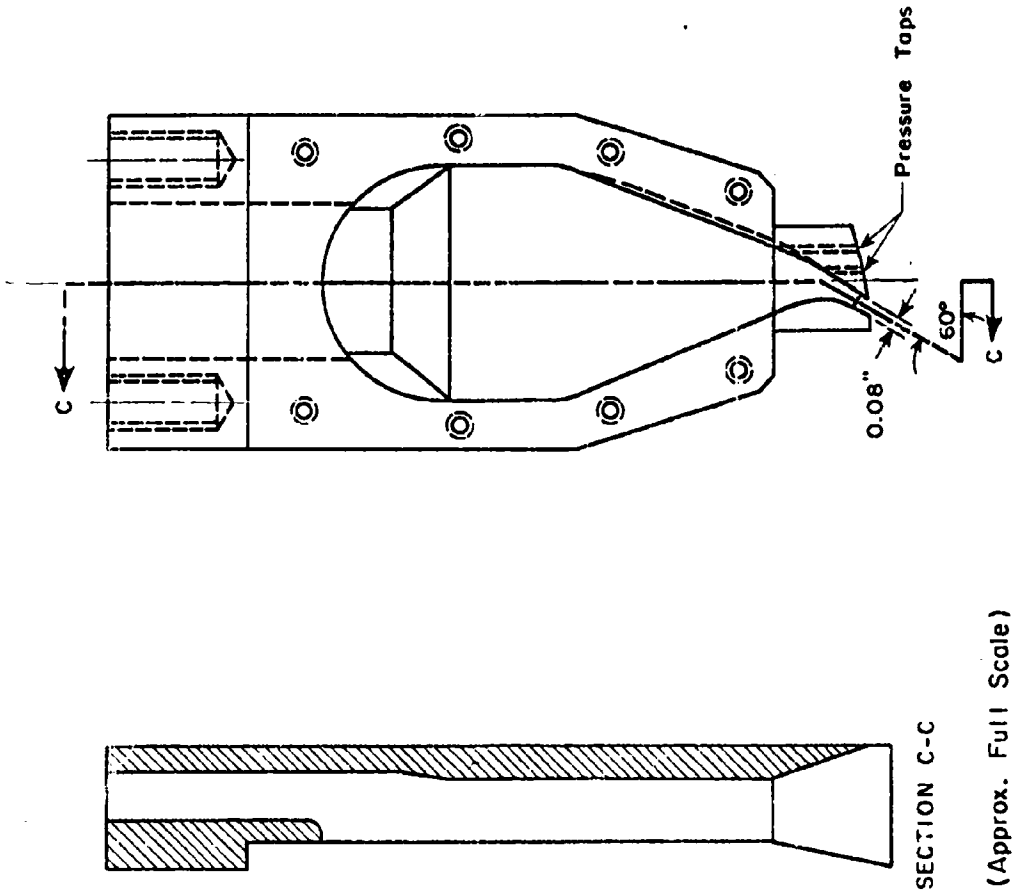

(Approx. Full Scale)

Figure 11. Injection insert details

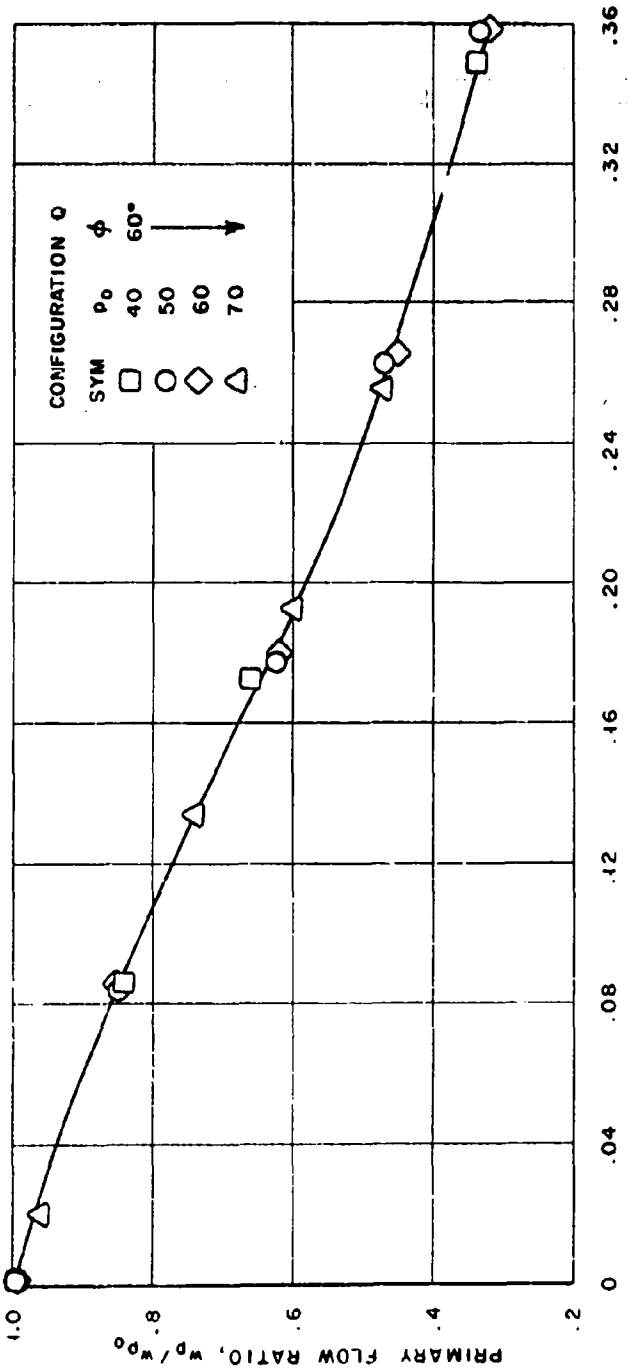

Figure 12. Flow throttling of the high pressure gradient nozzle at various stagnation pressures ($\phi = 60°$)

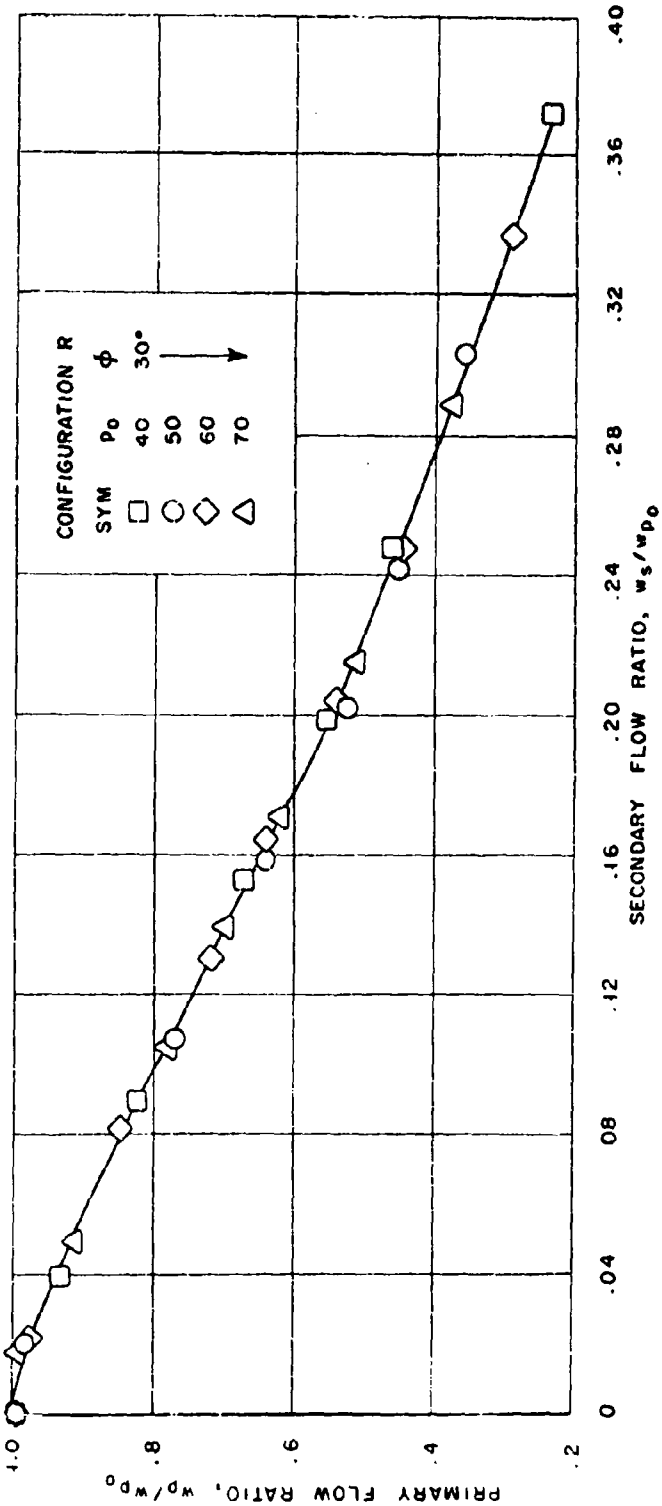

Figure 13. Flow throttling of the high pressure gradient nozzle at various stagnation pressures (ϕ = 30°)

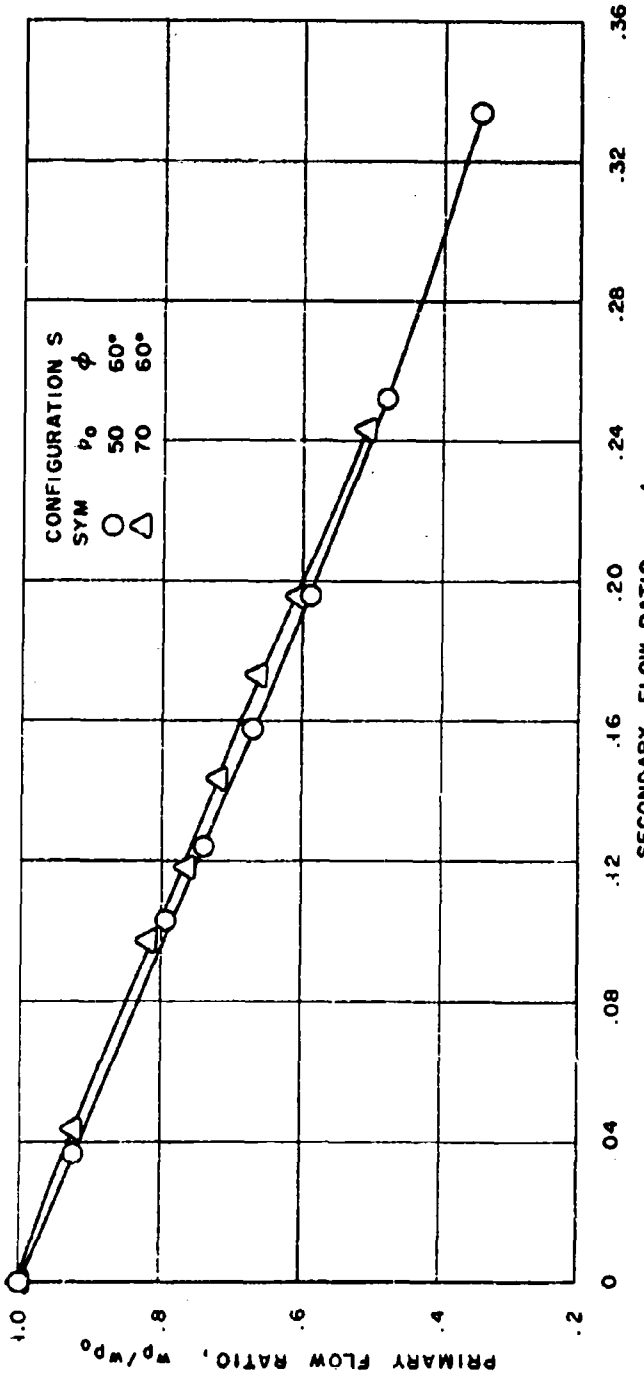

Figure 14. Flow throttling of the low pressure gradient nozzle at various stagnation pressures (ϕ = 60°)

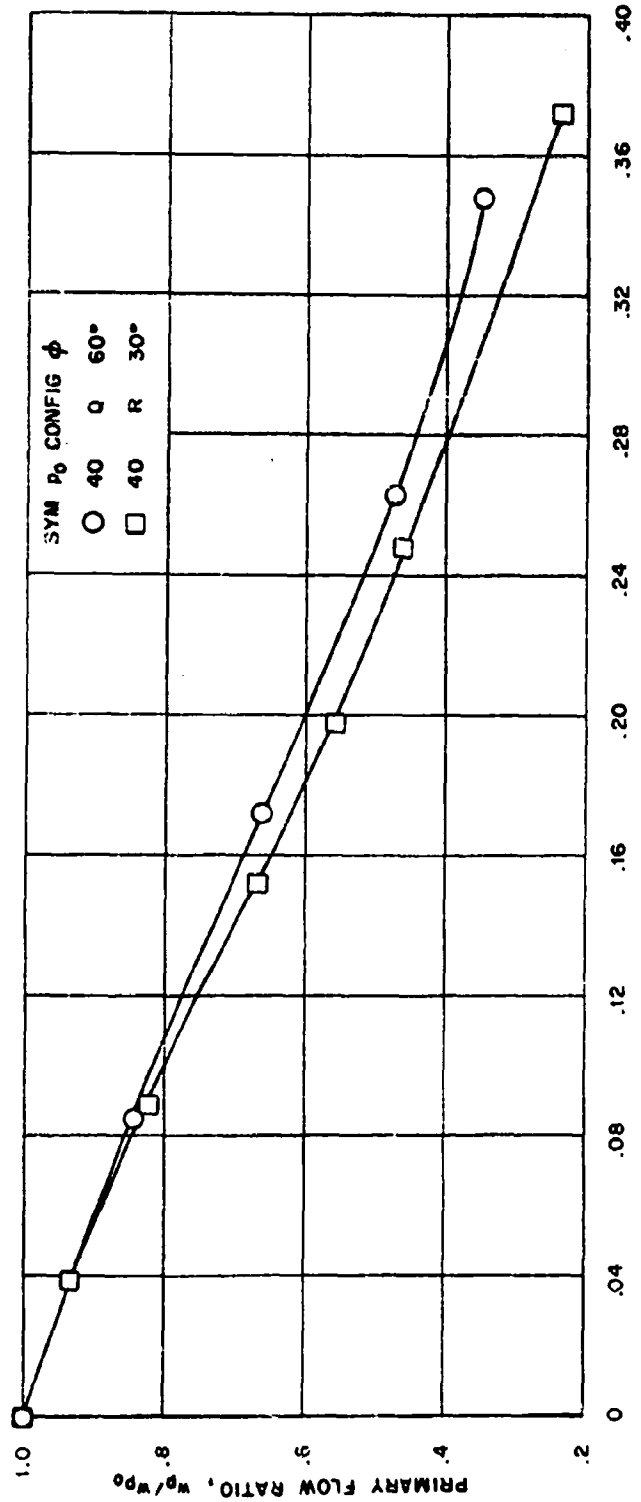

Figure 15a. Effect of injection angle on flow throttling of the high pressure gradient nozzle

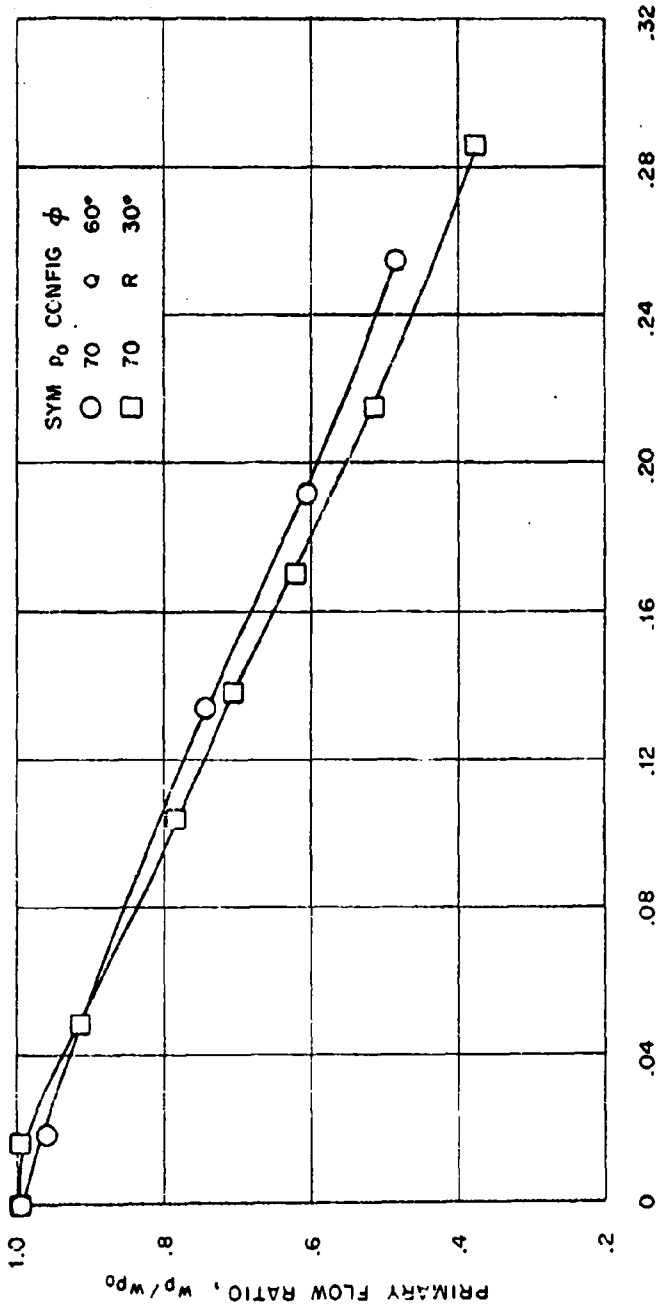

Figure 15b. Effect of injection angle on flow throttling of the high pressure gradient nozzle

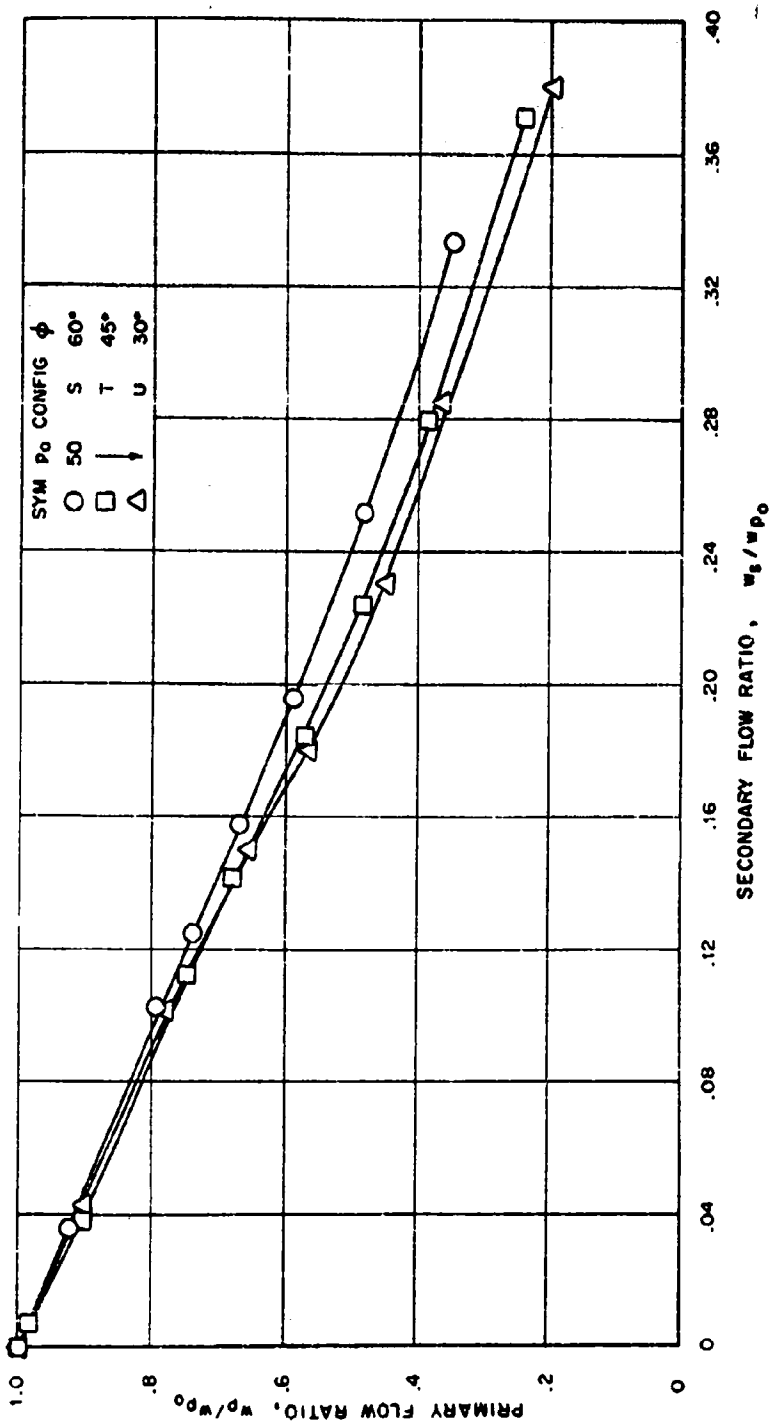

Figure 16a. Effect of injection angle on flow throttling of the low pressure gradient nozzle.

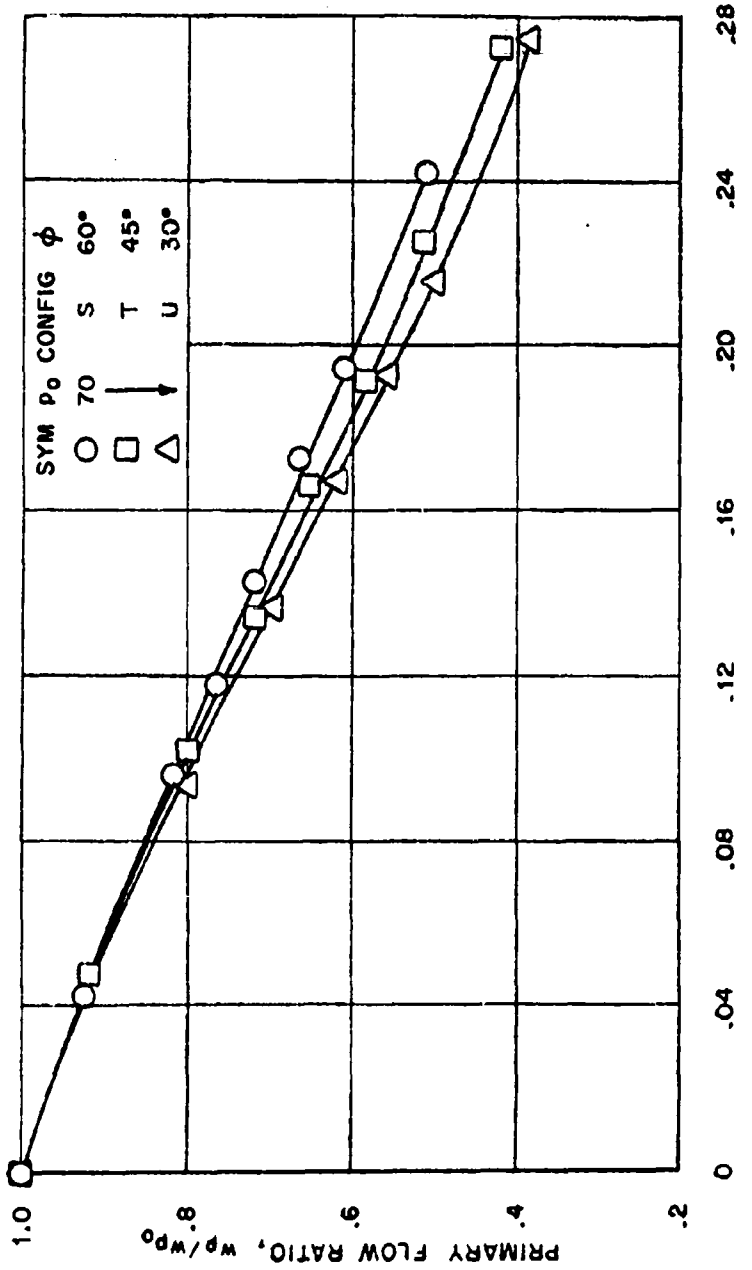

Figure 16b Effect of injection angle on flow throttling of the low pressure gradient nozzle

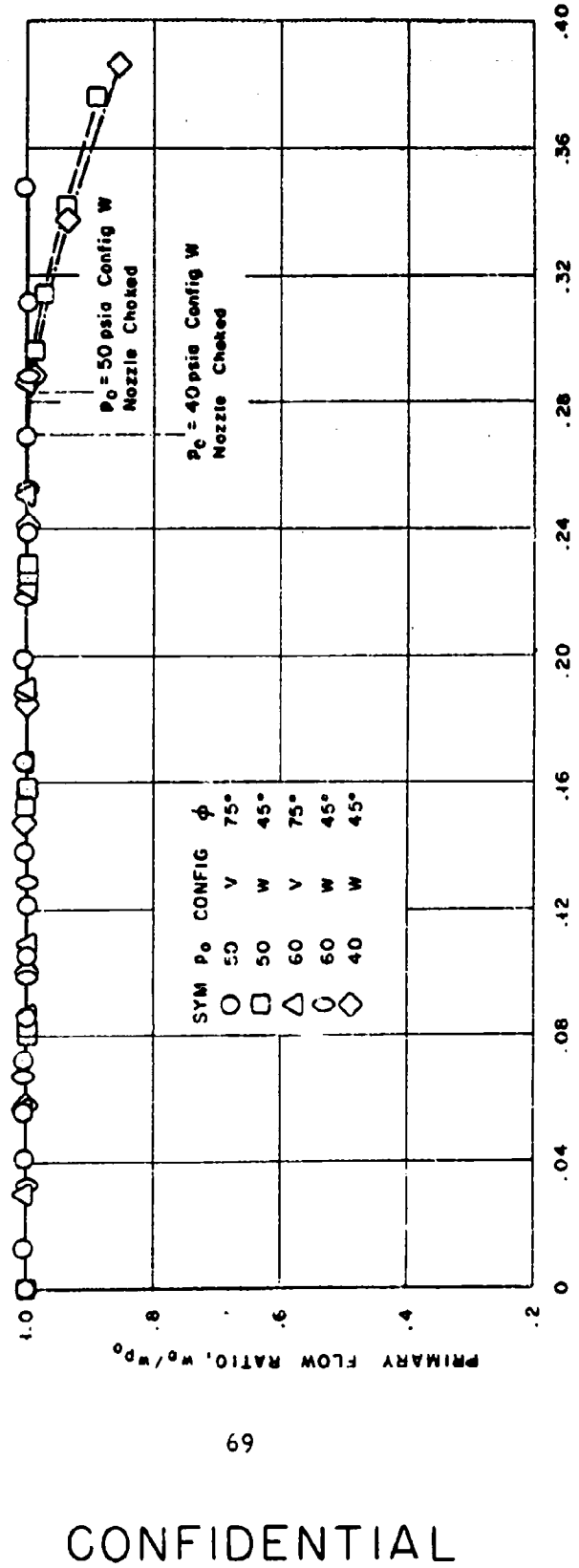

Figure 17. Flow throttling of the low pressure gradient nozzle with injection at a supersonic station

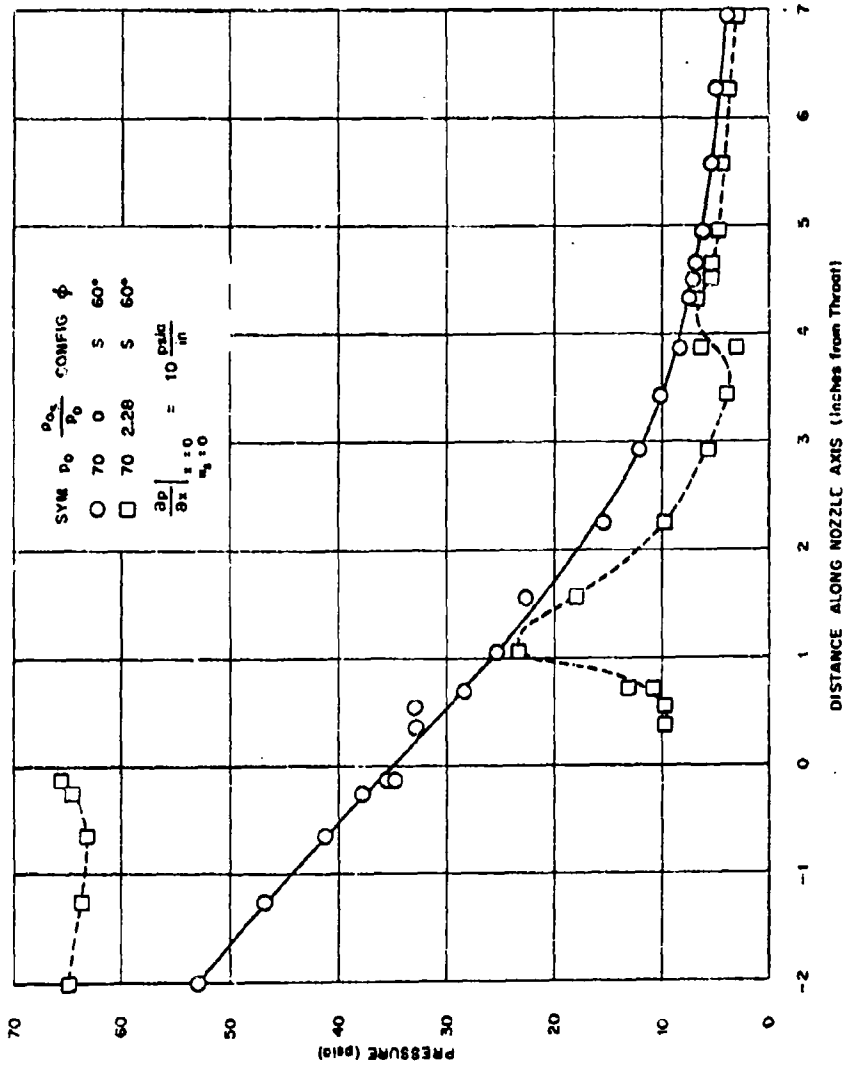

Figure 18. Typical pressure distributions in the low pressure gradient nozzle

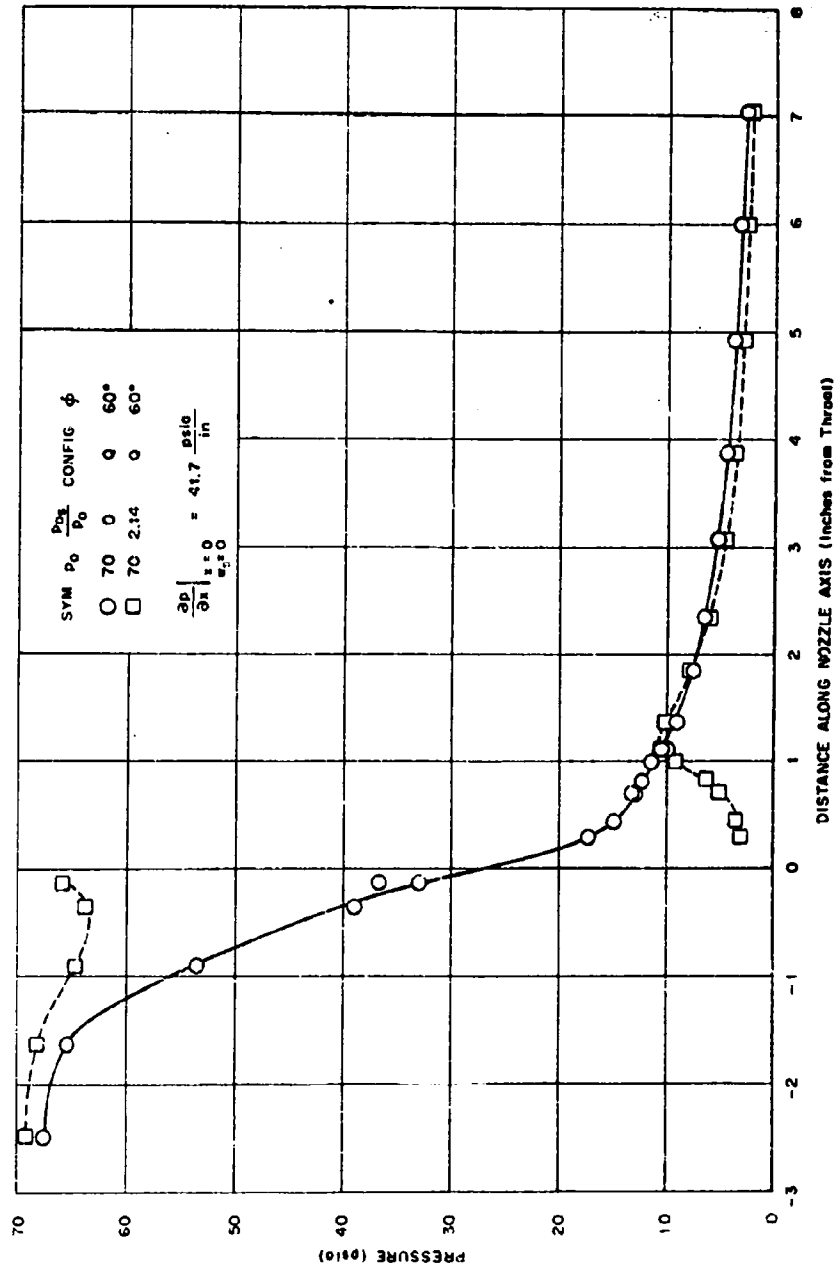

Figure 19. Typical pressure distributions in the high pressure gradient nozzle

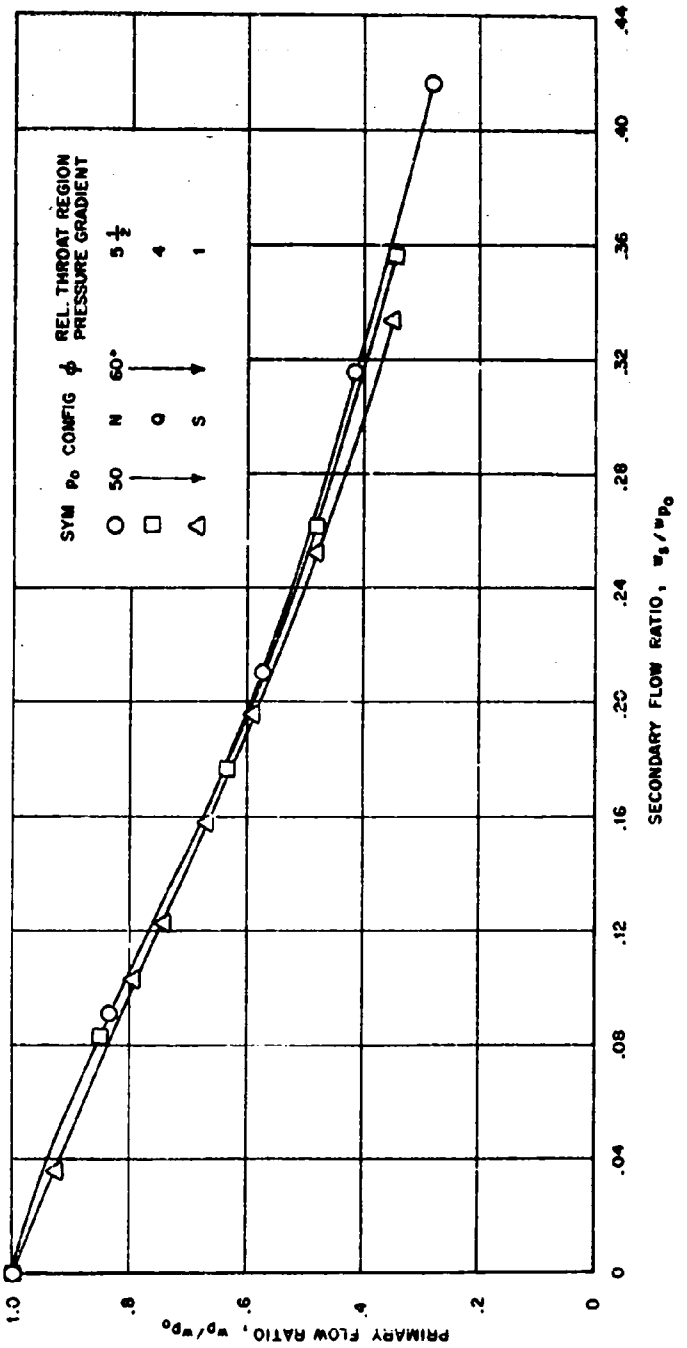

Figure 20a. Effect of pressure gradient on flow throttling at an injection angle of 60°

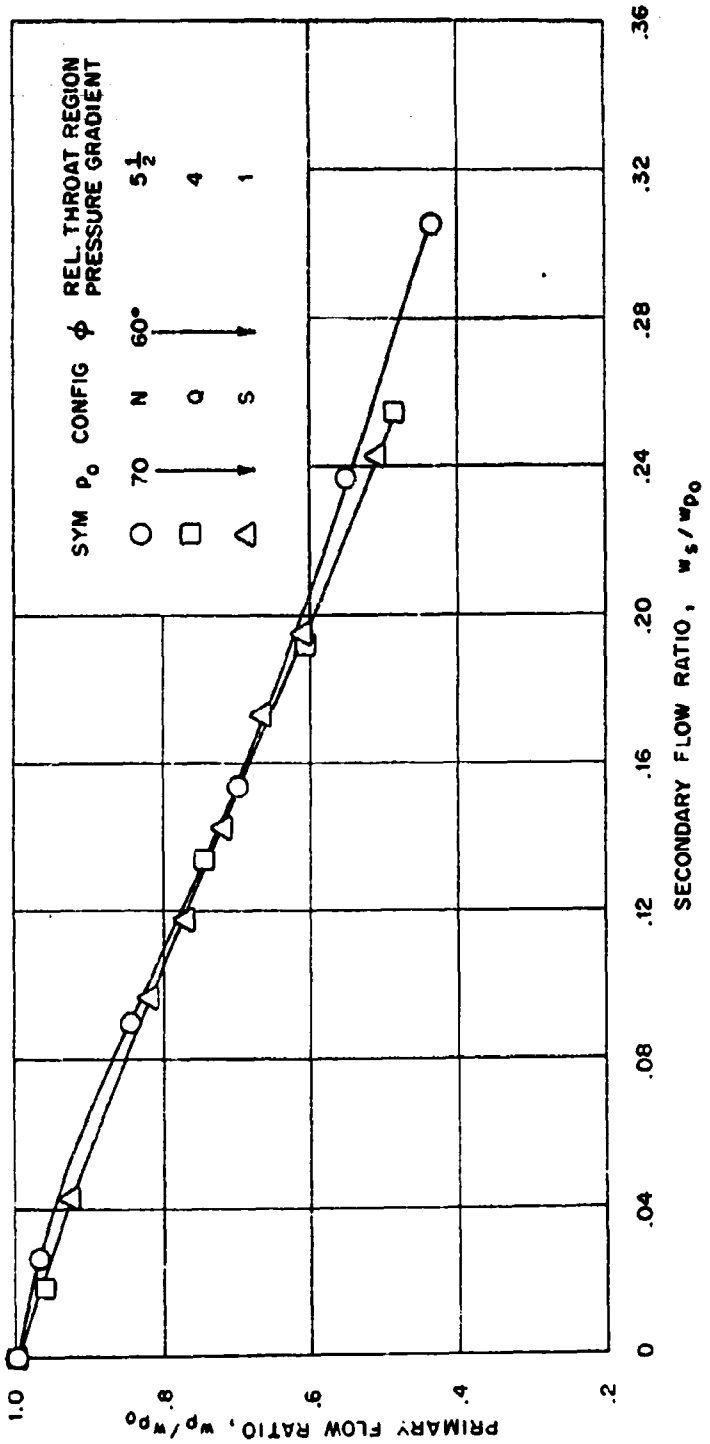

Figure 20b. Effect of pressure gradient on flow throttling at an injection angle of 60°

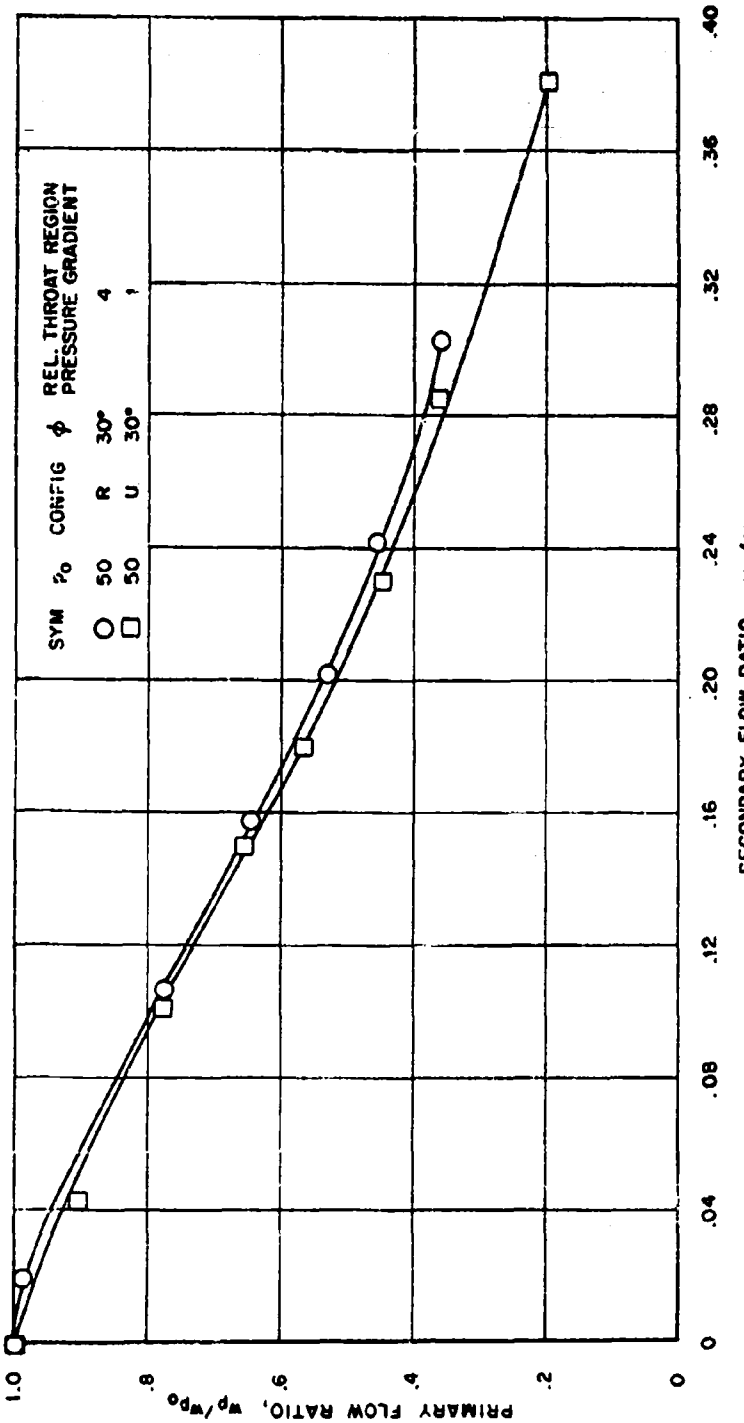

Figure 21a. Effect of pressure gradient on flow throttling at an injection angle of 30°

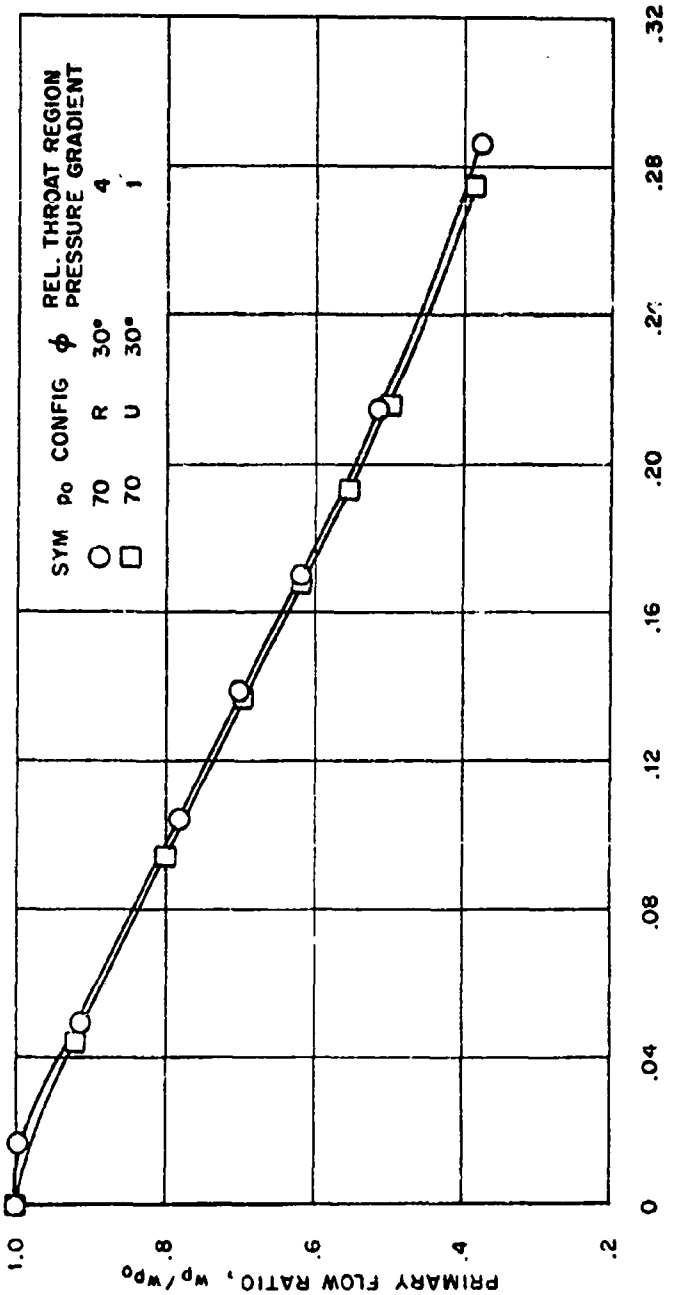

Figure 21b. Effect of pressure gradient on flow throttling at an injection angle of 30°

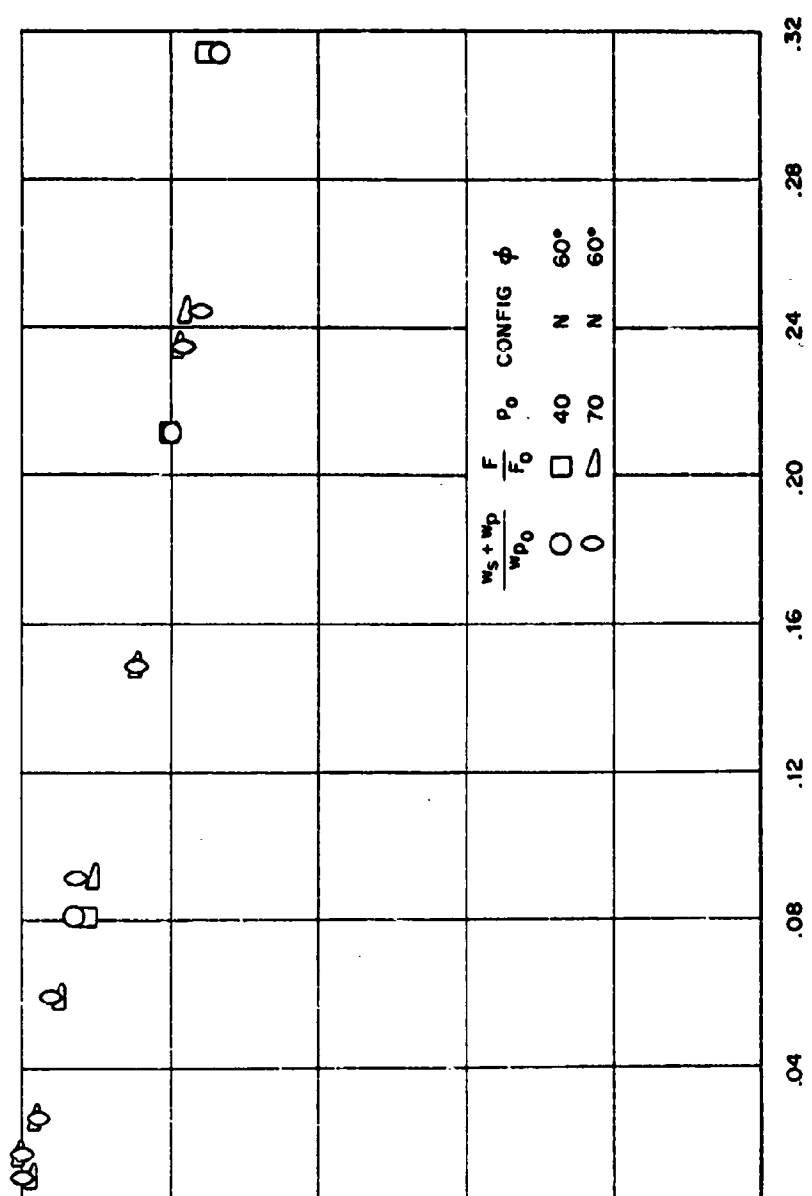

Figure 22. Typical variation of thrust and total nozzle flow with injection in the conical nozzle

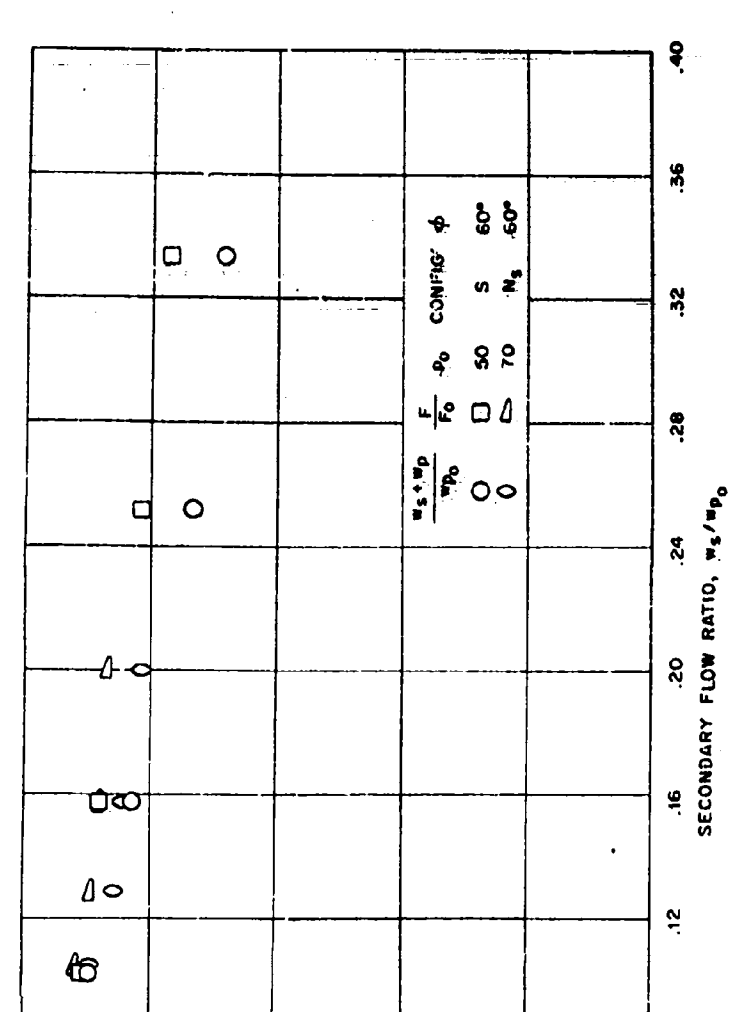

Figure 23. Typical variation of thrust and total nozzle flow with injection in the low pressure gradient nozzle and with asymmetric injection

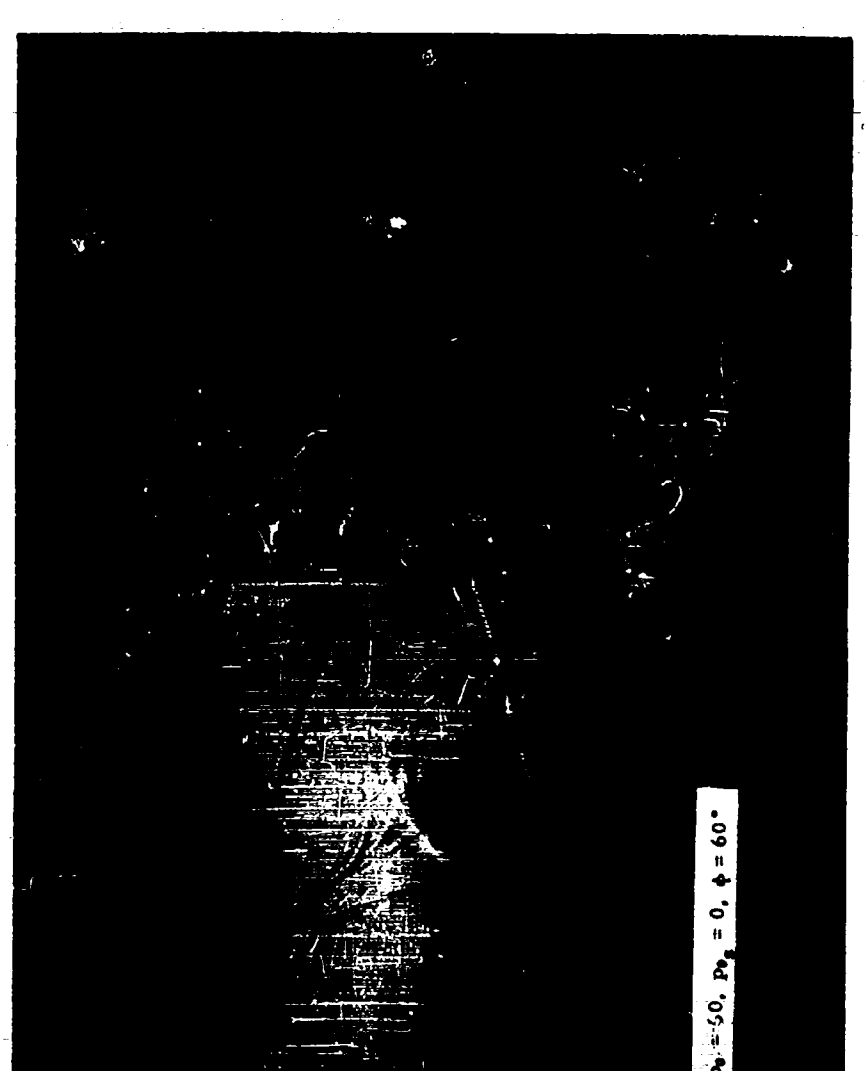

Figure 24a. Schlieren photograph of injection in the high pressure gradient nozzle.

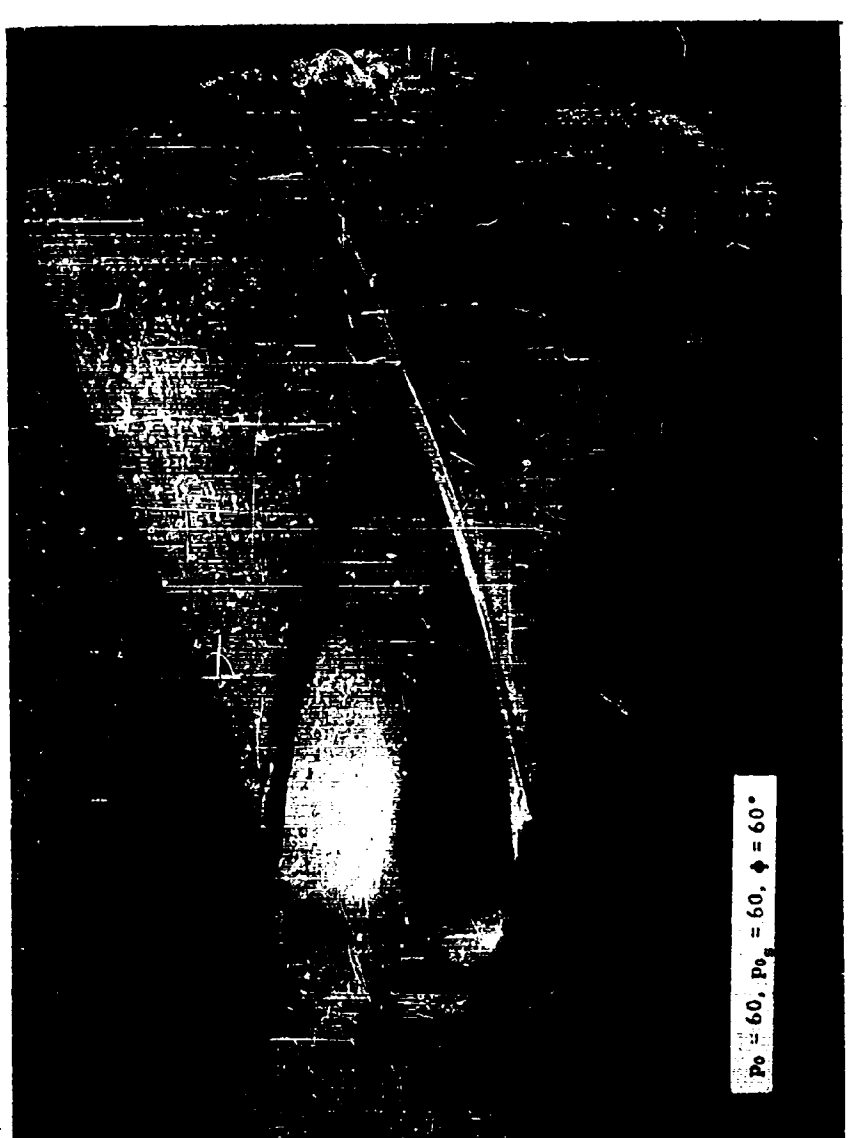

Figure 24b. Schlieren photograph of injection in the high pressure gradient nozzle.

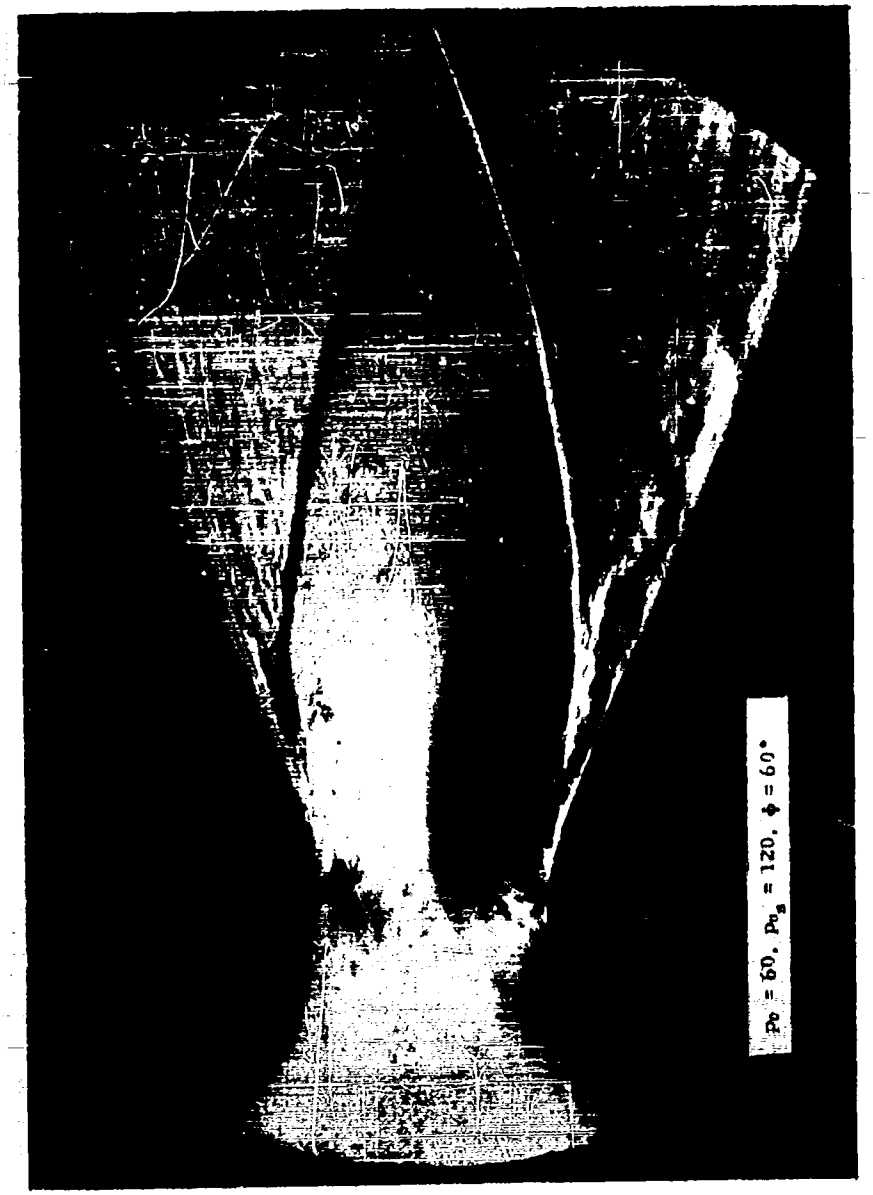

Figure 24c. Schlieren photograph of injection in the high pressure gradient nozzle.

Figure 24. Schlieren photograph of injection the high pressure gradient nozzle.

Figure 24e. Schlieren photograph of injection in the high pressure gradient nozzle.

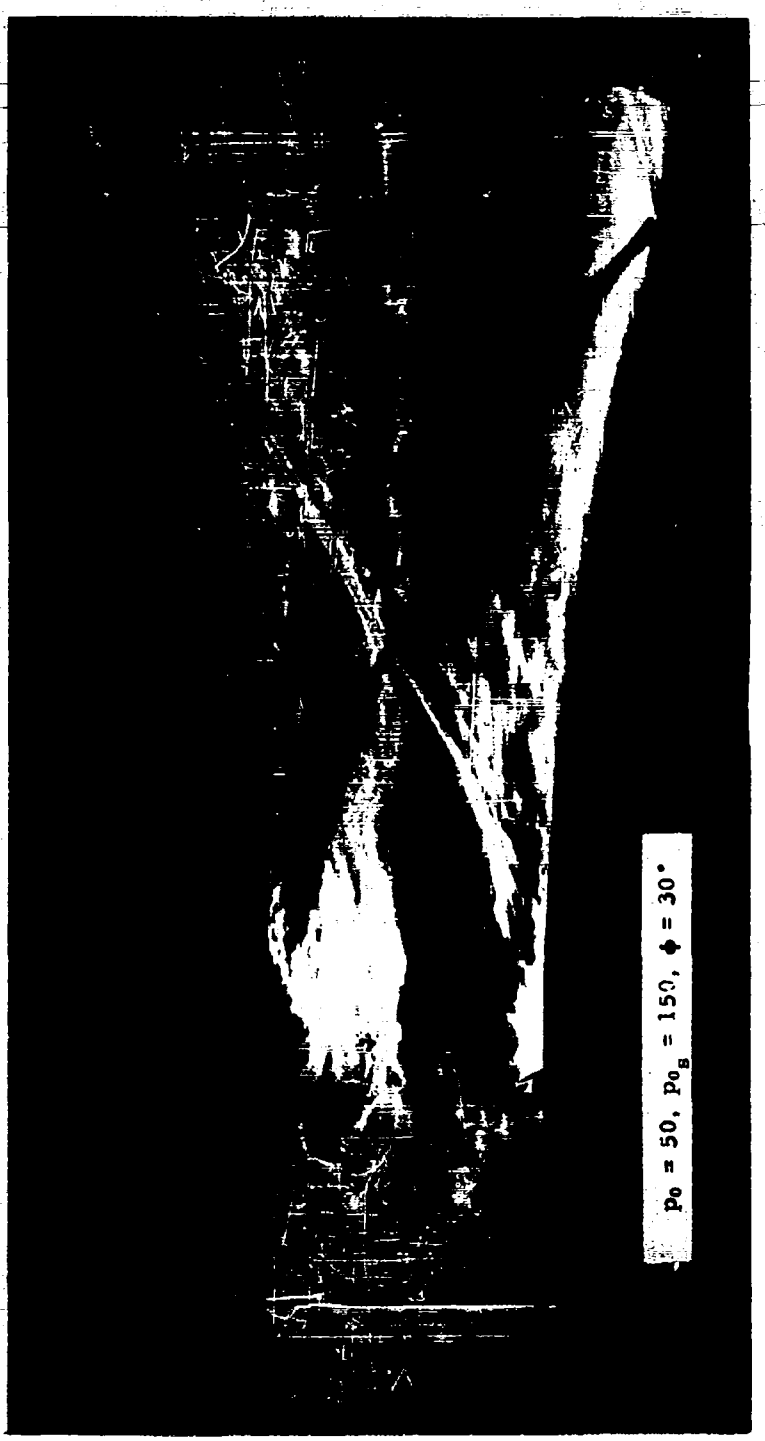

Figure 25. Schlieren photograph on injection in the low pressure gradient nozzle.

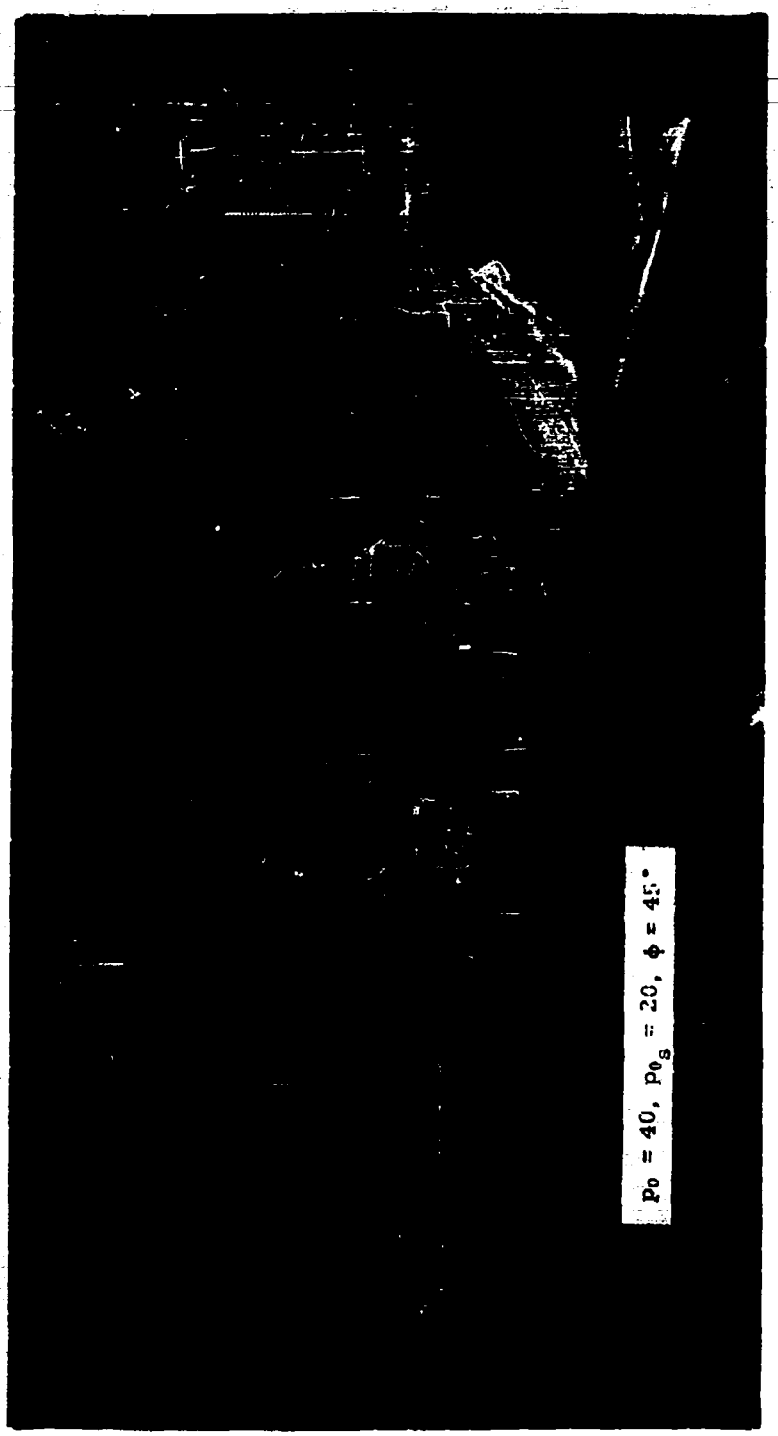

Figure 26a. Schlieren photograph of injection at a supersonic station in the low pressure gradient nozzle.

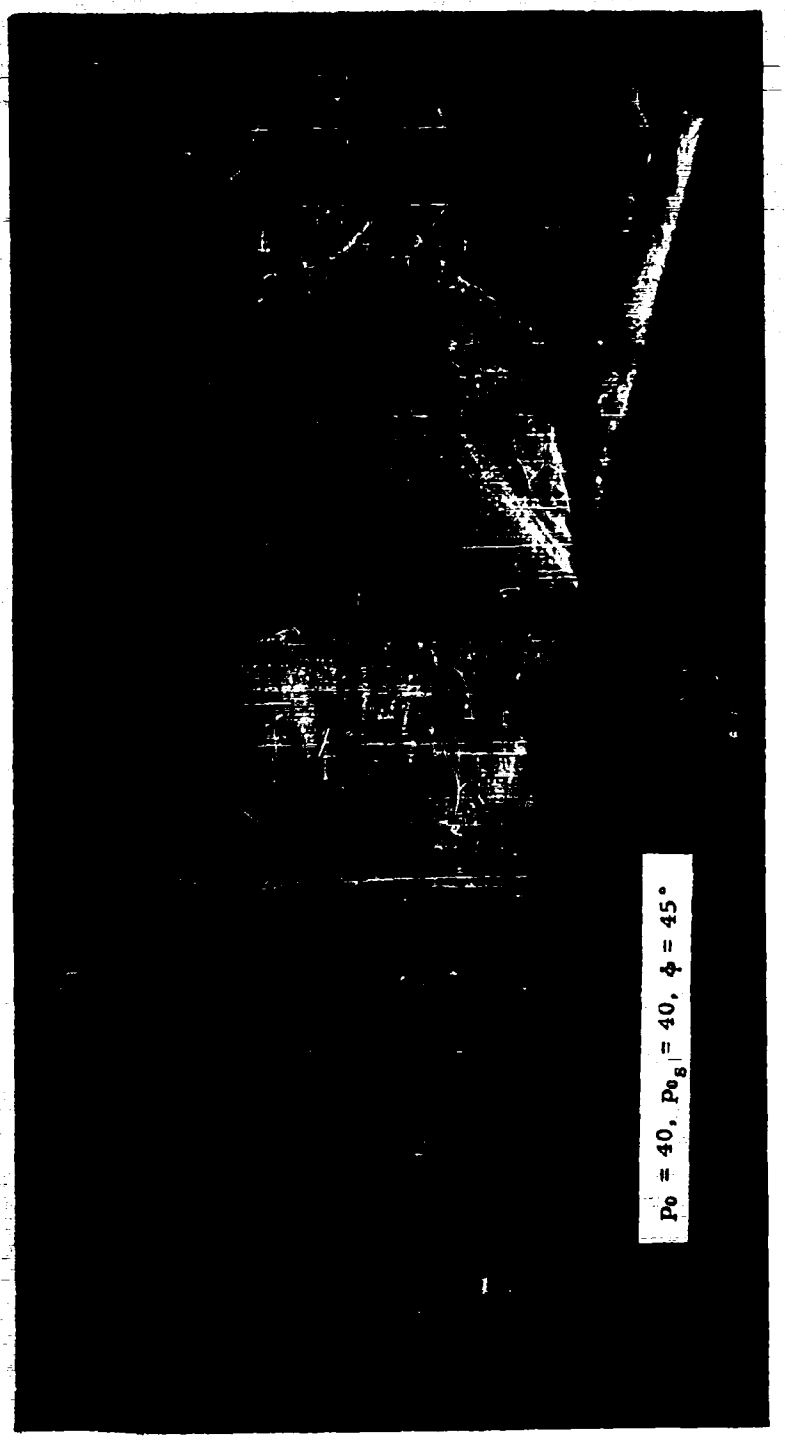

Figure 26b. Schlieren photograph of injection at a supersonic station in the low pressure gradient nozzle.

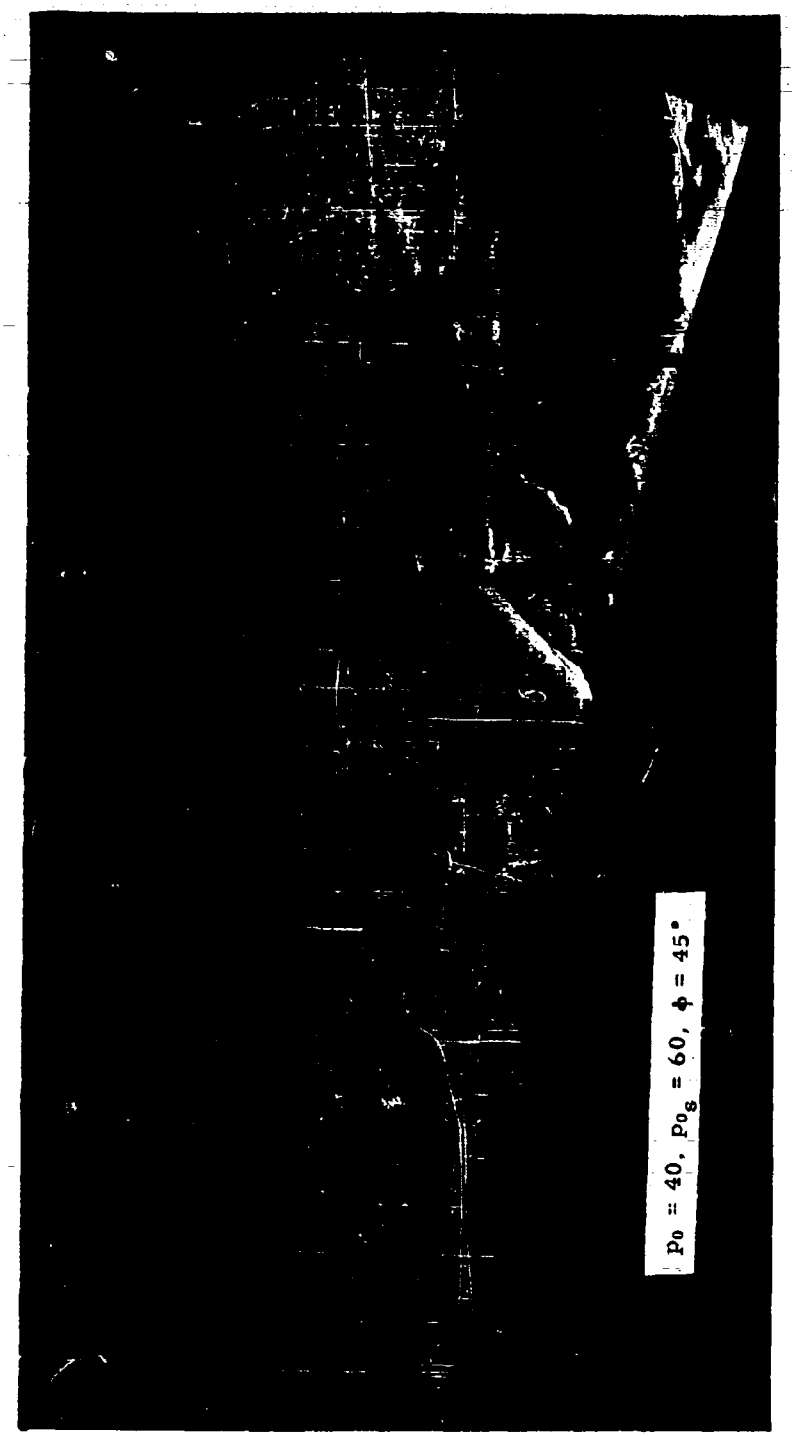

Figure 26c. Schlieren photograph of injection at a supersonic station in the low pressure gradient nozzle.

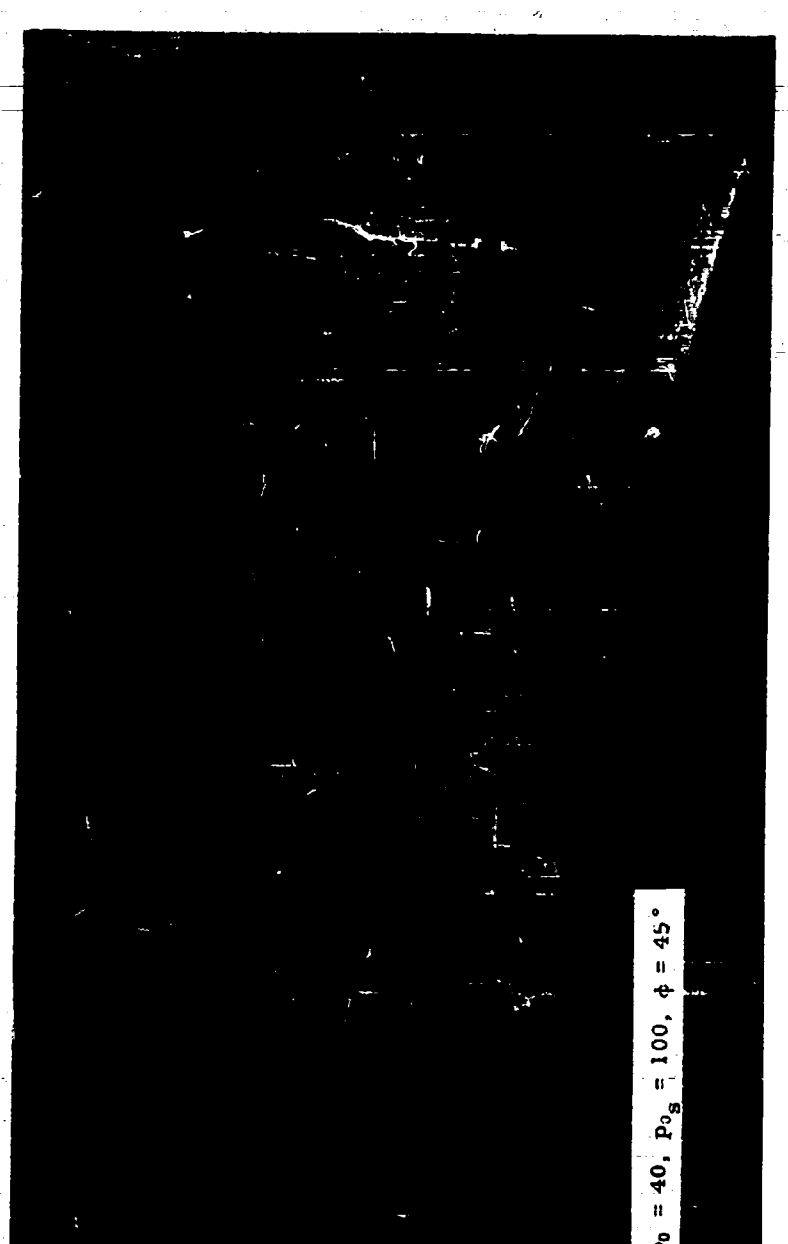

Figure 26d. Schlieren photograph of injection at a supersonic station in the low pressure gradient nozzle.

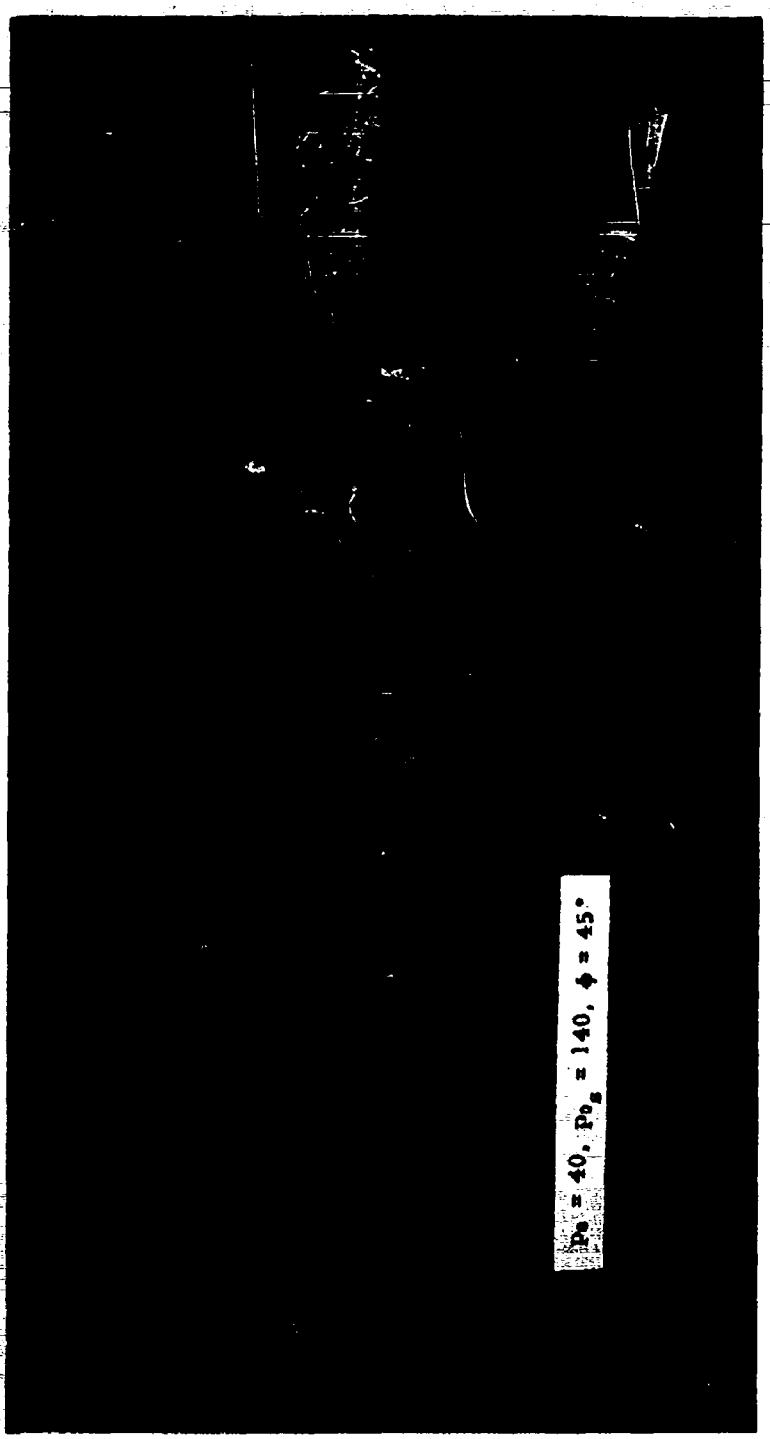

Figure 26e. Schlieren photograph of injection at a supersonic station in the low pressure gradient nozzle.

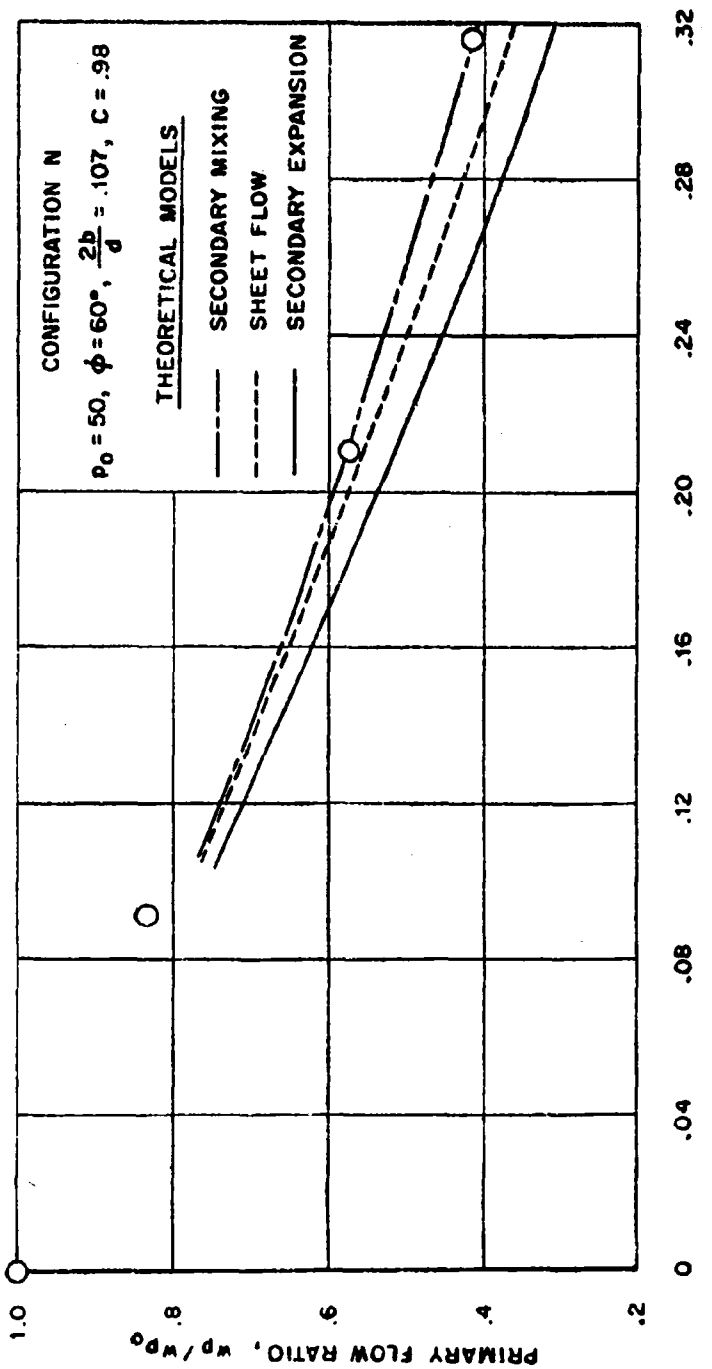

Figure 27. Theoretical and experimental flow throttling of the conical nozzle

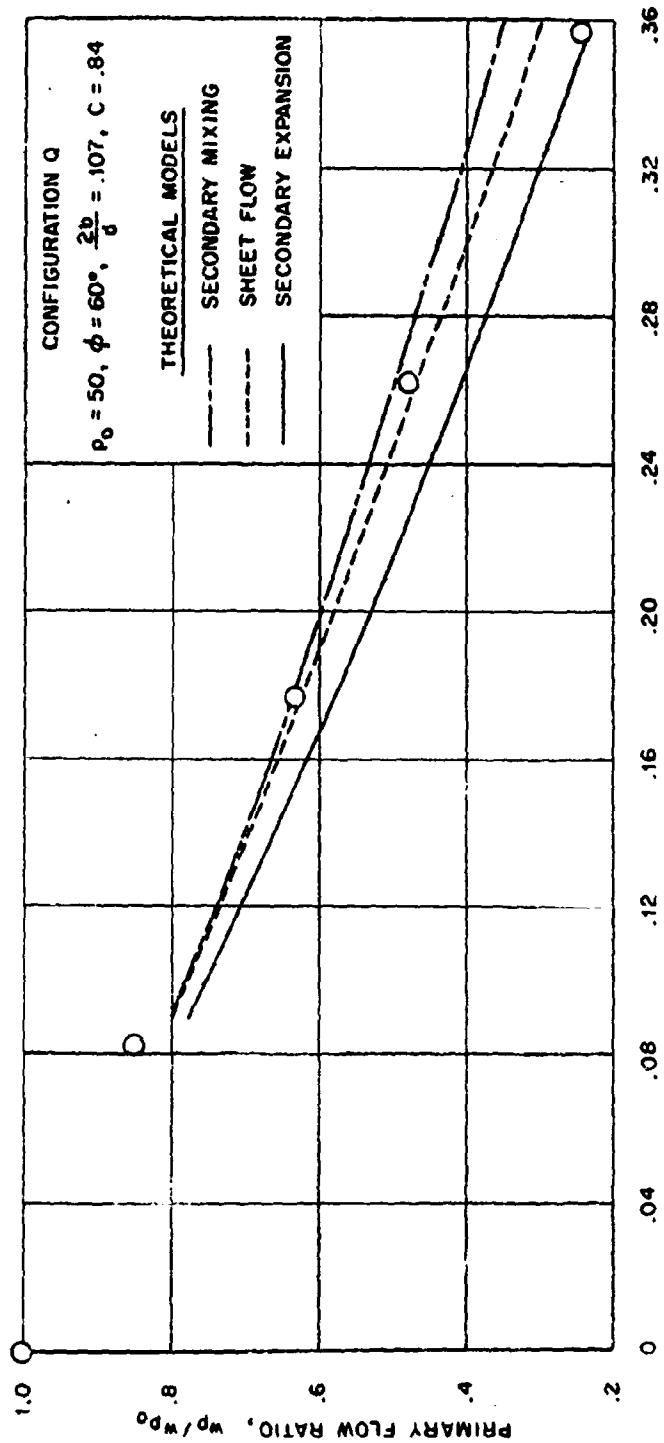

Figure 28. Theoretical and experimental flow throttling of the high pressure gradient nozzle with ϕ = 60°

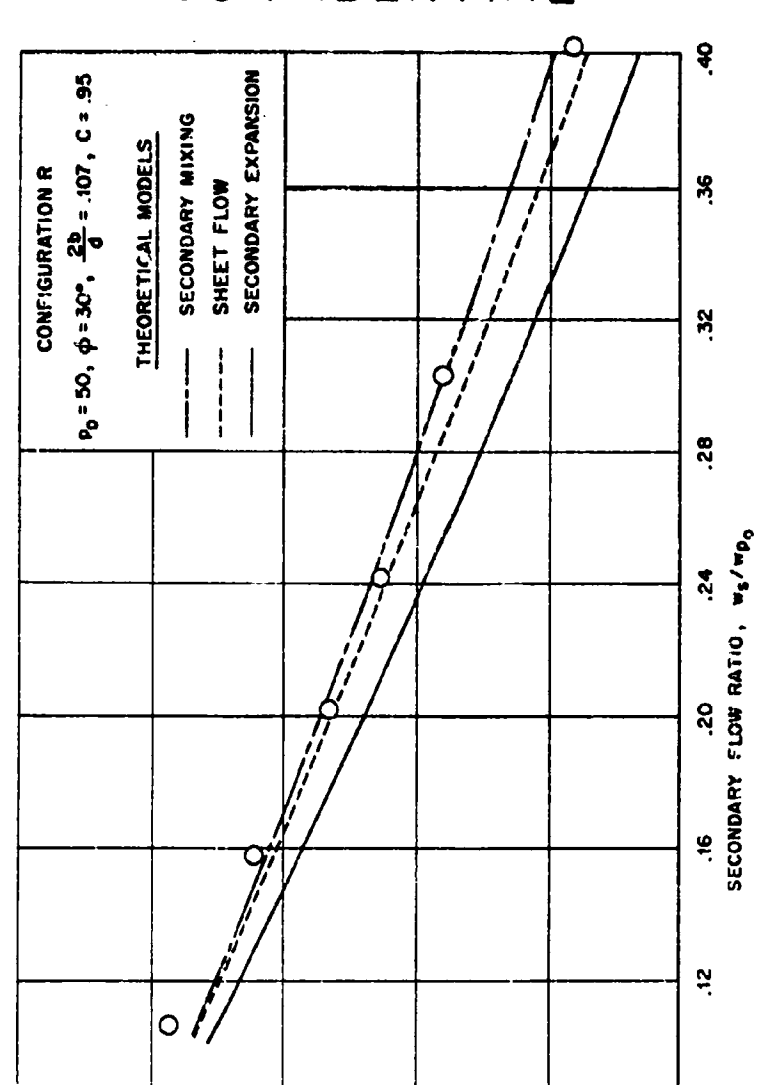

Figure 29. Theoretical and experimental flow throttling of the high pressure gradient nozzle with ϕ = 30°

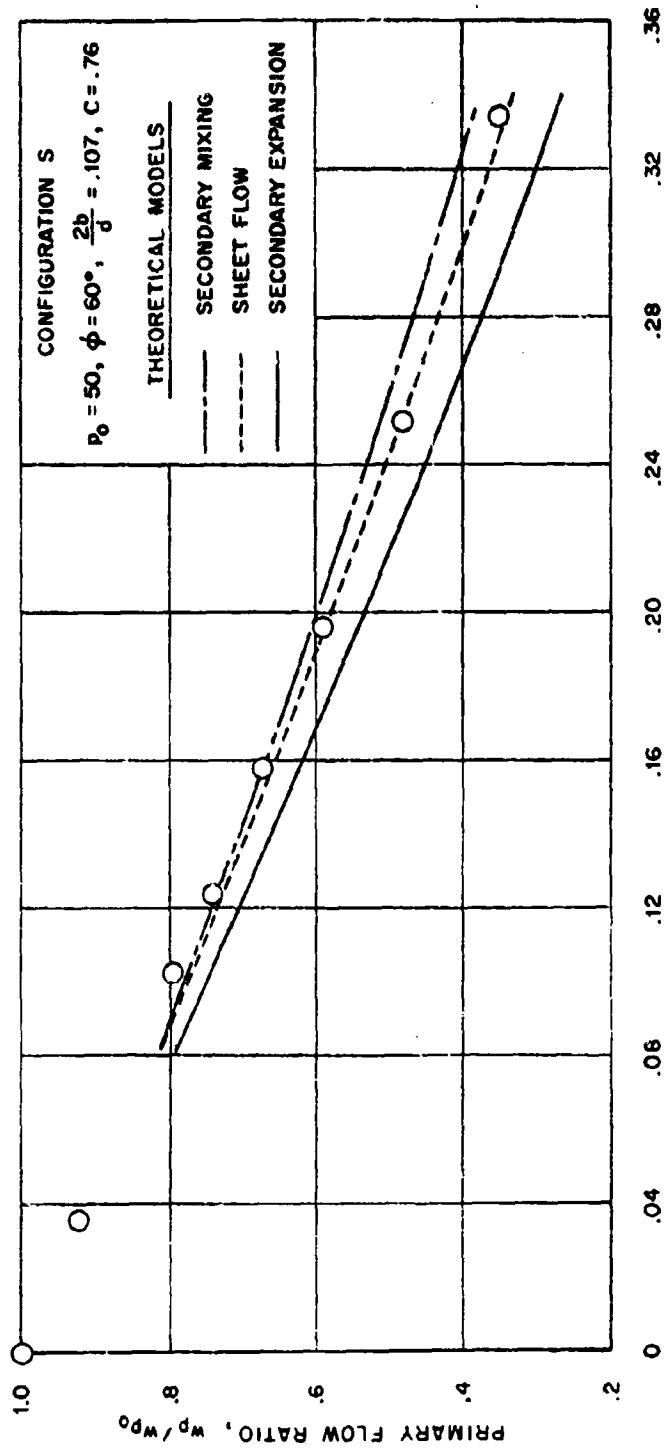

Figure 30. Theoretical and experimental flow throttling of low pressure gradient nozzle with ϕ = 60°

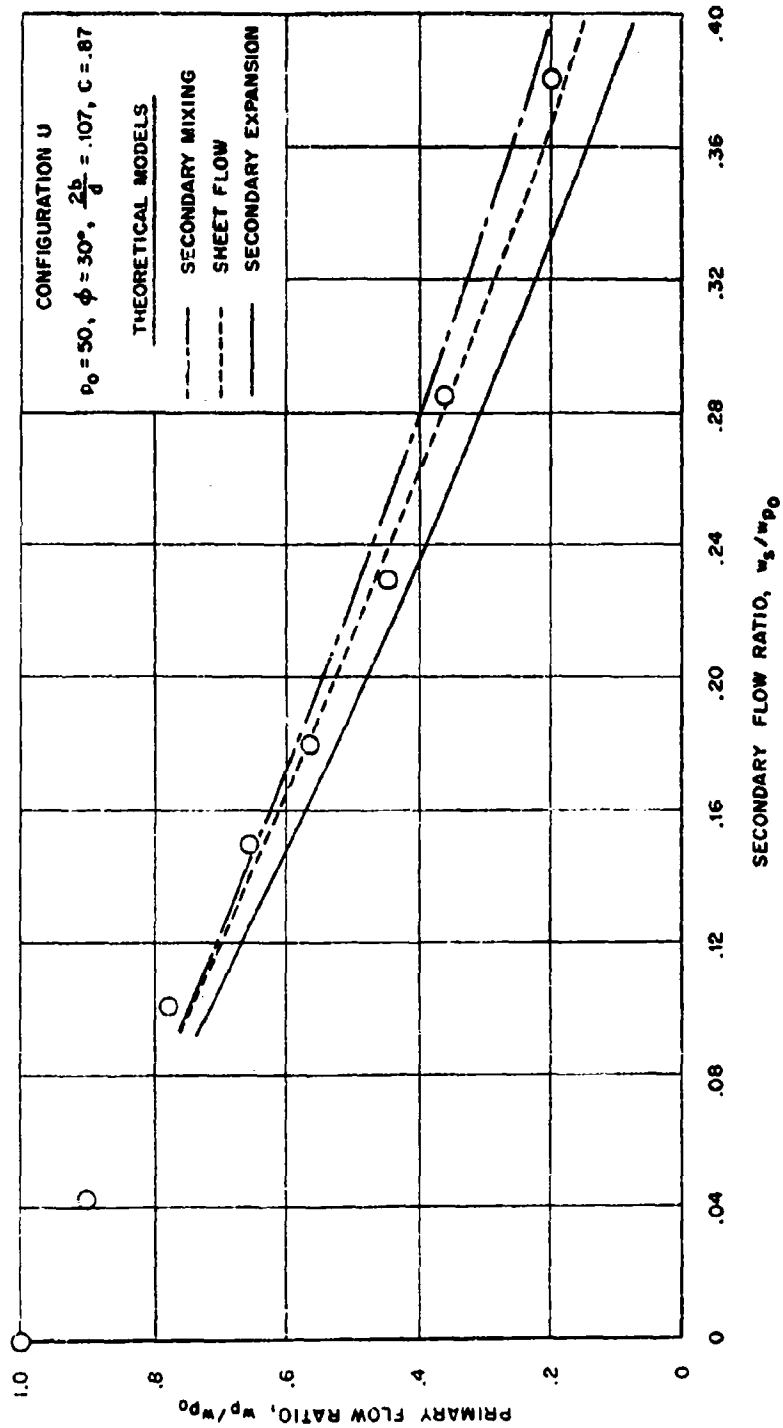

Figure 31. Theoretical and experimental flow throttling of the low pressure gradient nozzle with ϕ = 30°

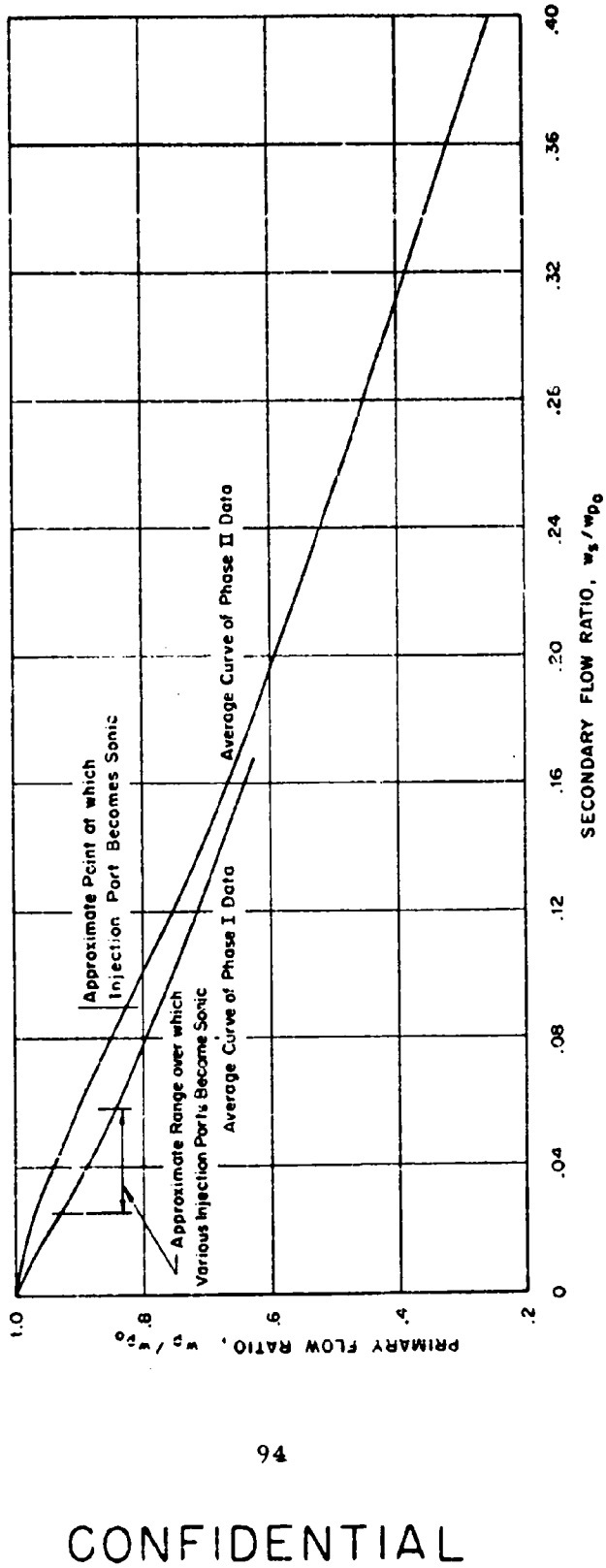

Figure 32. Phase I and Phase II flow throttling data ($\phi = 60°$)

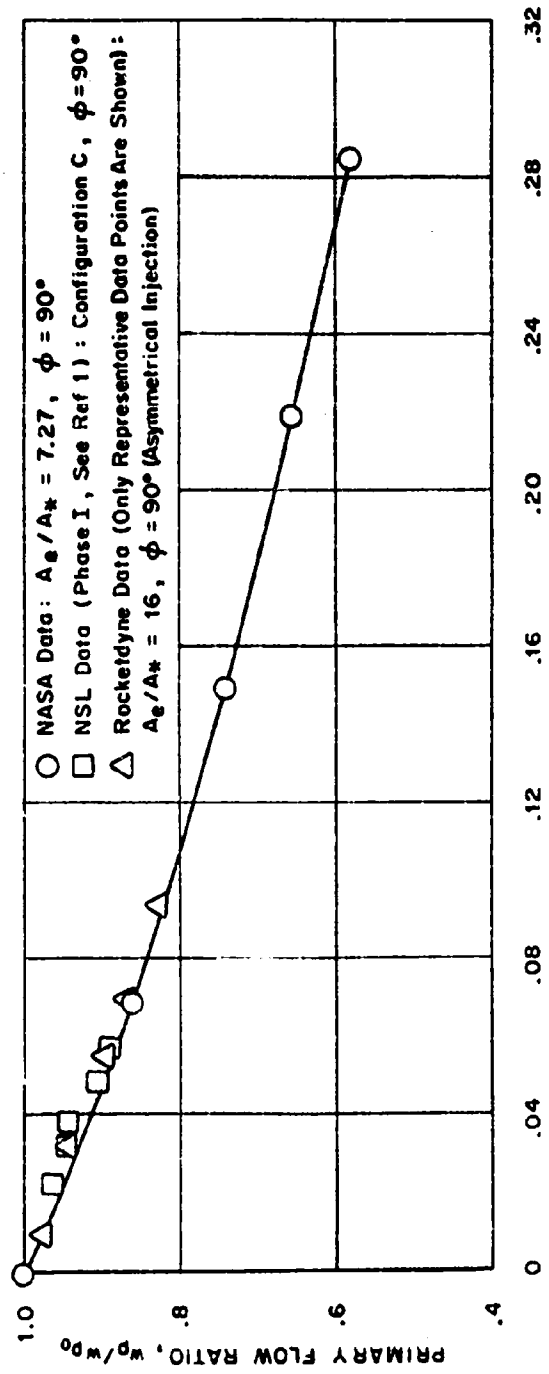

Figure 33. Some NSL and other flow throttling data

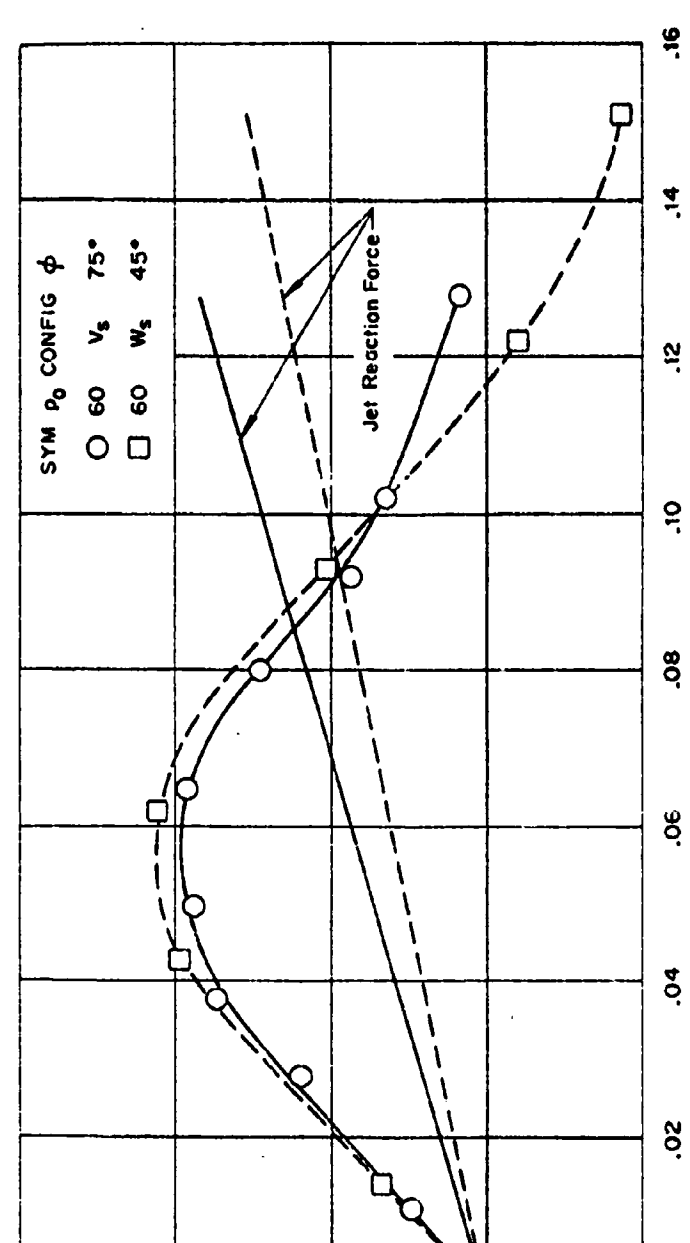

Figure 34. Typical side force data for asymmetric, supersonic-station injection in the low pressure gradient nozzle.

Figure 35a. Schlieren photograph of asymmetric, supersonic-station injection in the low pressure gradient nozzle.

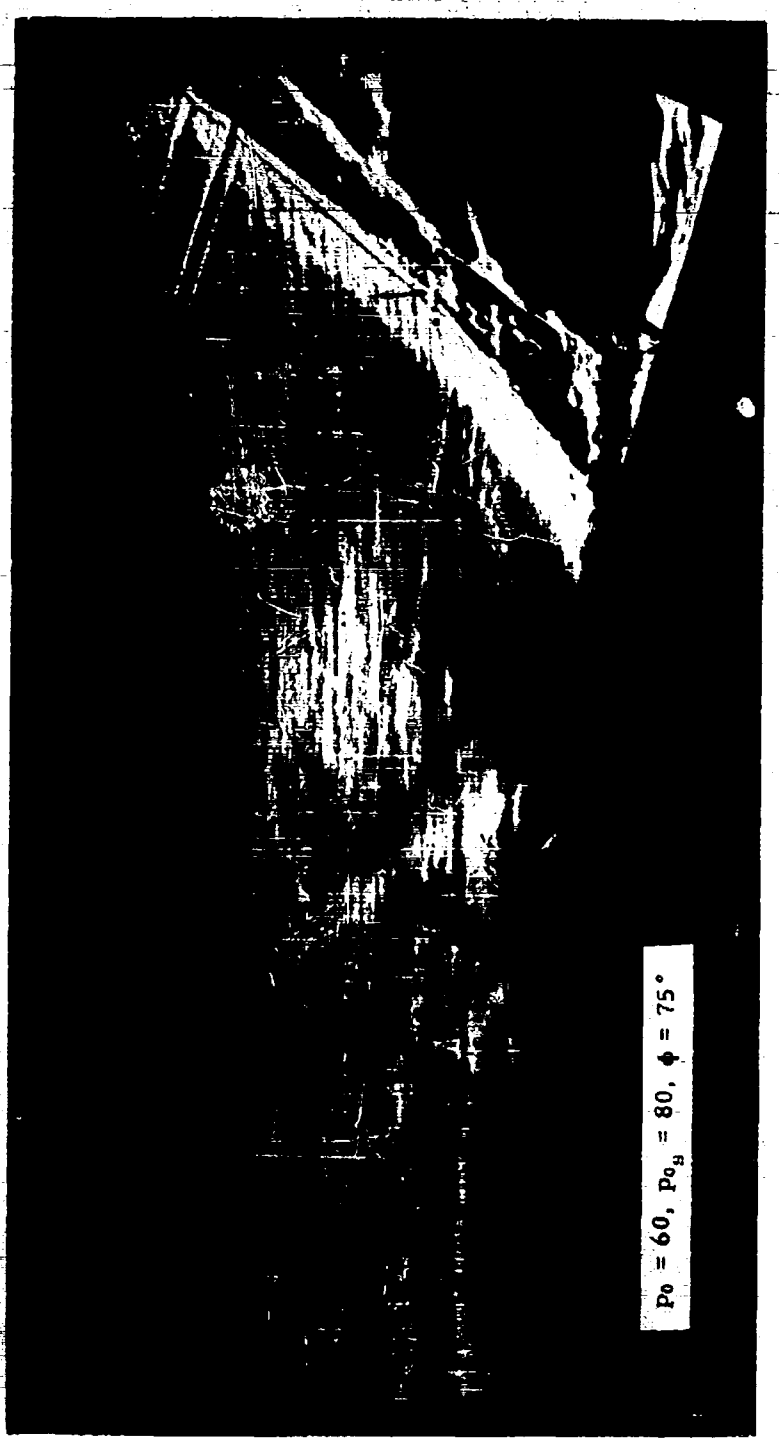

Figure 35b. Schlieren photograph of asymmetric, supersonic-station injection in the low pressure gradient nozzle.

Figure 35c. Schlieren photograph of asymmetric, supersonic-station injection in the low pressure gradient nozzle.

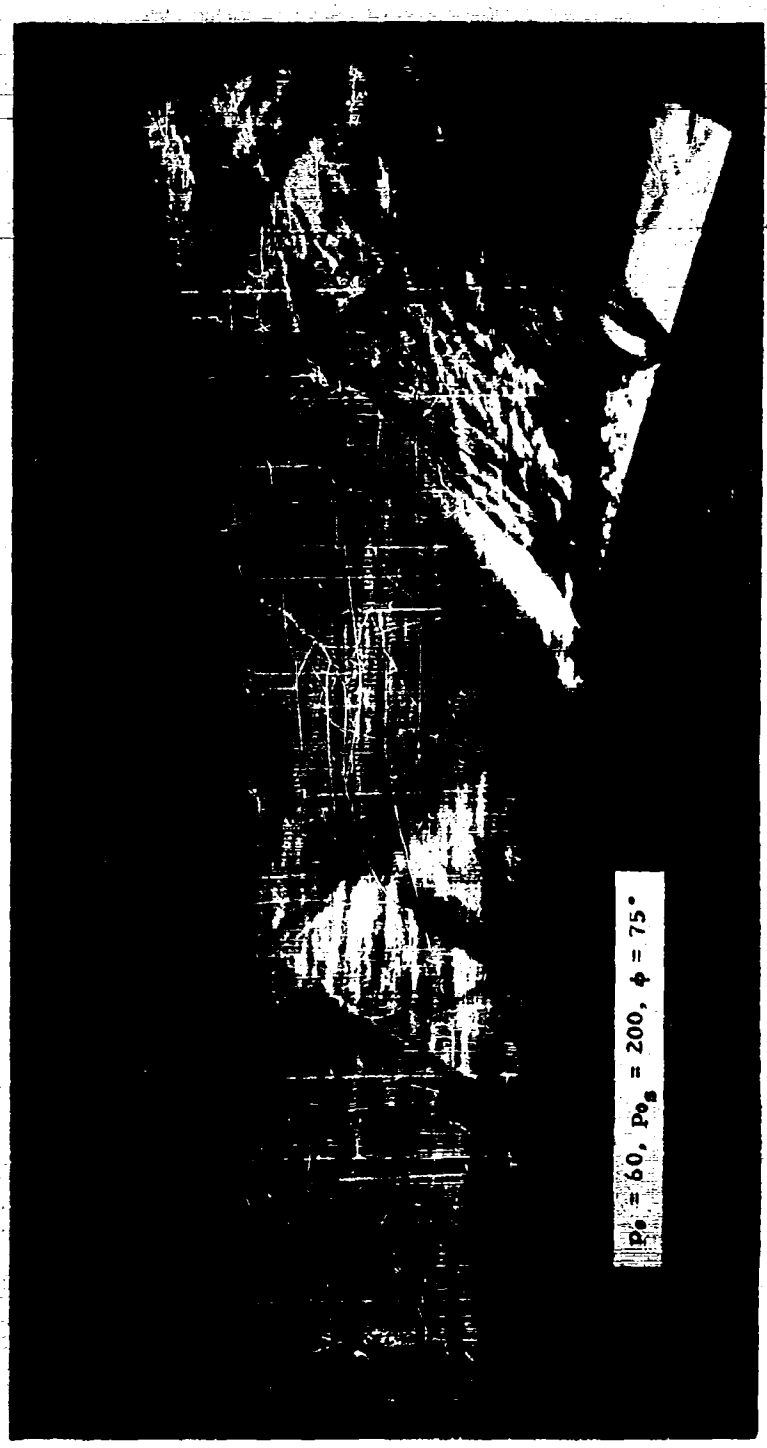

Figure 35d. Schlieren photograph of asymmetric, supersonic-station injection in the low pressure gradient nozzle.

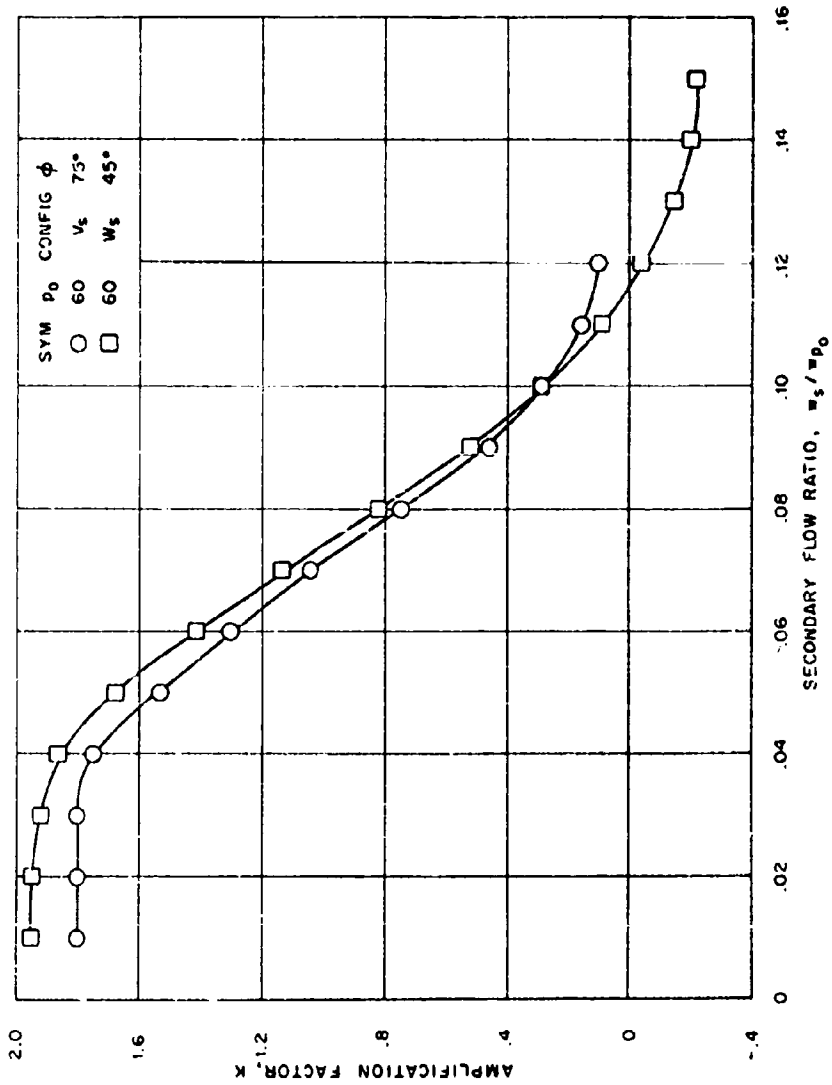

Figure 36. Variation of the side force amplification factor (K) with injection rate

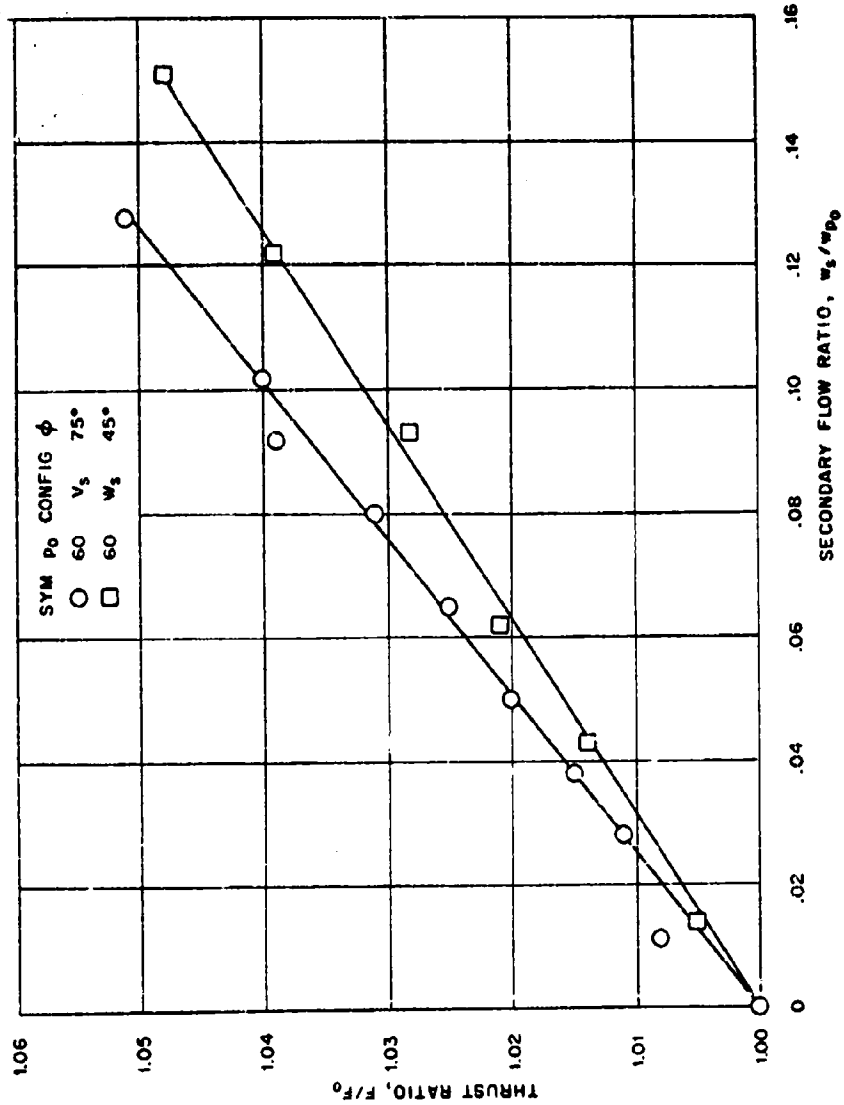

Figure 37. Axial thrust variation with asymmetric injection

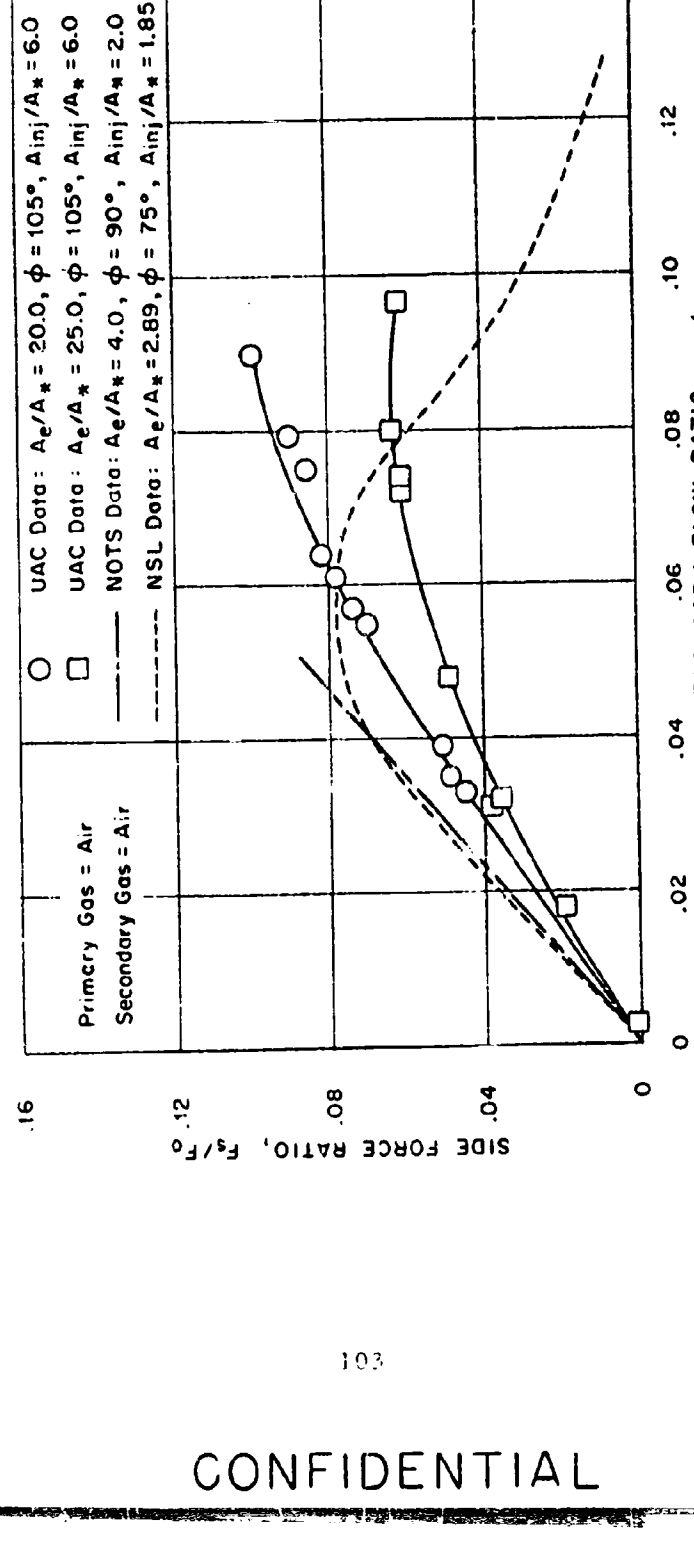

Figure 38. Side force data of the NSL, UAC, and NOTS

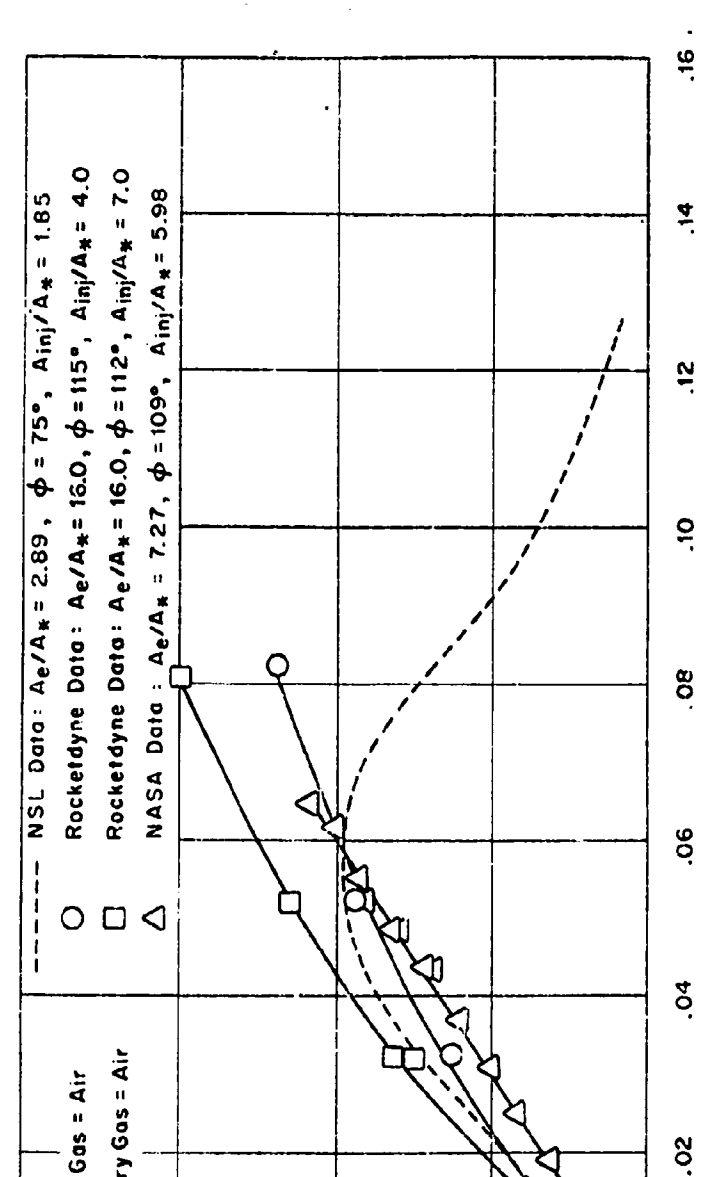

Figure 39. Side force data of the NSL, NASA, and Rocketdyne

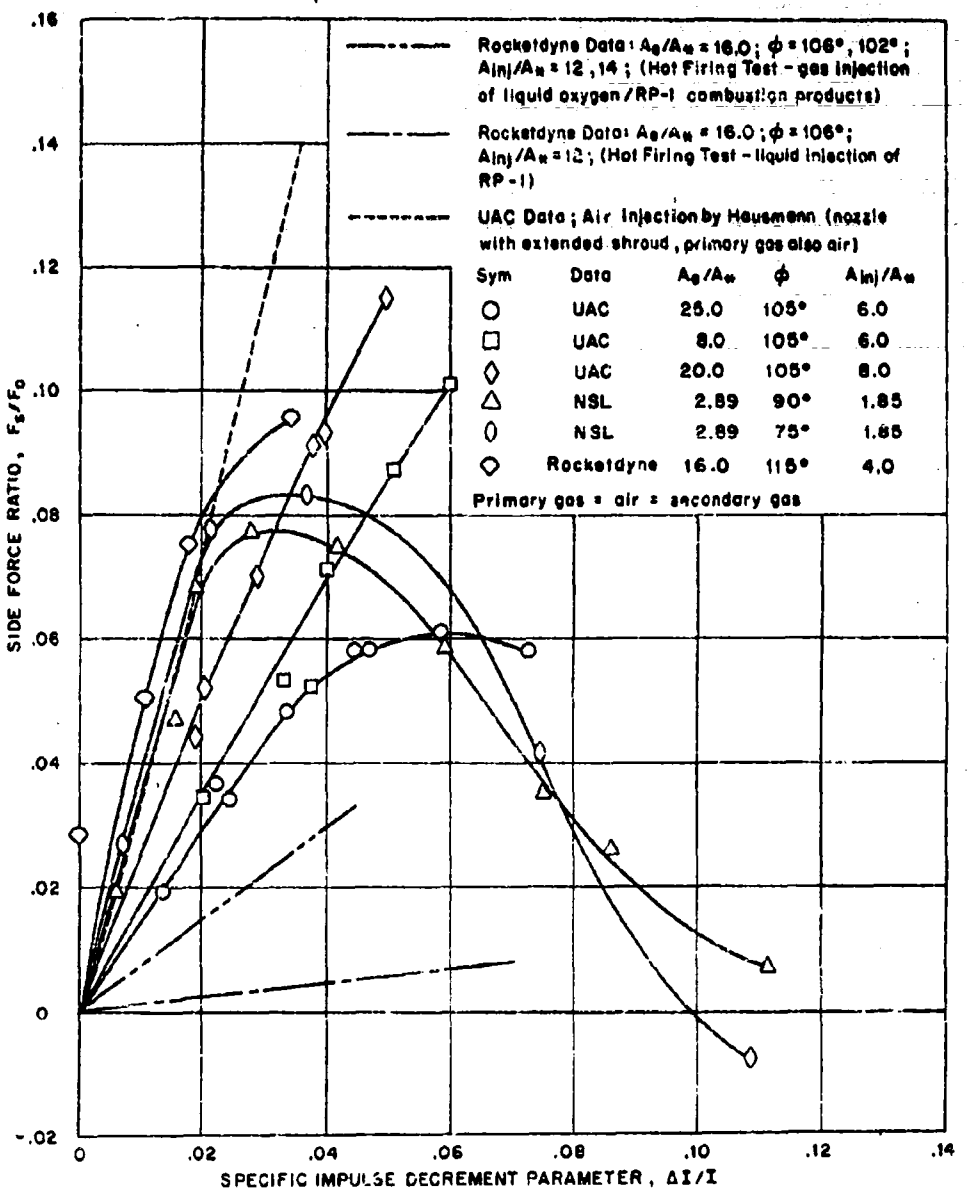

Figure 40. Side force variation of NSL and other data with specific impulse decrement parameter

APPENDIX A

METHOD OF SOLVING FLOW MODEL EQUATIONS

The final equations for all of the flow models were solved by a graphical technique. As shown in Sections A1, A2 and A3, a problem solution finally derives from a pair of simultaneous equations with unknown $(R_2/R_1)^2$ and M_1. However, these equations cannot be solved explicitly in the form given. Thus, a graphical method was used in which each of the simultaneous equations was solved for $(R_2/R_1)^2$ with both results being plotted as a function of M_1, as shown in the sketch below.

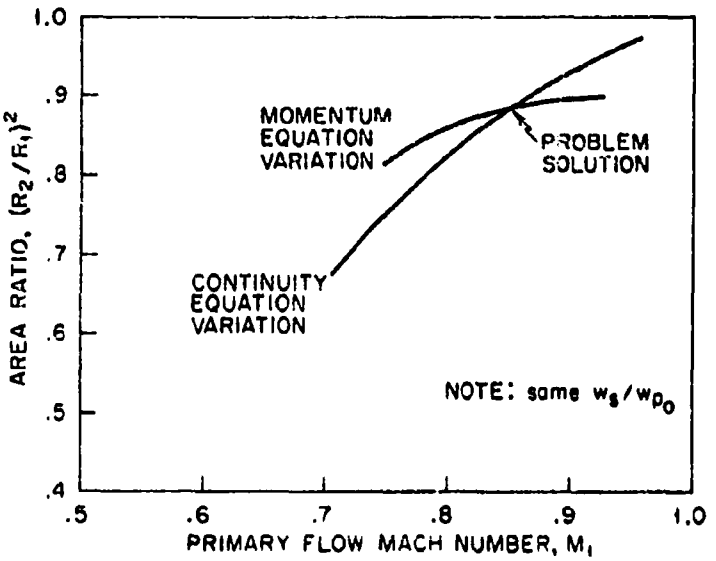

The intersection point is a solution with the corresponding M_1 and $(R_2/R_1)^2$ satisfying the simultaneous equations. A solution was thus determined for each assumed secondary flow rate.

The area ratio $(R_2/R_1)^2$ found from the above procedure is a flow throttling parameter in all of the models. The continuity equation (Eq. (5)) for the secondary mixing model shows that

$$\left[\frac{R_2}{R_1}\right]^2 = \frac{w_p + w_s}{w_{p_0}}$$

Thus, the primary flow throttling, the ratio w_p/w_{p_0}, is determined by subtracting the associated value of w_s/w_{p_0} from $(R_2/R_1)^2$. In the sheet flow and secondary expansion models Eq. (10) shows that

$$\left[\frac{R_2}{R_1}\right]^2 = \frac{w_p}{w_{p_0}}$$

since the primary and secondary streams flow without mixing.

APPENDIX B

SHEET FLOW MODEL DETAILS

The isentropic flow area ratio is a form of the continuity equation for a perfect gas and, as shown in Ref. 3, is given by

$$\frac{A}{A_*} = \frac{1}{M}\left[\frac{2}{\gamma+1}\left(1+\frac{\gamma-1}{2}M^2\right)\right]^{\frac{\gamma+1}{2(\gamma-1)}}$$

where M is the Mach number at the station where A is the area, in a streamtube flow.

The value of M_{2_s} in Eq. (10) is derived from the assumption that $p_{2_s} = p_2$. It is obvious that

$$\frac{p_2}{p_0} = \frac{p_{2_s}}{p_0}$$

A value of p_{0_s}/p_0 is implied by the assumption of a w_s/w_{p_0} and thus

$$\frac{p_0}{p_{0_s}} \times \frac{p_{2_s}}{p_0} = \frac{p_{2_s}}{p_{0_s}}$$

which implies the value of M_{2_s} according to Eq. (3).

APPENDIX C

SECONDARY EXPANSION FLOW MODEL DETAILS

The area ratio A_{2_s}/A_{*_s}, which determines M_{2_s}, is determined from

$$\frac{A_{2_s}}{A_{*_s}} = \frac{\pi\,(R_1^{\,2} - R_2^{\,2})}{A_{*_s}} = \frac{\left[1 - \left(\frac{R_2}{R_1}\right)^2\right]}{\frac{A_{*_s}}{\pi R_1^{\,2}}}$$

Since A_{2_s}/A_{*_s}, and thus M_{2_s}, depends on $(R_2/R_1)^2$, a trial value is needed for the $(R_2/R_1)^2$ in the above equation in order to solve Eq. (12) for the same parameter. However, as mentioned on page 8, the area ratio $(R_2/R_1)^2$ found from the continuity and momentum equations (Eqs. (8) and (12)) is determined for various assumed values of M_1. Thus, in the present case the assumed M_1 yields an $(R_2/R_1)^2$ from Eq. (8) which is then used as a trial value in the above equation so that Eq. (12) may also be solved for $(R_2/R_1)^2$. The M_{2_s} corresponding to the A_{2_s}/A_{*_s} in the above equation is used to obtain the pressure ratio p_{2_s}/p_{0_s} in Eq. (12).

MIT NSL TR 448

CONFIDENTIAL

Naval Supersonic Laboratory, Massachusetts Institute of Technology, Cambridge 39, Massachusetts.

FINAL REPORT ON A STUDY OF ROCKET THRUST CONTROL BY GAS INJECTION by Fred L. Gunter and Fred E. Fahrenholz. Contract Nonr 1841 (61), May 1961 xii and 110 pages.

A theoretical and experimental investigation of thrust control by secondary gas injection has been completed. Thrust control is treated from the two aspects of thrust modulation and vector control with the emphasis being on the former.

The thrust modulation study is concerned with the use of injection as a means of throttling the main nozzle flow. Since experimental data shows that thrust is proportional to total nozzle flow, the thrust is thus also proportional to flow throttling or injection rate. The performance (flow throttling and thrust) of a variety of secondary injection configurations was measured with a low pressure-ratio, axially symmetric nozzle as well as a high pressure-ratio, two-dimensional nozzle. Cold air (530°R) was the working fluid in the primary and secondary flows. The flow throttling results agree with an analysis based on three flow models and the schlieren photographs (from the two-dimensional tests) show that all three types of flow occur. The effects of the important variables are determined analytically and/or experimentally.

1. Nozzle Aerodynamics
2. Thrust Control

I. Gunter, Fred L.
II. Fahrenholz, Fred E.
III. MIT NSL TR 448

CONFIDENTIAL

MIT NSL TR 448

CONFIDENTIAL

Naval Supersonic Laboratory, Massachusetts Institute of Technology, Cambridge 39, Massachusetts.

FINAL REPORT ON A STUDY OF ROCKET THRUST CONTROL BY GAS INJECTION by Fred L. Gunter and Fred E. Fahrenholz. Contract Nonr 1841 (61), May 1961 xii and 110 pages.

A theoretical and experimental investigation of thrust control by secondary gas injection has been completed. Thrust control is treated from the two aspects of thrust modulation and vector control with the emphasis being on the former.

The thrust modulation study is concerned with the use of injection as a means of throttling the main nozzle flow. Since experimental data shows that thrust is proportional to total nozzle flow, the thrust is thus also proportional to flow throttling or injection rate. The performance (flow throttling and thrust) of a variety of secondary injection configurations was measured with a low pressure-ratio, axially symmetric nozzle as well as a high pressure-ratio, two-dimensional nozzle. Cold air (530°R) was the working fluid in the primary and secondary flows. The flow throttling results agree with an analysis based on three flow models and the schlieren photographs (from the two-dimensional tests) show that all three types of flow occur. The effects of the important variables are determined analytically and/or experimentally.

1. Nozzle Aerodynamics
2. Thrust Control

I. Gunter, Fred L.
II. Fahrenholz, Fred E.
III. MIT NSL TR 448

CONFIDENTIAL

MIT NSL TR 448

CONFIDENTIAL

Naval Supersonic Laboratory, Massachusetts Institute of Technology, Cambridge 39, Massachusetts.

FINAL REPORT ON A STUDY OF ROCKET THRUST CONTROL BY GAS INJECTION by Fred L. Gunter and Fred E. Fahrenholz. Contract Nonr 1841 (61), May 1961 xii and 110 pages.

A theoretical and experimental investigation of thrust control by secondary gas injection has been completed. Thrust control is treated from the two aspects of thrust modulation and vector control with the emphasis being on the former.

The thrust modulation study is concerned with the use of injection as a means of throttling the main nozzle flow. Since experimental data shows that thrust is proportional to total nozzle flow, the thrust is thus also proportional to flow throttling or injection rate. The performance (flow throttling and thrust) of a variety of secondary injection configurations was measured with a low pressure-ratio, axially symmetric nozzle as well as a high pressure-ratio, two-dimensional nozzle. Cold air (530°R) was the working fluid in the primary and secondary flows. The flow throttling results agree with an analysis based on three flow models and the schlieren photographs (from the two-dimensional tests) show that all three types of flow occur. The effects of the important variables are determined analytically and/or experimentally.

1. Nozzle Aerodynamics
2. Thrust Control

I. Gunter, Fred L.
II. Fahrenholz, Fred E.
III. MIT NSL TR 448

CONFIDENTIAL

MIT NSL TR 448

CONFIDENTIAL

Naval Supersonic Laboratory, Massachusetts Institute of Technology, Cambridge 39, Massachusetts.

FINAL REPORT ON A STUDY OF ROCKET THRUST CONTROL BY GAS INJECTION by Fred L. Gunter and Fred E. Fahrenholz. Contract Nonr 1841 (61), May 1961 xii and 110 pages.

A theoretical and experimental investigation of thrust control by secondary gas injection has been completed. Thrust control is treated from the two aspects of thrust modulation and vector control with the emphasis being on the former.

The thrust modulation study is concerned with the use of injection as a means of throttling the main nozzle flow. Since experimental data shows that thrust is proportional to total nozzle flow, the thrust is thus also proportional to flow throttling or injection rate. The performance (flow throttling and thrust) of a variety of secondary injection configurations was measured with a low pressure-ratio, axially symmetric nozzle as well as a high pressure-ratio, two-dimensional nozzle. Cold air (530°R) was the working fluid in the primary and secondary flows. The flow throttling results agree with an analysis based on three flow models and the schlieren photographs (from the two-dimensional tests) show that all three types of flow occur. The effects of the important variables are determined analytically and/or experimentally.

1. Nozzle Aerodynamics
2. Thrust Control

I. Gunter, Fred L.
II. Fahrenholz, Fred E.
III. MIT NSL TR 448

CONFIDENTIAL